UNIVERSITY OF SOUTHAMPTON

FACULTY OF NATURAL AND ENVIRONMENTAL SCIENCES

SCHOOL OF OCEAN AND EARTH SCIENCES

Characterising Carbon Cycle Perturbations in the Cenomanian Western Interior Seaway of North America

by

Sameer Y. Patel

A thesis submitted to the University of Southampton in accordance with the requirements for the degree of Doctor of Philosophy

July 2017

UNIVERSITY OF SOUTHAMPTON

FACULTY OF NATURAL AND ENVIRONMENTAL SCIENCES

Palaeoclimate and palaeoceanography

Thesis for the degree of Doctor of Philosophy

CHARACTERISING CARBON CYCLE PERTURBATIONS IN THE CENOMANIAN WESTERN INTERIOR SEAWAY OF NORTH AMERICA

Sameer Yogesh Patel

ABSTRACT

As current global temperatures continue to rise at an accelerated pace, it is becoming increasingly important to examine how the planet has responded to previous periods of global warming in order to gain valuable insights into how the Earth system may react in the future. The mid-Cretaceous (~101-91 Ma) provides an excellent case study of a prolonged greenhouse climatic state, where high rates of oceanic crust production and enhanced large igneous province-related volcanism released vast quantities of greenhouse gases into the atmosphere. Consequently, global temperatures reached their highest level for the past 450 Myr during the Cenomanian to Turonian stages, and peak sea levels led to the development of epeiric seas such as the Western Interior Seaway (WIS), which extended southwards from the northern Boreal Ocean, across central North America, and into the Tethys Ocean. Superimposed upon this greenhouse climate were a series of even more extreme climate perturbations, of which Oceanic Anoxic Event 2 (OAE 2), spanning the Cenomanian-Turonian boundary (94.1 Ma), was the most prominent, globally widespread, extreme climatic event of the Late Cretaceous. OAE 2 represents a major global carbon cycle perturbation, during which enhanced marine productivity coupled with the expansion of oxygen minimum zones across global oceans led to the extensive deposition of organic-rich black shale deposits. An earlier Mid-Cenomanian Event (MCE I; ~96.5 Ma) is taken to be a precursor to OAE 2, as it marks the beginning of a ~2 Myr oceanographic reorganisation during which bottom waters started to become increasingly oxygen-depleted. MCE I is identified on a global scale by a distinct dual-peaked positive carbon isotope excursion. However, with little evidence of widespread organic-rich mudrock deposition, most studies of MCE I are from carbonate-rich successions, thus limiting the range of analyses that can be undertaken.

Here, a high-resolution, integrated organic and inorganic multi-proxy study of the Rebecca K Bounds-1 core from western Kansas has been undertaken in order to elucidate environmental and oceanographic changes during MCE I and the interval leading up to OAE 2 in the central-eastern WIS. MCE I is identified in an organic-rich sequence through a dual-peaked, positive organic carbon isotope excursion (MCE 1a and MCE 1b, respectively), and is determined to coincide with the establishment of a fully connected seaway that extended from the northern Boreal Ocean to the Tethyan Ocean in the south via the WIS in the mid-Cenomanian, as evidenced by diversified palynological, foraminiferal, and geochemical changes between MCE 1a and MCE 1b. Periodically enhanced planktic productivity is linked to ~50 kyr obliquity cycles across MCE I through cyclostratigraphic analysis. This heightened productivity is attributed to the strengthening of meridional winds during obliquity maxima, which may have increased upwelling-related nutrient input into Tethyan surface waters in equatorial regions. Palynological, redox-sensitive trace metal, lipid biomarker, and sedimentological data reveal that a complex dynamic oceanographic system prevailed in the central region of the WIS, with mixed early Cenomanian Tethyan-Boreal waters eventually being replaced by a northward migrating Tethyan water mass in the mid- to late Cenomanian. This situation prevailed until OAE 2 set in, when a rapid southward incursion of Boreal waters extended as far as the southern margin of the seaway. This multi-faceted study provides a new in-depth, high-resolution example of how Earth systems and environmental conditions reacted to periods of stressed, greenhouse climatic conditions.

Table of Contents

List of Tables

List of Figures

List of Accompanying Materials

All palynological, palynofacies, geochemical, and sedimentological data are stored digitally and can be downloaded from the U.S. Geological Survey archives by going to the following web addresses:

- Scanning electron microscopy images of polished thin sections: http://my.usgs.gov/crc-data/core/12001/core_analysis_84870_E006Data26.pptx

- ICP-MS data: http://my.usgs.gov/crc-data/core/12001/core_analysis_73303_E006Data17.xlsx

- XRF data: http://my.usgs.gov/crc-data/core/12001/core_analysis_74814_E006data19.xlsx

- TOC, $CaCO_3$, $\delta^{13}C_{org}$, palynofacies, palynology, lipid biomarker, and sedimentation rate data: http://my.usgs.gov/crc-data/core/12001/core_analysis_99848_E006Data28.xlsx

Total kerogen residues from palynological processing, palynofacies slides and fractionated lipid biomarker extracts are stored at the National Oceanography Centre, Southampton, U.K.

DECLARATION OF AUTHORSHIP

I, SAMEER Y. PATEL

declare that this thesis and the work presented in it are my own and has been generated by me as the result of my own original research.

Characterising Extreme Climate Events in the Cenomanian Western Interior Seaway of North America

I confirm that:

1. This work was done wholly or mainly while in candidature for a research degree at this University;
2. Where any part of this thesis has previously been submitted for a degree or any other qualification at this University or any other institution, this has been clearly stated;
3. Where I have consulted the published work of others, this is always clearly attributed;
4. Where I have quoted from the work of others, the source is always given. With the exception of such quotations, this thesis is entirely my own work;
5. I have acknowledged all main sources of help;
6. Where the thesis is based on work done by myself jointly with others, I have made clear exactly what was done by others and what I have contributed myself;
7. None of this work has been published before submission.

Signed: .....

Date: .....

Acknowledgements

This thesis represents a significant chapter in my life, and I am indebted to my supervisors, family, friends, and colleagues who have provided guidance, support, advice, and laughter throughout this journey.

To Ian, John, and James. I could not have asked for a better supervisory team. You were always available to discuss my work, continuously provided me with excellent feedback throughout the past four years, and as a result, you never left me feeling isolated or that I was out of my depth. You have helped me develop my scientific skills, my ability to write concisely and coherently, and improved my critical thinking, for which I am extremely appreciative. I must also give a special mention to Jessica, who was more than happy to help me with my organic geochemistry work, even though she was not part of the original supervisory panel and already had and immense amount on her plate. To all of you, thank you.

To my Mum, my brother, Siobhan, little baby Ani, and the rest of my family, without question, I could always count on you for your unwavering support. Knowing you were always just a phone call or a short train ride away (*if* they ever ran on time…) gave me great comfort.

Where do I even begin when it comes to all of my friends at NOCS? Whilst not a comprehensive list, here's a shout out to a few. Having the same awesome housemates throughout my time in Southampton made things that much easier. I look forward to continuing on the annual Bernard Street Christmas dinners! Richy D, Sam, and Chris: the beers, barbeques, golf sessions, and *that* four-year long group chat – if only I could put a gif here. Will, those daily coffees and the Tenby trips will never be forgotten! Smithers, the delusional dreams of getting that Kensington pad kept me going after we spent hours staring down those microscopes. I was lucky enough to be a part of two lively, sociable offices. Liz, Catherine and the rest of the crew made coming to work that much more fun. And who can forget *Slumdog Migniolet* – the academic football team of dreams. We were once champions, who then let others have a chance over the next three years. That's how I remember it anyway…

I owe a special thanks to Shir, Matt, Sarge, Richard, and Megan who took time to train me on how to complete various lab methods, how to use specialised equipment, and kept spirits high during the repetitive tasks! In a similar vein, I appreciate the help and advice Paul Dodsworth offered regarding identifying palynological specimens. I would also like to thank Paul Wilson, who offered his thoughts and insights on the carbon isotope data I produced.

I extend my gratitude to NERC and Shell for providing funding for the duration of the programme, and to those that were involved in the process. Finally, I thank the USGS in allowing me to sample archived core material, without which this project would not have been possible!

Once again, thank you to everyone for making this such an amazing, memorable experience.

Chapter 1: Introduction

1.1 Introduction

Global temperatures continue to rise at an unnaturally accelerated rate due to anthropogenic greenhouse gas (GHG) emissions (IPCC AR5: Pachauri et al., 2014). As such, it is important to understand how the planet has responded to previous periods of global warming, as this allows us to calibrate, validate, and improve climate models, and also gives us valuable insights into how environments and Earth systems (e.g., the global carbon cycle) may react in future scenarios.

1.2 The mid-Cretaceous climate and oceanography

The mid-Cretaceous provides an excellent case study of a prolonged greenhouse climatic state (Wang et al., 2014). High rates of oceanic crust production and enhanced large igneous province (LIP)-related volcanism released vast quantities of GHGs into the atmosphere (e.g., Larson, 1991; Seton et al., 2009; Hong and Lee, 2012). During this period, atmospheric carbon dioxide (pCO_2) concentrations rose to 800 – 1500 ppmv, ~2 – 4 times that of present levels (Berner, 2006; Beerling et al., 2011). This outgassing resulted in the development of a Late Cretaceous thermal maximum (Fig. 1.1) spanning the latest Albian to the early Coniacian (~101-91 Ma; Laurin et al., 2015; O'Brien et al., 2017), as indicated by numerous palaeo-temperature proxies such as bulk carbonate $\delta^{18}O$ records (Clarke and Jenkyns, 1999), fish tooth enamel-derived oxygen isotopes ($\delta^{18}O$: Pucéat et al., 2003), TEX_{86} lipid biomarkers: Forster et al., 2007), and benthic and planktic foraminiferal $\delta^{18}O$ records (e.g., Friedrich et al., 2012). Within this interval, Cretaceous global temperatures reached their peak in the Cenomanian – Turonian stages (e.g., Wilson et al., 2002; Friedrich et al., 2012).

During this thermal maximum there was an absence of permanent polar-ice cover as mean Arctic temperatures exceeded 14°C (Tarduno et al., 1998), and the warmest tropical surface (>35°C) and deep-ocean (>20°C) water temperatures of the past 450 Myr (in the early Turonian) resulted in reduced pole-equator thermal gradients (Huber et al., 2002; Norris et al., 2002; Forster et al., 2007a; Friedrich et al., 2008; O'Brien et al., 2017). This, together with the thermal expansion of seawater (Wendler and Wendler, 2016) led to high mid-Cretaceous sea levels (Fig. 1.1), which peaked at ~240-250 meters above mean present day values during the Cenomanian – Turonian (Haq, 2014) and allowed for the development of expanded shallow shelf environments and the formation of epicontinental seas, such as the Western Interior Seaway (WIS) of North America (Kauffman, 1977).

Along with higher sea levels, the evolving distribution of continental land masses and oceanic basins impacted upon water mass circulation in the mid-Cretaceous (Poulsen et al., 2001; Trabucho Alexandre et al., 2010). At this time, the North American and Eurasian continental landmasses were still connected at high latitudes, the proto-Atlantic Ocean was in its early evolutionary phase, and the subtropical Tethys Ocean extended from the Indo-Pacific Ocean to the central Atlantic Ocean (Fig. 1.2; Scotese et al., 1988; Trabucho Alexandre et al., 2010). Furthermore, during peak transgression in the Cenomanian – Turonian, the epeiric WIS extended from the proto-Gulf of Mexico to the Arctic Ocean, creating an important gateway between the Boreal and Tethyan realms (Kauffman, 1985; Elderbak and Leckie, 2016).

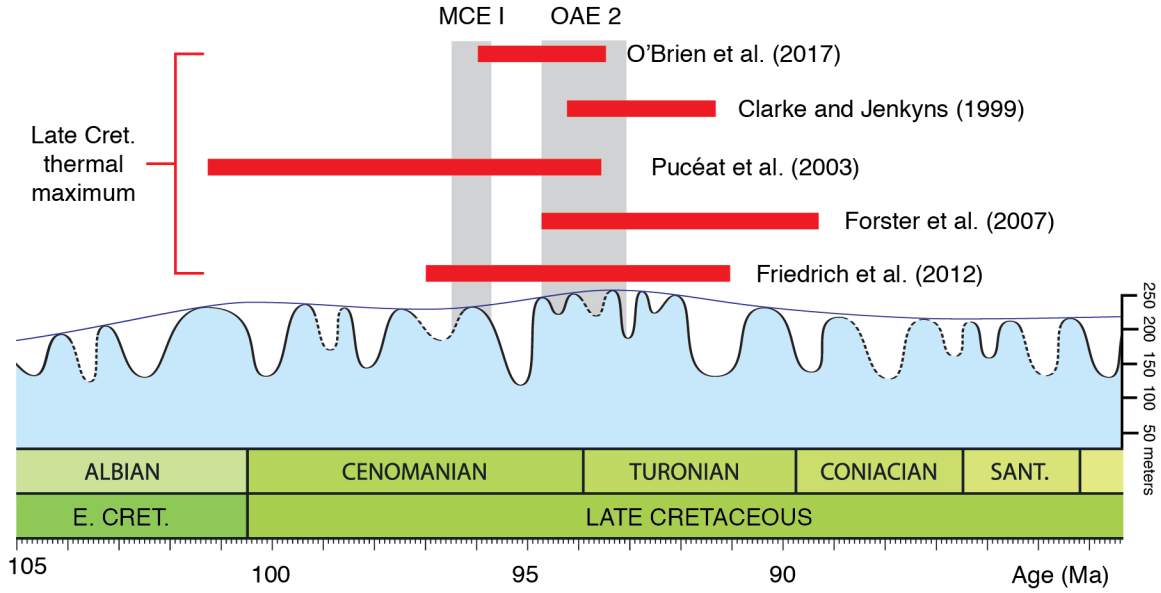

Figure 1.1: Range of Late Cretaceous thermal maximum (red bars) as identified by listed authors (from Laurin et al., 2015 and O'Brien et al., 2017), with prominent, global Cenomanian carbon cycle perturbations shown in grey (MCE I: Mid-Cenomanian Event); OAE 2: Oceanic Anoxic Event 2). MCE I duration from Eldrett et al. (2015a) and OAE 2 duration from Jarvis et al. (2006). Cretaceous short-term (light blue) and long-term (dark blue) sea level curves from Haq (2014).

Simulations using the GENESIS 2.0 Earth Systems Model demonstrate that trade winds travelled southwards from warm, humid-temperate high and mid-latitudinal regions towards arid, hot equatorial areas (Fig. 1.2; Hay and Floegel, 2012), and were subsequently deflected westwards in the northern hemisphere due to the Coriolis Effect (Fig. 1.3; Trabucho Alexandre et al., 2010). This mechanism was a key component of the North Equatorial Current, which drove European estuarine surface waters in a southwestern direction, across the Tethyan and Atlantic oceans towards the Central American Seaway (Poulsen et al., 2001; Trabucho Alexandre et al., 2010) – an oceanic gateway that separated North and South America (Fig. 1.3). Denser, more saline subsurface waters, originating from evaporitic low-latitudinal sites (Glancy et al., 1993) and/or the Southern Ocean, travelled along the western margins of both American continental landmasses before flowing eastwards into the Atlantic and Tethyan oceans as a result of salinity-driven convective forces (Poulsen et al., 2001; Trabucho Alexandre et al., 2010). These counter-flowing surface and

subsurface waters in the Tethyan Ocean created important nutrient traps in intermediate waters that allowed for enhanced productivity and large accumulations of organic-rich sediments along upwelling zones across the southern margin of the North Atlantic Ocean (Friedrich et al., 2008; Trabucho Alexandre et al., 2010).

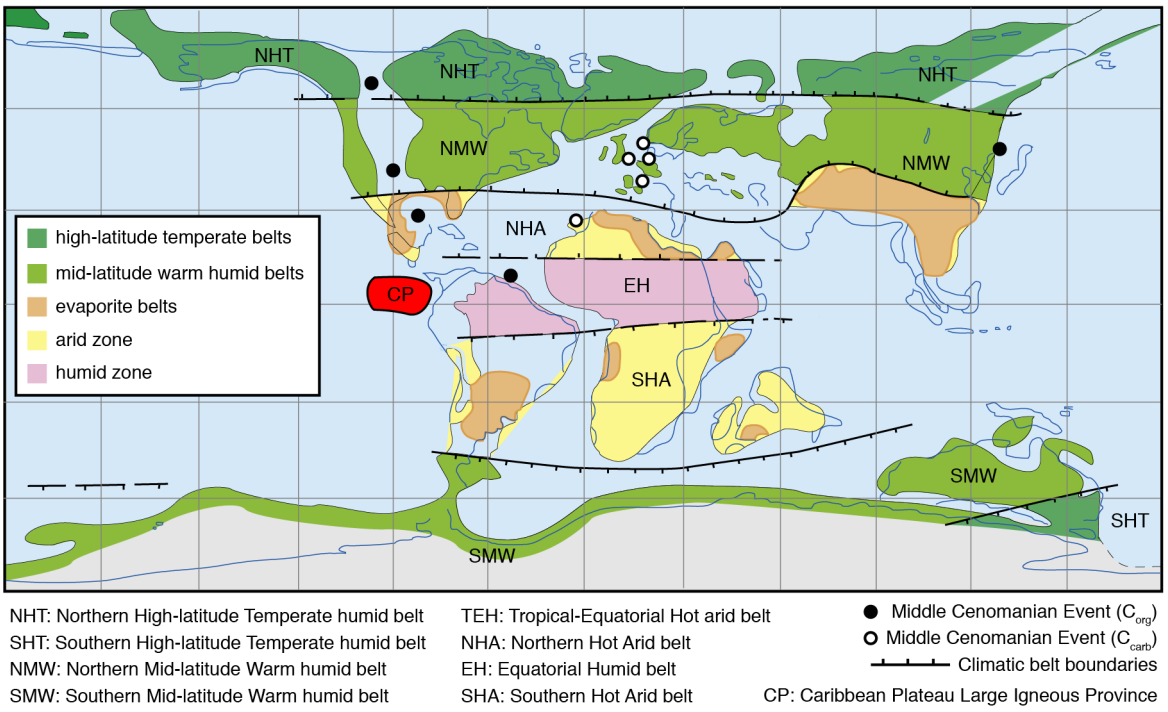

Figure 1.2: Mid-Cretaceous (Cenomanian) palaeogeographic and climatic reconstruction showing a selection of sites where the Mid-Cenomanian Event has been identified. Modified from Hay and Floegel, (2012).

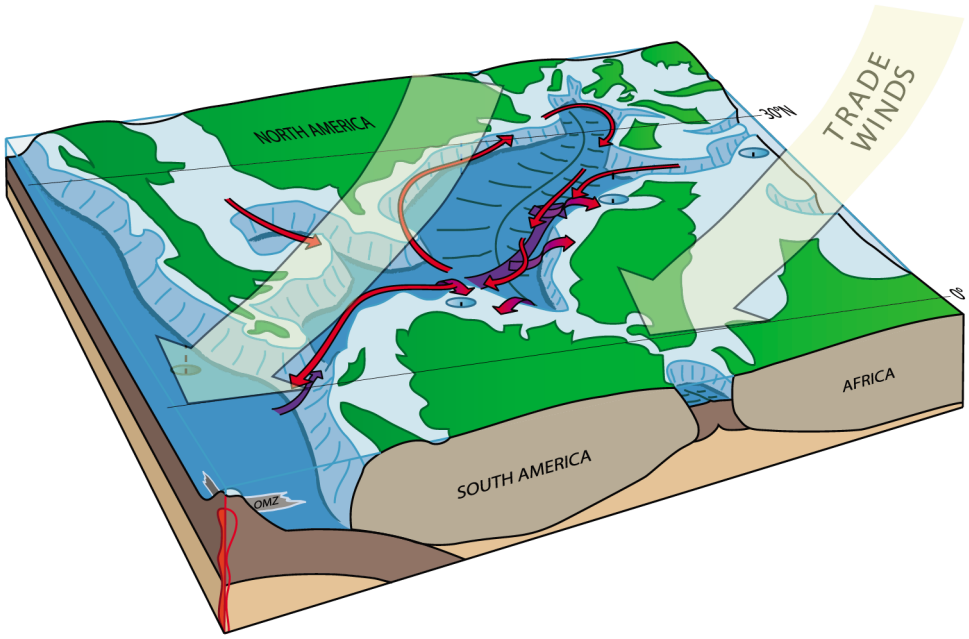

Figure 1.3: Mid-Crteaceous model of trade winds (yellow arrows) driving estuarine circulation (surface waters: red arrows; deep water: purple arrows) across the North Atlantic. From Trabucho Alexandre et al., 2010.

1.3 Extreme mid-Cretaceous climate events

A number of transient climatic perturbations occurred during the mid-Cretaceous greenhouse world (Fig. 1.4). These perturbations, characterised by expanded marine oxygen minimum zones and referred to as oceanic anoxic events (OAEs; Schlanger and Jenkyns, 1976), represent intervals of enhanced productivity and/or widespread preservation of finely laminated, organic-rich sediments (Calvert and Pedersen, 1993). Isotopically light carbon (^{12}C) is preferentially utilised over ^{13}C during photosynthesis (Farquhar et al., 1989). Thus, during periods of increased productivity, atmospheric and oceanic reservoirs became depleted in ^{12}C and thus enriched in ^{13}C, which was subsequently mobilized, buried, and preserved under the prevailing anoxic conditions (Jenkyns and Clayton, 1986). Therefore, stable organic carbon and biogenic carbonate isotope records that denote positive carbon isotope excursions (CIEs) can be used as indicators of past global carbon cycle perturbations associated with OAEs (e.g., Fig. 1.4; Jarvis et al., 2006).

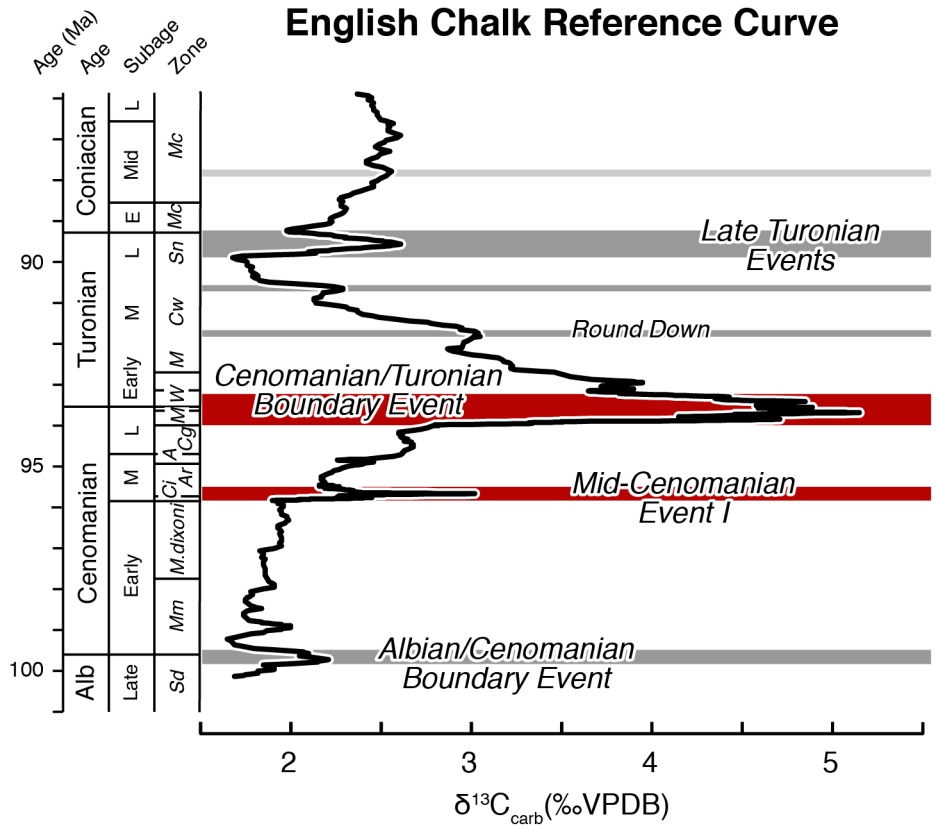

Figure 1.4: Composite mid-Cretaceous carbonate isotope record from the English Chalk, highlighting major carbon cycle perturbations, with OAE 2 and MCE I highlighted in red and other events in grey. Adapted from Jarvis et al. (2006).

Changes in the Earth's orbit around the Sun (eccentricity), in Earth's axial tilt (obliquity), and in axial precession result in solar insolation variations (Milankovitch cycles), which have long been understood to also force climatic change, both on longer and short timescales (e.g., Berger et al.,

1992; Laskar et al., 2004; Kuiper et al., 2008). However, the use of current astronomical solutions further than 50 million years into the past has been limited by modelling sensitivity (Laskar et al., 2004, 2011). Geochronological data (e.g., radio-isotopic dating of ash beds) have been used to calibrate astronomical models in the Cretaceous (e.g., Meyers et al., 2012b; Eldrett et al., 2015a; Ma et al., 2017), and have revealed that extreme climate events in the Cretaceous may have been paced by ~1.2 – 1.3 Myr chaotic orbital resonances (Laurin et al., 2015; Ma et al., 2017) that were the result of dynamic interplays between the orbits of Earth and Mars (Mitchell et al., 2008; Ma et al., 2017). On shorter timescales, eccentricity cycles (e.g., ~100 – 405 kyr), obliquity cycles (~40 – 50 kyr), and precession cycles (~18-23 kyr) influenced climatic and environmental fluctuations within individual OAEs (e.g., Meyers et al., 2012a; Eldrett et al., 2015b; Batenburg et al., 2016), as recorded in rhythmically interbedded organic- and carbonate-rich sediments.

The Cenomanian – Turonian boundary event (OAE 2) has been studied extensively, and is considered one of the most pronounced global carbon cycle perturbations of the Late Cretaceous, and thus provides an excellent insight into the development of these climate episodes (e.g., Arthur et al., 1987; Gale and Christensen, 1996; Friedrich et al., 2006; Trabucho Alexandre et al., 2010; Jarvis et al., 2011; Meyers et al., 2012a; Eldrett et al., 2015a; van Helmond et al., 2016). A combination of environmental (e.g., Friedrich et al., 2006; Prauss, 2012), climate (e.g., Jarvis et al., 2011; Zheng et al., 2016), and astronomical drivers (e.g., Meyers et al., 2012b; Eldrett et al., 2015b) influenced widespread anoxic marine conditions and thus orchestrated the development of OAE 2.

Enhanced LIP-related volcanism during the Late Cretaceous thermal maximum, such the emplacement of the Late Cenomanian Caribbean Plateau (Fig. 1.2) introduced large quantities of reduced metals and sulphides into the oceanic system, which subsequently depleted oxygen levels as they became oxidized (e.g., Snow et al., 2005; Turgeon and Creaser, 2008; van Bentum et al., 2009; Jarvis et al., 2011). LIP-related activity also increased global temperatures (see above), which in turn intensified and accelerated hydrological cycles (van Helmond et al., 2014). As a result, enhanced continental weathering elevated nutrient supplies to the oceans, which in turn promoted increased planktic productivity (e.g., Arthur et al., 1987; Trabucho Alexandre et al., 2010). As greater fluxes of organic matter became degraded by microbial action as it descended through the water column, oxygen levels became rapidly depleted and hydrogen sulphide concentrations increased, leading to anoxic-euxinic conditions (Kump et al., 2005). Stratified oceans (e.g., Friedrich et al., 2006) and the development of silled basins from enhanced oceanic crust production (Seton et al., 2009; Meyers et al., 2012a) impeded the reoxygenation of bottom waters, creating ideal conditions for organic matter preservation, thus perturbing the global carbon cycle (Arthur et al., 1987).

Although OAE 2 occurred during a dominantly warm period, a shorter-lived but prominent worldwide cooling (Plenus Cold Event) and bottom water reoxygenation pulse has been identified

during the early part of the event (e.g., in Europe: Gale and Christensen, 1996; Pearce at a., 2009; Voigt et al., 2004; the North Atlantic: Forster et al., 2007b; van Helmond et al., 2016; and the WIS: van Helmond et al., 2014; Eldrett et al., 2017). This pulse has been linked to a heightened pCO_2 drawdown as a result of increased productivity and subsequent black shale deposition (Jarvis et al., 2011; van Bentum et al., 2012), and the equatorial migration of Boreal waters (Gale and Christensen, 1996; van Helmond et al., 2016; Zheng et al., 2016).

Obliquity-paced high-latitude insolation variations periodically increased and decreased meridional temperature differences, which in turn controlled wind intensities (Meyers et al., 2012a). During times of strengthened winds, enhanced upwelling of nutrient-rich deep waters could have promoted enhanced productivity in equatorial regions (e.g., Demerara Rise; Meyers et al., 2012a), explaining high organic matter accumulations at these sites during OAE 2 (Friedrich et al., 2006). In the WIS, interbedded organic-rich mudrocks, marls, and limestones are also attributed to climate changes driven by Milankovitch-paced solar insolation intensity variances, with carbonate-rich lithologies associated with insolation maxima, and the converse for organic-rich sediments (Fig. 1.4; Eldrett et al., 2015b). As such, organic matter accumulation across the North Atlantic and the WIS was, in part, controlled by obliquity during OAE 2 (Meyers et al., 2012a).

Together, these studies demonstrate the influences of different Earth system processes on the development of short-term climatic anomalies. Thus, multiple driving forces must be taken into account when studying these episodes.

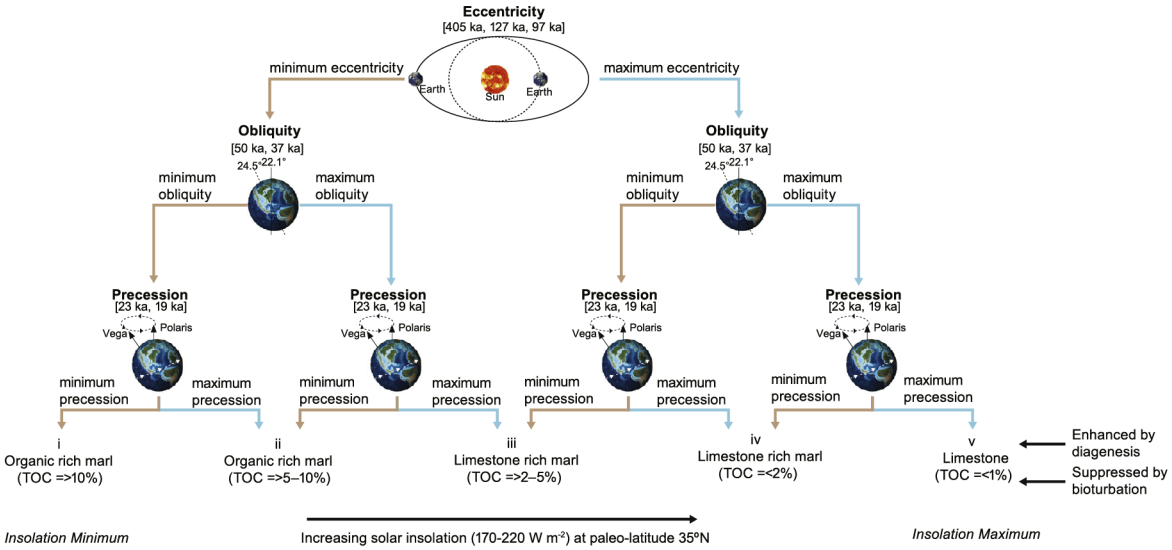

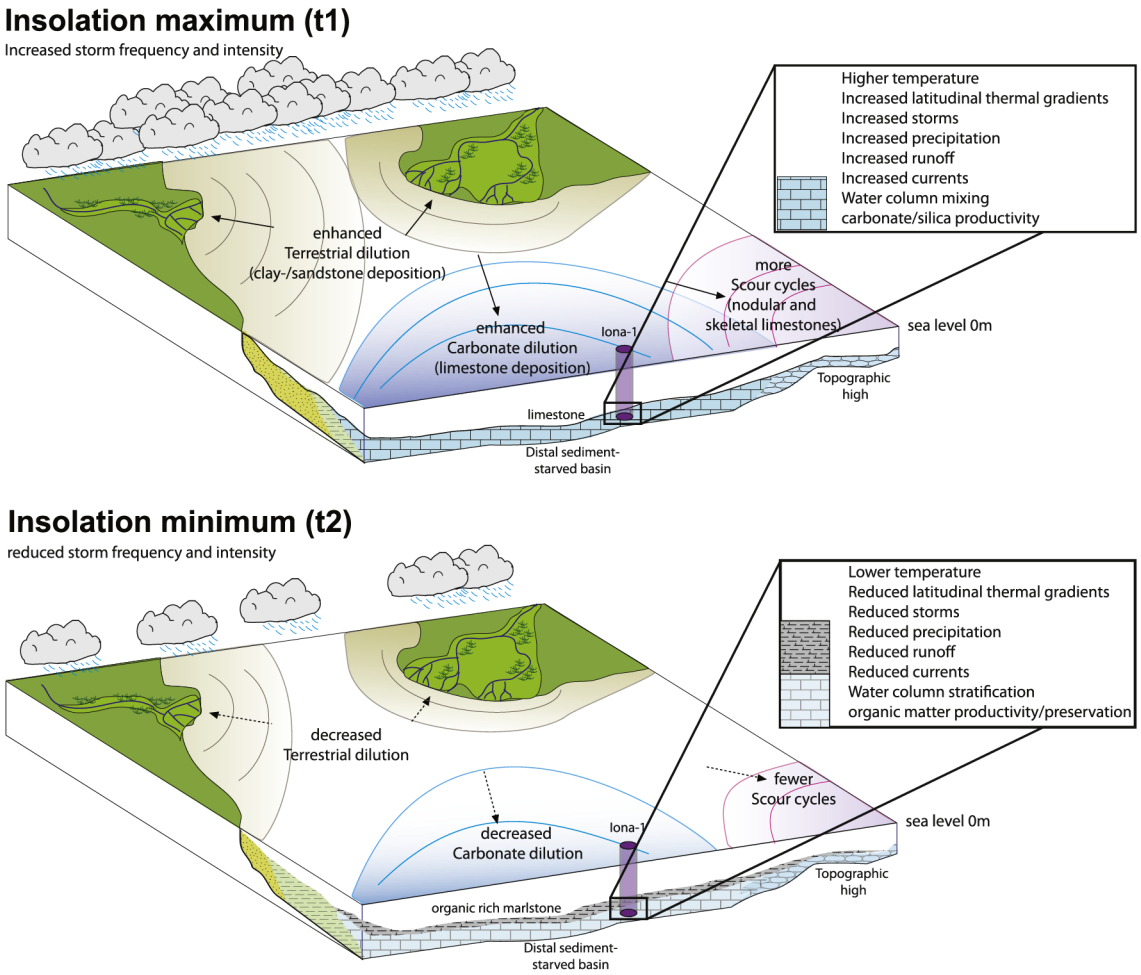

Figure 1.5: Conceptual model for orbital control on lithology (top), and diagrams illustrating the geographic variability in the lithologic expression of Milankovitch climate forced cycles for greenhouse climates within a restricted anoxic carbonate shelf setting (bottom). From Eldrett et al. (2015b).

1.4 The Mid-Cenomanian Event

The Mid Cenomanian Event (MCE I; ~96.57 – 96.36 Ma Eldrett et al., 2015a) is a globally recognised carbon cycle perturbation proposed as a precursor to OAE 2 (Coccioni and Galeotti, 2003; Friedrich et al., 2009), although MCE I is currently much less well understood than OAE 2. To better understand the nature of MCE I, and its impact on global oceanography, a number of granular (e.g., palaeoproductivity-focussed; Hardas et al., 2012) and multi-proxy studies have been completed (e.g., Friedrich et al., 2009; Giraud et al., 2013;Gambacorta et al., 2014; Zheng et al., 2016).

The first description of a "Cenomanian Event" was from a fossiliferous Cenomanian nodular limestone in North-West Germany (Ernst et al., 1983; Meyer, 1990). "Twin-peaked" positive CIEs (MCE 1a: $\delta^{13}C_{carb}$ +0.5 ‰ and MCE 1b: $\delta^{13}C_{carb}$ +1.0 ‰; Fig. 1.4) were later recorded in geologically older carbonate successions from the basal Middle Cenomanian in southern England, and used to define MCE I (see: Jenkyns et al., 1994; Paul et al., 1994; Mitchell, 1996). This same event has now been identified in numerous marine carbonate successions (e.g., England and France: Voigt et al., 2004; Jarvis et al., 2006; Giraud et al., 2013; Reboulet et al., 2013; Andrieu et al., 2015; Zheng et al., 2016; Spain: Rodriguez-Lázaro et al., 1998; Stoll and Schrag, 2000; Portugal: Coimbra et al., 2016; Italy: Stoll and Schrag, 2000; Gambacorta et al., 2015; Batenburg et al., 2016; Germany: Gale, 1995; Wilmsen, 2007; Janetschke et al., 2015; Oman: Wohlwend et al., 2015), organic carbon-rich mudrock successions (e.g., Morocco: Gertsch et al., 2010; North Atlantic: Friedrich et al., 2008; Ando et al., 2009; North America: Schröder-Adams et al., 1996; Gale et al., 2008; Joo and Sageman, 2014; Eldrett et al., 2015a; Phelps et al., 2015; Peru: Navarro-Ramirez et al., 2016), and also in terrestrial successions (e.g., Japan: Uramoto et al., 2007).

However, MCE I is not characterised by widespread black shale deposition (Jenkyns et al., 1994; Friedrich et al., 2009), despite being marked by positive CIEs, and is thus not considered a global OAE. However, although not global in distribution, organic-rich mud rocks with high total organic carbon (TOC) contents spanning, but not restricted to, this interval *have* been recovered from the North Atlantic (e.g., Blake Nose: Ando et al., 2009; Demerara Rise: Friedrich et al., 2008) and from the WIS (e.g., Texas: Eldrett et al., 2015a; Colorado: Joo and Sageman, 2014; Canada: Schröder-Adams et al., 1996), indicating that anoxic conditions did manifest in these regions (Friedrich et al., 2009; Hardas et al., 2012; Eldrett et al., 2017).

Conditions during MCE I have been associated with dysaerobic bottom waters at some sites (e.g., Europe: Mitchell and Carr, 1998; Rodriguez-Lázaro et al., 1998; Coccioni and Galeotti, 2003; Tropical North Atlantic: Friedrich et al., 2009; Hardas et al., 2012; WIS: Eldrett et al., 2017), and oligotrophic surface waters in some regions where there was limited productivity (e.g., Demerara Rise: Hardas et al., 2012; France: Giraud et al., 2013). A number of ecological studies have determined MCE I marked the beginning of a ~2 Myr interval leading to OAE 2 that was

characterised by stepwise extinctions and extreme biotic turnovers of benthic and planktic foraminifera, dinoflagellates, bivalves, ammonites and belemnites, with up to 26% of all radiolarian species becoming extinct during the event (Paul et al., 1994; Erbacher and Thurow, 1997; Mitchell and Carr, 1998; Coccioni and Galeotti, 2003; Wilmsen, 2003; Friedrich et al., 2009). Conversely, some European sites (e.g., Anglo-Paris basin, Basque basin) show no discernible changes in planktic or benthic foraminiferal assemblages, indicating conditions remained stable across MCE I (Paul et al., 1994; Rodriguez-Lázaro et al., 1998). Furthermore, other European sites (e.g., the Umbria Marche Basin, and in northern Germany) show elevated productivity from the onset of, or during MCE I (Stoll and Schrag, 2001; Coccioni and Galeotti, 2003; Wilmsen, 2003). With such variation in the expression of MCE I at different locations, it is evident that local environmental conditions were driven by global, regional, and local oceanographic and climatic forces.

The European sections show distinct lithological changes have been identified during the onset of MCE I, such as inclusions of dark grey-black chert in white limestones in the Italian Umbria Marche Basin (Coccioni and Galeotti, 2003; Gambacorta et al., 2015). In the same region, sedimentological evidence demonstrates that pronounced increases in bottom current activity coincided with the onset of MCE I (Gambacorta et al., 2016). This has been attributed to the formation of high-salinity, dense intermediate and deep waters (Gambacorta et al., 2016), which may have developed during arid climatic conditions across MCE 1a (Giraud et al., 2013) as this could have led to enhanced evaporation of surface waters, thus increasing salinity contents and creating highly stratified waters (Mitchell and Carr, 1998; Gambacorta et al., 2015).

High-resolution benthic foraminiferal $\delta^{18}O$ records from the Demerara Rise suggest extremely warm bottom waters prior to MCE I may have weakened the thermal stratification of the water column. This would have induced stronger vertical mixing and subsequently enhanced nutrient availability to the upper photic zone (Friedrich et al., 2008). During MCE I, however, a greater abundance of oligotrophic surface-dwelling calcareous nannoplankton (e.g., *Prediscosphaera cretacea*), and a proliferation of deeper-dwelling taxa (e.g., *Eprolithus florali*) suggest the nutricline deepened and the water column became stratified (Hardas et al., 2012). Furthermore, high-salinity, dense intermediate waters were present at the Demerara Rise, where benthic foraminiferal assemblages of decreasing diversity and abundances from the onset of the MCE have been attributed to limited nutrient availability as water-column stratification intensified (Friedrich et al., 2008, 2009). This intensified stratification has been linked to incursions of highly saline epicontinental waters into the Tethys, forming intermediate to deep waters that led to the creation of a distinctive halocline (Friedrich et al., 2009), reflecting similar conditions to those in southern Europe at the same time (Gambacorta et al., 2015, 2016).

In a similar manner to those reported for OAE 2, incursions of northerly Boreal water masses southwards into European MCE I successions have also been documented. For MCE I, these have been demonstrated by the appearance of benthic Boreal faunas coincident with the MCE 1a and

MCE 1b CIE maxima (Paul et al., 1994; Gale, 1995), positive neodymium isotope (ε_{Nd}) excursions just prior to the CIE maxima (Zheng et al., 2016), and a 2-3°C cooling event recorded across MCE I from brachiopod $\delta^{18}O$ records (Voigt et al., 2004). Originally, these incursions were attributed to relatively rapid glacioeustatic sea level changes (Stoll and Schrag, 2000; Miller et al., 2003, 2005; Gale et al., 2008), however, consistent planktic $\delta^{18}O$ values across the Cenomanian from the North Atlantic argue against a glaciation event during this interval (Moriya et al., 2007). Concomitant fluctuating benthic foraminiferal $\delta^{18}O$ records indicate changes to deep water circulation (Moriya et al., 2007; Ando et al., 2009) were driven by climatic variability rather than glacioeustasy (Zheng et al., 2016). This being said, sea-level fluctuation cannot be ruled out as a major driver of environmental change as a mid-Cenomanian eustatic low is recorded through observations of winnowed micro-wackestones and mass-flow deposits in chalk successions in European sections (Wilmsen, 2003; Hancock, 2004). The earliest section of the mid-Cenomaninan *Turrilites costatus* biozone is also missing in many European sites, sometimes extending down into the earliest mid-Cenomanian *Cunningtoniceras inerme* biozone (Hancock, 2004). The occurrence of the mid-Cenomanian skeletal Thatcher Limestone bed in the WIS reflects a carbonate bed that promoted carbonate productivity in shallow waters (<100 meters), and the identification of *Ostrea beloiti* fossils suggest water depths may have been as shallow as 15 meters (Kauffman et al., 1977). Together, these records demonstrate the mid-Cenomanian eustatic low likely persisted on a global scale.

The foregoing discussion demonstrates that MCE I was a complex, dynamic climatic event. Although it shows some similarities to OAE 2, it did not develop in entirely similar environmental conditions, and the underlying driving forces behind MCE I are thus far unresolved. To date, most studies of MCE I have been in carbonate-rich sequences from European localities, and whilst more recently, some analyses of organic-rich sediments been published, most of these records focus on single-proxy data (e.g., Friedrich et al., 2009; Hardas et al., 2012) or are of low resolution (e.g., Eldrett et al., 2017), and thus cannot provide a complete understanding of MCE I at these sites.

1.5 Aims and objectives

MCE I has been identified in organic-rich mudrocks of the central WIS (Joo and Sageman, 2014) but has yet to be studied in high resolution (Eldrett et al., 2017). Studying this event in the WIS will permit better constraint of the environmental, climatic, and oceanographic evolution of MCE I in a region that is yet to be investigated in great detail. Therefore, the key objectives of this research are:

1. To develop a high-resolution, multi-proxy framework for MCE I by integrating organic and inorganic datasets obtained from sedimentological, geochemical, and palynological analyses of organic-rich sediments from the Amoco Rebecca K Bounds-1 core, Kansas;

2. To further our understanding of the driving forces behind MCE I by exploring environmental changes;
3. To evaluate longer-term oceanographic changes across Cenomanian WIS by creating a multiproxy environmental dataset from the central-eastern Kansas site and integrating this information with that from other sites across the seaway.

In order to achieve these goals, three individual, thematic scientific investigations have been completed, written in a format suitable for submission as journal publications, and are reported in the following chapters:

- Chapter 2: Tethyan water mass incursions and orbital control of productivity in the Cenomanian Western Interior Seaway
- Chapter 3: Oceanographic and environmental influence on the Mid-Cenomanian Event in the Western Interior Seaway of North America
- Chapter 4: Environmental evolution of the central-eastern margin of the Cenomanian Western Interior Seaway

1.6 Geological setting

The WIS extended from the Tethys Ocean (the present day Gulf of Mexico) northwards to the Boreal Sea (present-day Arctic Ocean), covering much of what is today mid-western North America to form one of the largest epicontinental seaways of the Late Cretaceous during maximum sea-level highstand (Kauffman, 1977; Nicholls & Russell, 1990; Fig. 1.5). Consisting of a north-south orientated retroarc foreland basin, it was enclosed to the west by the Sevier Orogenic Belt, which formed from the Late Jurassic through to the Late Cretaceous and was associated with numerous volcanic centres and intrusive igneous bodies (Armstrong, 1968; Kauffman and Caldwell, 1993). Continued Cretaceous thrusting caused prolonged subsidence on the western WIS margin, and accelerated uplift and subsequent deposition of sediment from the orogenic belt led to further subsidence on the western side of the basin (Jordan, 1981; Wright, 1987). Conversely, a much more stable cratonic platform developed on the eastern side. Thus the basin was asymmetric, with the western side being much deeper and consisting of a thicker sediment fill than the eastern margin (Kauffman 1985).

The first stage in the development of the Cretaceous WIS took place during the Aptian, when Boreal waters flooded southwards forming the main northern arm of the seaway (McGookey et al., 1972). During the mid-Albian, Tethyan waters transgressed northward into the basin, forming a fully connected North-South seaway (Kauffman, 1977). After a short regressive pulse which produced an east-west land bridge, the northern and southern arms of the seaway reconnected in the early/mid-Cenomanian and remained a continuous seaway for ~35 Myr (Fig. 1.5). During the mid-Cretaceous, the third-order Greenhorn transgressive cycle, related to intensified sea-floor spreading

and associated oceanic crust production and subsequent global sea-level rises, records a change from siliclastic to carbonate facies, and the highest sea levels in the centre of the basin being coincident with OAE 2 (Kauffman, 1977). A number of fourth-order cycles have also been recorded in various parts of the basin, but are thought to be primarily the product of regional climatic influences and to a lesser extent "local" tectonic events (Elderbak et al., 2014).

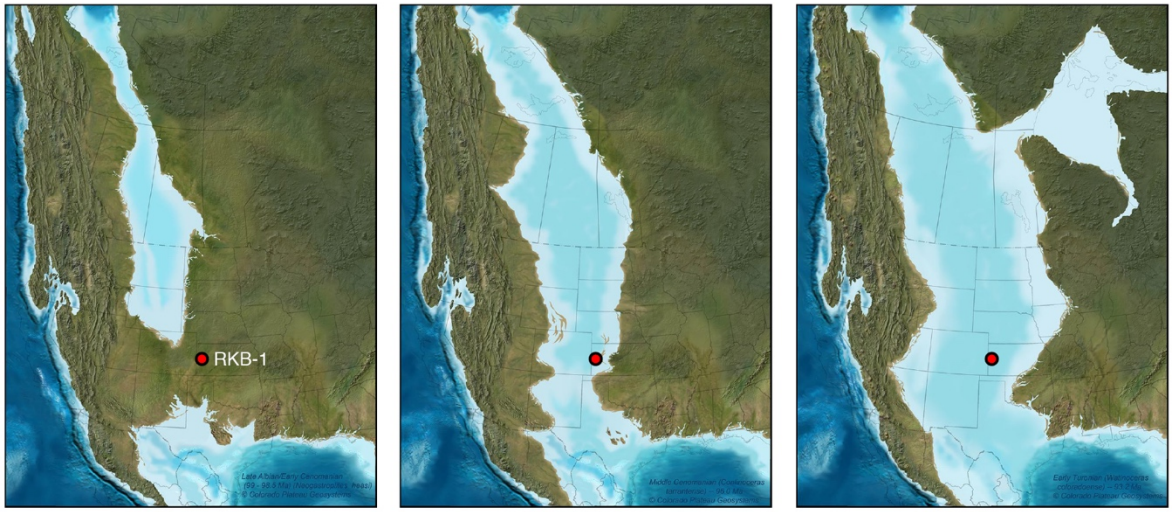

Figure 1.6: Palaeogeographic reconstructions of the mid-Cretaceous WIS showing the location of the Rebecca K Bounds-1 core (red circle). Adapted from Blakey (2014).

Intense volcanic activity resulted in the formation of over six hundred volcanic ash layers (bentonites) during the evolution of the WIS, which provide excellent geochronological reference points and have been used for stratigraphic correlation (e.g., Kauffman, 1977; Meyers et al., 2012b; Eldrett et al., 2015a). Furthermore, high-resolution ammonite, inoceramid, and foraminiferal biostratigraphic frameworks have been created to further constrain basin-wide correlations from the mid-Cenomanian onwards (e.g., Cobban and Scott, 1972; Cobban, 1984; Cobban and McKinney, 2007).

1.7 Study material

The Rebecca K Bounds-1 (RKB-1) core from western Kansas was drilled by the Amoco Production Company in 1988 with >90 % recovery, and spans from the Albian to the Santonian (Dean et al., 1995). The interval studied in this report extends from the Albian/Cenomanian boundary to Cenomanian-Turonian boundary, and consists of three formations: the Dakota Formation, the Graneros Shale, and the Greenhorn Formation, and members within each formation have been lithostratigraphically correlated to those found in Colorado (Dean et al., 1995; Scott et al., 1998).

The Dakota Formation contains the Cenomanian "upper" Dakota Sandstone, which was deposited in a delta plain/estuarine palaeoenvironment (Hattin et al., 1987; Roberts and Kirschbaum, 1995). The Graneros Shale Formation consists of the Lower Graneros Shale, the Thatcher Limestone, and the Upper Graneros Shale members.

The Lower Graneros Shale Member is chiefly composed of marine mudstones and is devoid of any macrofossils, and only scarce microfauna in the form of benthic foraminifera have been reported (Eicher, 1965). The Thatcher Limestone Member is a skeletal limestone package, formed by a process of storm winnowing during sea-level fall, and condensation due to starvation during the subsequent sea level rise (Sageman, 1996). As such, this tempestite member can be considered as a marker for a sea level lowstand and/or a deposit of early transgression, and marks the point when the Boreal influenced WIS re-established connection with southern Tethyan waters (Kauffman, 1986; Gale et al., 2008). From this point, younger sediments show substantially increased abundances and diversities of molluscan macrofauna and foraminifera throughout the basin (Cobban and Scott, 1972; Kauffman, 1988; Hook and Cobban, 2007). The Upper Graneros Shale contains numerous calcareous fossils, both microscopic and macroscopic, the latter in the form of bivalve shells, suggesting these were deposited under more oxygenated conditions than the Lower Graneros Shale (Cobban & Scott, 1976). A number of volcanic ash beds are present in the Graneros Shale, with the most prominent the "x-bentonite" in the Upper Graneros Shale Member, which has been used for stratigraphic and geochronologic age calibration across the WIS (Obradovich, 1993; Gale et al., 2008). The x-bentonite has been identified in the RKB-1 core at ~318 m, and an Ar/Ar date of 95.53 ± 0.159 Ma has been given for this bentonite close to the core in an outcrop in Russell County, Kansas (Miggins, 2004). This date is within error of the first date from the x-bentonite in Wyoming, at 94.93 ± 0.53 Ma (Obradovich, 1993) and the most recently obtained age for the same ash bed obtained from Texas (95.80 ± 0.092; Eldrett et al., 2015a).

The Greenhorn Formation records a distinct shift from mudrocks to carbonate-rich marlstones and limestone in the mid to late Cenomanian (Cobban and Scott, 1972; Kauffman, 1977). In Colorado, the base of the Lincoln Limestone Member directly overlays the x-bentonite. However, in the RKB-1 core, the Upper Graneros Shale extends above the x-bentonite, and then transitions into the Lincoln Limestone. Highly bioturbated strata across the Greenhorn Formation indicate ventilated bottom waters prevailed. However, high total organic carbon contents (Joo and Sageman, 2014) and high abundances of prasinophyte phycomata in the Coloradan Lincoln Limestone and Hartland Shale members indicate the water column was stratified and environmental conditions permitted the preservation of organic-rich sediments (Eldrett et al., 2017), thus demonstrating a complex, dynamic oceanographic regime prevailed (Sageman, 1985, 1989). In RKB-1, all members of the Greenhorn Formation contain numerous volcanic ash horizons, demonstrating volcanic activity was persistent throughout this section of the core. In the Bridge Creek Limestone Member, a prominent positive bulk organic CIE (Dean et al., 1995) has been identified as OAE 2 by using the occurrence

of three basin-wide bentonites (the "A-bentonite", "B-bentonite", and "C-bentonite"; Elder, 1985; Dean et al., 1995) as temporal constraints, as they have been identified within strata that contain the OAE 2 CIE elsewhere in the basin (e.g., Sageman et al., 1998; Eldrett et al., 2015a).

1.8 MCE I in the WIS

A "Mid-Cenomanian Event" was first identified from a positive $\delta^{13}C_{carb}$ excursion in the Hartland Shale Member in a study from Pueblo, Colorado (the Global Boundary Stratotype Section and Point for the Cenomanian/Turonian Boundary), and was assigned an age of 95.80 - 95.71 Myr, based on extrapolated sedimentation rates downwards from OAE 2 (Keller and Pardo, 2004). However, more recent studies from successions in Texas, Colorado, and Alberta suggest the MCE is recorded in older sedimentary units, such as in the Lower Eagle Ford Shale, the Graneros Shale, and the Belle Fourche Member, respectively (Schröder-Adams et al., 2012; Joo and Sageman, 2014; Eldrett et al., 2015a). Within all of these successions, the MCE I CIE correlates with that in the English Chalk Reference Curve (Jarvis et al., 2006), which dates the commencement of the event to slightly prior to 96.14 Ma, or at least ~340-430 kyr before the level suggested by Keller and Pardo (2004). The Coloradan isotope curve and the English Chalk Reference Curve have been correlated to the newly established astronomically calibrated age model for the mid-Cretaceous WIS, indicating all of these signals represent the same climatic event (Eldrett et al., 2015a). Calculated commencement and termination dates of 96.57 Ma to 96.36 Ma , respectively (Eldrett et al., 2015a), confirm the identification of MCE I by Keller & Pardo (2004) is incorrect. It is possible that the "MCE" identified by Keller and Pardo (2004) is the later, secondary Mid Cenomanian Event (MCE II), which occurred after the MCE, but prior to OAE2 (Melinte-Dobrinescu and Bojar, 2008). Thus, this study takes the stratigraphic position of MCE I as that according to Joo & Sageman (2014) and Eldrett et al. (2015a).

1.9 References

Ando, A., Huber, B.T., MacLeod, K.G., Ohta, T., Khim, B.K., 2009. Blake Nose stable isotopic evidence against the mid-Cenomanian glaciation hypothesis. Geology 37, 451–454. doi:10.1130/G25580A.1

Andrieu, S., Brigaud, B., Rabourg, T., Noret, A., 2015. The Mid-Cenomanian Event in shallow marine environments: Influence on carbonate producers and depositional sequences (northern Aquitaine Basin, France). Cretac. Res. 56, 587–607. doi:10.1016/j.cretres.2015.06.018

Armstrong, R., 1968. Sevier orogenic belt in Nevada and Utah. Geol. Soc. Am. Bull.

Arthur, M.A., Schlanger, S.O., Jenkyns, H.C., 1987. The Cenomanian-Turonian Oceanic Anoxic Event, II. Palaeoceanographic controls on organic-matter production and preservation. Geol.

Soc. London, Spec. Publ. 26, 401–420. doi:10.1144/GSL.SP.1987.026.01.25

Batenburg, S.J., Vleeschouwer, D. De, Sprovieri, M., Hilgen, F.J., Gale, A.S., Singer, B.S., Koeberl, C., Coccioni, R., Claeys, P., Montanari, A., 2016. Orbital control on the timing of oceanic anoxia in the Late Cretaceous. Climate of the Past. doi:10.5194/cp-2015-182

Beerling, D.J., Fox, A., Stevenson, D.S., Valdes, P.J., 2011. Enhanced chemistry-climate feedbacks in past greenhouse worlds. Proc. Natl. Acad. Sci. 108, 9770–9775.

Berger, A., Loutre, M.-F., Laskar, J., 1992. Stability of the astronomical frequencies over the Earth's history for paleoclimate studies. Science 255, 560-566.

Berner, R.A., 2006. GEOCARBSULF: a combined model for Phanerozoic atmospheric O_2 and CO_2. Geochim. Cosmochim. Acta 70, 5653–5664.

Blakey, R.C., 2014. Paleogeography and Paleotectonics of the Western Interior Seaway, Jurassic-Cretaceous of North America. AAPG Search Discov. Artic. 30392, 1–72.

Calvert, S., Pedersen, T., 1993. Geochemistry of recent oxic and anoxic marine sediments: implications for the geological record. Mar. Geol. 113, 67-88.

Clarke, L.J., Jenkyns, H.C., 1999. New oxygen isotope evidence for long-term Cretaceous climatic change in the Southern Hemisphere. Geology 27, 699–702.

Cobban, W.A., 1984. Mid-Cretaceous ammonite zones , Western Interior , United States. Bull. Geol. Soc. Denmark 33, 71–89.

Cobban, W.A., McKinney, K.C., 2007. A USGS Zonal Table for the Upper Cretaceous Middle Cenomanian−Maastrichtian of the Western Interior of the United States Based on Ammonites, Inoceramids, and Radiometric Ages. U.S. Geological Survey Open-File Report 2006-1250, 45.

Cobban, W.A., Scott, G.R., 1972. Stratigraphy and Ammonite Fauna of the Graneros Shale and Greenhorn Limestone Near Pueblo , Colorado Stratigraphy and Ammonite Fauna of the Graneros Shale and Greenhorn Limestone Near Pueblo, Colorado. Geol. Surv. Prof. Pap. 645, 1–195.

Coccioni, R., Galeotti, S., 2003. The mid-Cenomanian Event: Prelude to OAE 2. Palaeogeography, Palaeoclimatology, Palaeoecology. 190, 427–440. doi:10.1016/S0031-0182(02)00617-X

Coimbra, R., Azerêdo, A.C., Cabral, M.C., Immenhauser, A., 2016. Palaeoenvironmental analysis of mid-Cretaceous coastal lagoonal deposits (Lusitanian Basin, W Portugal). Palaeogeogr. Palaeoclimatol. Palaeoecol. 446, 308–325.

Dean, W.E., Arthur, M.A., Sageman, B.B., Lewan, M.D., 1995. Core descriptions and preliminary geochemical data for the Amoco Production Company Rebecca K. Bounds# 1 well, Greeley County, Kansas. US Geological Survey.

Eicher, D.L., 1965. Foraminifera and biostratigraphy of the Graneros Shale. J. Paleontol. 39, 875–909.

Elder, W.P., 1985. Biotic patterns across the Cenomanian-Turonian extinction boundary near Pueblo, Colorado, in: Pratt, L.M., Kauffman, E.G., Zelt, F.B. (Eds.), Field Trip Guidebook No. 4, 157e169. Special Publications of SEPM.

Elderbak, K., Leckie, R.M., 2016. Paleocirculation and foraminiferal assemblages of the Cenomanian-Turonian Bridge Creek Limestone bedding couplets: Productivity vs. dilution during OAE2. Cretac. Res. 60, 52–77. doi:10.1016/j.cretres.2015.11.009

Elderbak, K., Leckie, R.M., Tibert, N.E., 2014. Paleoenvironmental and paleoceanographic changes across the Cenomanian-Turonian Boundary Event (Oceanic Anoxic Event 2) as indicated by foraminiferal assemblages from the eastern margin of the Cretaceous Western Interior Sea. Palaeogeogr. Palaeoclimatol. Palaeoecol. 413, 29–48. doi:10.1016/j.palaeo.2014.07.002

Eldrett, J.S., Dodsworth, P., Bergman, S.C., Wright, M., Minisini, D., 2017. Water-mass evolution in the Cretaceous Western Interior Seaway of North America and equatorial Atlantic. Clim. Past 13, 1–34. doi:https://doi.org/10.5194/cp-13-1-2017

Eldrett, J.S., Ma, C., Bergman, S.C., Lutz, B., Gregory, F.J., Dodsworth, P., Phipps, M., Hardas, P., Minisini, D., Ozkan, A., Ramezani, J., Bowring, S.A., Kamo, S.L., Ferguson, K., Macaulay, C., Kelly, A.E., 2015a. An astronomically calibrated stratigraphy of the Cenomanian, Turonian and earliest Coniacian from the Cretaceous Western Interior Seaway, USA: Implications for global chronostratigraphy. Cretac. Res. 56, 316–344. doi:10.1016/j.cretres.2015.04.010

Eldrett, J.S., Ma, C., Bergman, S.C., Ozkan, A., Minisini, D., Lutz, B., Jackett, S-J., Macaulay, C., Kelly, A.E., 2015b. Origin of limestone-marlstone cycles: Astronomic forcing of organic-rich sedimentary rocks from the Cenomanian to early Coniacian of the Cretaceous Western Interior Seaway, USA. Earth Planet. Sci. Lett. 423, 98–113. doi:10.1016/j.epsl.2015.04.026

Erbacher, J., Thurow, J., 1997. Influence of oceanic anoxic events on the evolution of mid-Cretaceous radiolaria in the North Atlantic and western Tethys. Mar. Micropaleontol.

Ernst, G., Schmid, F., Seibertz, E., Wood, C., 1983. Event-stratigraphie im Cenoman und Turon von NW-Deutschland. Zitteliana.

Farquhar, G.D., Ehleringer, J.R., Hubick, K.T., 1989. Carbon isotope discrimination and photosynthesis. Annu. Rev. Plant Biol. 40, 503–537.

Forster, A., Schouten, S., Baas, M., Sinninghe Damsté, J.S., 2007a. Mid-Cretaceous (Albian-Santonian) sea surface temperature record of the tropical Atlantic Ocean. Geology 35, 919–922. doi:10.1130/G23874A.1

Forster, A., Schouten, S., Moriya, K., Wilson, P.A., Damsté, J.S.S., 2007b. Tropical warming and intermittent cooling during the Cenomanian/Turonian oceanic anoxic event 2: Sea surface temperature records from the equatorial Atlantic. Paleoceanography 22, 1–14. doi:10.1029/2006PA001349

Friedrich, O., Erbacher, J., Moriya, K., Wilson, P.A., Kuhnert, H., 2008. Warm saline intermediate waters in the Cretaceous tropical Atlantic Ocean. Nat. Geosci. 1, 453–457. doi:10.1038/ngeo217

Friedrich, O., Erbacher, J., Mutterlose, J., 2006. Paleoenvironmental changes across the Cenomanian/Turonian Boundary Event (Oceanic Anoxic Event 2) as indicated by benthic foraminifera from the Demerara Rise (ODP Leg 207). Rev. Micropaleontol. 49, 121–139. doi:10.1016/j.revmic.2006.04.003

Friedrich, O., Erbacher, J., Wilson, P.A., Moriya, K., Mutterlose, J.J., 2009. Paleoenvironmental changes across the Mid Cenomanian Event in the tropical Atlantic Ocean (Demerara Rise, ODP Leg 207) inferred from benthic foraminiferal assemblages. Mar. Micropaleontol. 71, 28–40. doi:10.1016/j.marmicro.2009.01.002

Friedrich, O., Norris, R.D., Erbacher, J., 2012. Evolution of middle to Late Cretaceous oceans-A 55 m.y. Record of Earth's temperature and carbon cycle. Geology 40, 107–110. doi:10.1130/G32701.1

Gale, A.S., 1995. Cyclostratigraphy and correlation of the Cenomanian Stage in Western Europe. Orbital Forcing Timescales and Cyclostratigraphy 85, 177–197. doi:10.1144/GSL.SP.1995.085.01.11

Gale, A.S., Christensen, W.K., 1996. Occurrence of the belemnite *Actinocamax plenus* in the Cenomanian of SE France and its significance. Bull. Geol. Soc. Denmark. 43, 68-77.

Gale, A.S., Voigt, S., Sageman, B.B., Kennedy, W.J., 2008. Eustatic sea-level record for the Cenomanian (Late Cretaceous) - Extension to the Western Interior Basin, USA. Geology 36, 859–862. doi:10.1130/G24838A.1

Gambacorta, G., Bersezio, R., Erba, E., 2014. Sedimentation in the Tethyan pelagic realm during the Cenomanian: Monotonous settling or active redistribution? Palaeogeogr. Palaeoclimatol.

Palaeoecol. 409, 301–319. doi:10.1016/j.palaeo.2014.05.011

Gambacorta, G., Bersezio, R., Weissert, H., Erba, E., 2016. Onset and demise of Cretaceous Oceanic Anoxic Events: the coupling of surface and bottom oceanic processes in two pelagic basins of the western Tethys. Paleoceanography 732–757. doi:10.1002/2015PA002922

Gambacorta, G., Jenkyns, H.C., Russo, F., Tsikos, H., Wilson, P.A., Faucher, G., Erba, E., 2015. Carbon- and oxygen-isotope records of mid-Cretaceous Tethyan pelagic sequences from the Umbria-Marche and Belluno Basins (Italy). Newsletters Stratigr. 48, 299–323. doi:10.1127/nos/2015/0066

Gertsch, B., Adatte, T., Keller, G., Tantawy, A.A.A.M., Berner, Z., Mort, H.P., Fleitmann, D., 2010. Middle and late Cenomanian oceanic anoxic events in shallow and deeper shelf environments of western Morocco. Sedimentology 57, 1430–1462. doi:10.1111/j.1365-3091.2010.01151.x

Giraud, F., Reboulet, S., Deconinck, J.F., Martinez, M., Carpentier, A., Bréziat, C., 2013. The Mid-cenomanian event in southeastern france: Evidence from palaeontological and clay mineralogical data. Cretac. Res. 46, 43–58. doi:10.1016/j.cretres.2013.09.004

Glancy, T.J., Arthur, M.A., Barron, E.J., Kauffman, E.G., 1993. A paleoclimate model for the North American Cretaceous (Cenomanian- Turonian) epicontinental sea. Geol. Assoc. Canada Spec. Pap. 39, 219–241.

Hancock, J., 2004. The mid-Cenomanian eustatic low. Acta Geologica Polonica, 54, 611-627.

Haq, B.U., 2014. Cretaceous eustasy revisited. Glob. Planet. Change 113, 44–58. doi:10.1016/j.gloplacha.2013.12.007

Hardas, P., Mutterlose, J., Friedrich, O., Erbacher, J., 2012. The Mid Cenomanian Event in the equatorial Atlantic: The calcareous nannofossil and benthic foraminiferal response. Mar. Micropaleontol. 96–97, 66–74. doi:10.1016/j.marmicro.2012.08.003

Hattin, D.E., Siemers, C.T., Stewart, G.F., 1987. Upper Cretaceous stratigraphy and depositional environments of western Kansas. Guidebook. Kansas Geol. Surv. 3, 1–30.

Hay, W.W., Floegel, S., 2012. New thoughts about the Cretaceous climate and oceans. Earth-Science Rev. 115, 262–272. doi:10.1016/j.earscirev.2012.09.008

Hong, S.K., Lee, Y. Il, 2012. Evaluation of atmospheric carbon dioxide concentrations during the Cretaceous. Earth Planet. Sci. Lett. 327–328, 23–28. doi:10.1016/j.epsl.2012.01.014

Hook, S.C., Cobban, W.A., 2007. A condensed middle Cenomanian succession in the Dakota Sandstone (Upper Cretaceous), Sevilleta National Wildlife Refuge, Socorro County , New

Mexico. New Mex. Geol. 29, 75–99.

Huber, B.T., Norris, R.D., MacLeod, K.G., 2002. Deep-sea paleotemperature record of extreme warmth during the Cretaceous. Geology 30, 123–126.

Janetschke, N., Niebuhr, B., Wilmsen, M., 2015. Inter-regional sequence-stratigraphical synthesis of the Plänerkalk, Elbtal and Danubian Cretaceous groups (Germany): Cenomanian-Turonian correlations around the Mid-European Island. Cretac. Res. 56, 530–549. doi:https://doi.org/10.1016/j.cretres.2015.04.007

Jarvis, I., Gale, A.S., Jenkyns, H.C., Pearce, M.A., 2006. Secular variation in Late Cretaceous carbon isotopes: a new delta C-13 carbonate reference curve for the Cenomanian-Campanian (99.6-70.6 Ma). Geol. Mag. 143, 561–608. doi:10.1017/S0016756806002421

Jarvis, I., Lignum, J.S., Gröcke, D.R., Jenkyns, H.C., Pearce, M.A., 2011. Black shale deposition, atmospheric CO_2 drawdown, and cooling during the Cenomanian-Turonian Oceanic Anoxic Event. Paleoceanography 26, 1–17. doi:10.1029/2010PA002081

Jenkyns, H.C., Clayton, C.J., 1986. Black shales and carbon isotopes in pelagic sediments from the Tethyan Lower Jurassic. Sedimentology 33, 87–106.

Jenkyns, H.C., Gale, A. S., Corfield, R.M., 1994. Carbon- and oxygen-isotope stratigraphy of the English Chalk and Italian Scaglia and its palaeoclimatic significance. Geol. Mag. 131, 1. doi:10.1017/S0016756800010451

Joo, Y.J.I., Sageman, B.B., 2014. Cenomanian to Campanian carbon isotope chemostratigraphy from the Western Interior Basin, USA. J. Sediment. Res. 84, 529–542. doi:dx.doi.org/10.2110/jsr.2014.38

Jordan, T., 1981. Thrust loads and foreland basin evolution, Cretaceous, western United States. Am. Assoc. Pet. Geol. Bull. 65, 2506-2520.

Kauffman, E., 1977. Geological and biological overview: Western Interior Cretaceous basin. Mt. Geol. 14, 75-99.

Kauffman, E.G., 1985. Paleobiogeography and evolutionary response dynamic in the Cretaceous Western Interior Seaway of North America, in: Jurassic-Cretaceous Biochronology and Paleogeography of North America. Geol. Assoc. Can. Sp. Pap, pp. 273–306.

Kauffman, E. G., 1986. High-resolution event stratigraphy: Regional and Global Cretaceous Bio-events, In: O. Walliser, ed., Global Bio-Events, Lecture Notes in Earth History, v. 8, Springer, Berlin, p. 279-335.

Kauffman, E.G., 1988. Concepts and methods of high-resolution event stratigraphy. Annu. Rev.

Earth Planet. Sci. 16, 605.

Kauffman, E.G., Caldwell, W.G.E., 1993. The Western Interior Basin in space and time. Evol. West. Inter. Basin Geol. Assoc. Canada, Spec. Pap. 39, 1–30.

Keller, G., Pardo, A., 2004. Age and paleoenvironment of the Cenomanian-Turonian global stratotype section and point at Pueblo, Colorado. Mar. Micropaleontol. 51, 95–128. doi:10.1016/j.marmicro.2003.08.004

Kuiper, K.F., Deino, A., Hilgen, F.J., Krijgsman, W., Renne, P.R., Wijbrans, J.R., 2008. Synchronizing Rock Clocks of Earth History. Science. 320, 500–504. doi:10.1126/science.1154339

Kump, L.R., Pavlov, A., Arthur, M.A., 2005. Massive release of hydrogen sulfide to the surface ocean and atmosphere during intervals of oceanic anoxia. Geology 33, 397–400. doi:10.1130/G21295.1

Larson, R.L., 1991. Latest pulse of Earth: Evidence for a mid-Cretaceous superplume. Geology 19, 547–550.

Laskar, J., Fienga, A., Gastineau, M., Manche, H., 2011. La2010: A new orbital solution for the long term motion of the Earth. Astron. Astrophys. 4, 17. doi:10.1051/0004-6361/201116836

Laskar, J., Robutel, P., Joutel, F., Gastineau, M., Correia, a. C.M., Levrard, B., 2004. A long-term numerical solution for the insolation quantities of the Earth. Astron. Astrophys. 428, 261–285. doi:10.1051/0004-6361:20041335

Laurin, J., Meyers, S.R., Uličný, D., Jarvis, I., Sageman, B.B., 2015. Axial obliquity control on the greenhouse carbon budget through middle- to high-latitude reservoirs. Paleoceanography 30, 133–149. doi:10.1002/2014PA002736

Ma, C., Meyers, S.R., Sageman, B.B., 2017. Theory of chaotic orbital variations confirmed by Cretaceous geological evidence. Nature 542, 468–470. doi:10.1038/nature21402

McGookey, D.P., Haun, J.D., Hale, L.A., Goodell, H.G., McCubbin, D.G., Weimer, R., Wulf, G.R., 1972. Cretaceous system. *in* Geologic atlas of the Rocky Mountain region: Denver, Colorado. Rocky Mt. Assoc. Geol. 190–228.

Melinte-Dobrinescu, M.C., Bojar, A.-V., 2008. Biostratigraphic and isotopic record of the Cenomanian–Turonian deposits in the Ohaba-Ponor section (SW Haţeg, Romania). Cretac. Res. 29, 1024–1034.

Meyer, T., 1990. Biostratigraphische und sedimentologische Untersuchungen in der Plänerfazies des Cenoman von Nordwestdeutschland.

Meyers, S.R., Sageman, B.B., Arthur, M.A., 2012a. Obliquity forcing of organic matter accumulation during Oceanic Anoxic Event 2. Paleoceanography 27, 1–19. doi:10.1029/2012PA002286

Meyers, S.R., Siewert, S.E., Singer, B.S., Sageman, B.B., Condon, D.J., Obradovich, J.D., Jicha, B.R., Sawyer, D.A., 2012b. Intercalibration of radioisotopic and astrochronologic time scales for the Cenomanian-Turonian boundary interval, western interior Basin, USA. Geology 40, 7–10. doi:10.1130/G32261.1

Miggins, D., 2004. $^{40}Ar/^{39}Ar$ results for Cretaceous bentonite beds of Colorado and Kansas, Report provided to USD A Forest Service under intra-agency agreement.

Miller, K.G., Kominz, M.A., Browning, J. V, Wright, J.D., Mountain, G.S., Katz, M.E., Sugarman, P.J., Cramer, B.S., Christie-Blick, N., Pekar, S.F., 2005. The Phanerozoic Record of Global Sea-level Change. Science. 310, 1293–1298. doi:10.1126/science.1116412

Miller, K.G., Sugarman, P.J., Browning, J. V., Kominz, M.A., Hernàndez, J.C., Olsson, R.K., Wright, J.D., Feigenson, M.D., Van Sickel, W., 2003. Late Cretaceous chronology of large, rapid sea-level changes: Glacioeustasy during the greenhouse world. Geology 31, 585–588. doi:10.1130/0091-7613(2003)031<0585:LCCOLR>2.0.CO;2

Mitchell, R.N., Bice, D.M., Montanari, A., Cleaveland, L.C., Christianson, K.T., Coccioni, R., Hinnov, L.A., 2008. Oceanic anoxic cycles? Orbital prelude to the Bonarelli Level (OAE 2). Earth Planet. Sci. Lett. 267, 1–16. doi:10.1016/j.epsl.2007.11.026

Mitchell, S.F., 1996. Foraminiferal assemblages from the late Lower and Middle Cenomanian of Speeton (North Yorkshire, UK): relationships with sea-level fluctuations and watermass distribution. J. Micropalaeontology 15, 37–54.

Mitchell, S.F., Carr, I.T., 1998. Foraminiferal response to mid-Cenomanian (Upper Cretaceous) palaeoceanographic events in the Anglo-Paris Basin (Northwest Europe). Palaeogeogr. Palaeoclimatol. Palaeoecol. 137, 103–125. doi:http://dx.doi.org/10.1016/S0031-0182(97)00087-4

Moriya, K., Wilson, P.A., Friedrich, O., Erbacher, J., Kawahata, H., 2007. Testing for ice sheets during the mid-Cretaceous greenhouse using glassy foraminiferal calcite from the mid-Cenomanian tropics on Demerara Rise. Geology 35, 615–618. doi:10.1130/G23589A.1

Navarro-Ramirez, J.P., Bodin, S., Immenhauser, A., 2016. Ongoing Cenomanian-Turonian heterozoan carbonate production in the neritic settings of Peru. Sediment. Geol. 331, 78–93. doi:http://dx.doi.org/10.1016/j.sedgeo.2015.10.011

Nicholls, E.L., Russell, A.P., 1990. Paleobiogeography of the Cretaceous Western Interior Seaway

of North America: the vertebrate evidence. Palaeogeogr. Palaeoclimatol. Palaeoecol. 79, 149–169. doi:10.1016/0031-0182(90)90110-S

Norris, R.D., Bice, K.L., Magno, E.A., Wilson, P.A., 2002. Jiggling the tropical thermostat in the Cretaceous hothouse. Geology 30, 299–302.

Obradovich, J.D., 1993. A Cretaceous time scale. Evol. West. Inter. Basin 39, 379–396.

O'Brien, Charlotte L., Stuart A. Robinson, Richard D. Pancost, Jaap S. Sinninghe Damsté, Stefan Schouten, Daniel J. Lunt, Heiko Alsenz et al., 2017. Cretaceous sea-surface temperature evolution: Constraints from TEX_{86} and planktonic foraminiferal oxygen isotopes. Earth-Science Reviews 172, 224-247.

Pachauri, R.K., Allen, M.R., Barros, V.R., Broome, J., Cramer, W., Christ, R., Church, J.A., Clarke, L., Dahe, Q., Dasgupta, P., 2014. Climate change 2014: synthesis report. Contribution of Working Groups I, II and III to the fifth assessment report of the Intergovernmental Panel on Climate Change. IPCC.

Paul, C., Mitchell, S., Marshall, J., Leafy, P., 1994. Palaeoceanographic events in the Middle Cenomanian of Northwest Europe. Cretac. Res. 15, 707–738.

Pearce, M.A., Jarvis, I. and Tocher, B.A., 2009. The Cenomanian–Turonian boundary event, OAE2 and palaeoenvironmental change in epicontinental seas: New insights from the dinocyst and geochemical records. Palaeogeography, Palaeoclimatology, Palaeoecology 280, 207-234.

Phelps, R.M., Kerans, C., Da-Gama, R.O.B.P., Jeremiah, J., Hull, D., Loucks, R.G., 2015. Response and recovery of the Comanche carbonate platform surrounding multiple Cretaceous oceanic anoxic events, northern Gulf of Mexico. Cretac. Res. 54, 117–144. doi:10.1016/j.cretres.2014.09.002

Poulsen, C.J., Barron, E.J., Arthur, M.A., Peterson, W.H., 2001. Response of the mid-Cretaceous global oceanic circulation to tectonic and CO_2 forcings. Paleoceanography 16, 576–592. doi:10.1029/2000PA000579

Prauss, M.L., 2012. The Cenomanian/Turonian Boundary event (CTBE) at Tarfaya, Morocco: Palaeoecological aspects as reflected by marine palynology. Cretac. Res. 34, 233–256. doi:10.1016/j.cretres.2011.11.004

Pucéat, E., Lécuyer, C., Sheppard, S.M.F., Dromart, G., Reboulet, S., Grandjean, P., 2003. Thermal evolution of Cretaceous Tethyan marine waters inferred from oxygen isotope composition of fish tooth enamels. Paleoceanography. 18, 1-12.

Reboulet, S., Giraud, F., Colombié, C., Carpentier, A., 2013. Integrated stratigraphy of the Lower

and Middle Cenomanian in a Tethyan section (Blieux, southeast France) and correlations with Boreal basins. Cretac. Res. 40, 170–189. doi:10.1016/j.cretres.2012.06.006

Roberts, L.N., Kirschbaum, M.A., 1995. Paleogeography of the Late Cretaceous of the Western Interior of Middle North America - Coal Distribution and Sediment Accumulation, U.S. Geological Survey Professional paper 1561.

Rodriguez-Lázaro, J., Pascual, A., Elorza, J., 1998. Cenomanian events in the deep western Basque Basin: the Leioa section. Cretac. Res. 19, 673–700. doi:http://dx.doi.org/10.1006/cres.1998.0125

Sageman, B.B., 1985. High-resolution stratigraphy and paleobiology of the Hartland Shale Member: analysis of an oxygen-deficient epicontinental sea. *In*: Fine-grained deposits and biofaces of the Cretaceous Western Interior Seaway: Evidence of cyclic sedimentary processes, L. M. Pratt, E. G. Kauffman, F. B. Zelt, eds., Society of economic paleontologists and mineralogists, 2nd annual midyear meeting. Fieldtrip guidebook 4, 110-121.

Sageman, B. B., 1989. The benthic boundary biofacies model: Hartland Shale Member, Greenhorn Formation (Cenomanian), Western Interior, North America. Palaeogeography, Palaeoclimatology, Palaeoecology. 74, 87-110.

Sageman, B.B., 1996. Lowstand tempestites: Depositional model for Cretaceous skeletal limestones, Western Interior basin. Geology 24, 888–892. doi:10.1130/0091-7613(1996)024<0888:LTDMFC>2.3.CO;2

Sageman, B.B., Rich, J., Arthur, M.A., Dean, W.E., Savrda, C.E., Bralower, T.J., 1998. Multiple Milankovitch cycles in the Bridge Creek Limestone (Cenomanian-Turonian), Western Interior Basin. Stratigraphy and Paleoenvironments of the Cretaceous Western Interior Seaway, USA, *in* SEPM Concepts in Sedimentology and Paleontology. 6, 153-171.

Schlanger, S.O., Jenkyns, H.C., 1976. Cretaceous oceanic anoxic events: causes and consequences. Netherlands J. Geosci. en Mijnb. 55, 179–184.

Schröder-Adams, C., Herrle, J.O., Tu, Q., 2012. Albian to Santonian carbon isotope excursions and faunal extinctions in the Canadian Western Interior Sea: Recognition of eustatic sea-level controls on a forebulge setting. Sediment. Geol. 281, 50–58. doi:10.1016/j.sedgeo.2012.08.004

Schröder-Adams, C.J., Leckie, D.A., Bloch, J., Craig, J., Mcintyre, D.J., Adams, P.J., 1996. Paleoenvironmental changes in the Cretaceous (Albian to Turonian) Colorado Group of western Canada : microfossil , sedimentological and geochemical evidence. Cretac. Res. 17, 311–365. doi:10.1006/cres.1996.0022

Scotese, C., Gahagan, L., Larson, R., 1988. Plate tectonic reconstructions of the Cretaceous and Cenozoic ocean basins. Tectonophysics. 155, 27-48.

Scott, R.W., Franks, P.C., Evetts, M.J., Bergen, J.A., Stein, J.A., 1998. Timing of mid-Cretaceous relative sea level changes in the Western Interior: Amoco No. 1 Bounds Core, in: Stratigraphy and Paleoenvironments of the Cretaceous Western Interior Seaway, USA. Special Publications of SEPM, pp. 35–58.

Seton, M., Gaina, C., Müller, R.D., Heine, C., 2009. Mid-Cretaceous seafloor spreading pulse: Fact or fiction? Geology 37, 687–690.

Snow, L.J., Duncan, R.A., Bralower, T.J., 2005. Trace element abundances in the Rock Canyon Anticline, Pueblo, Colorado, marine sedimentary section and their relationship to Caribbean plateau construction and ocean anoxic event 2. Paleoceanography 20, 1–14. doi:10.1029/2004PA001093

Stoll, H.M., Schrag, D.P., 2001. Sr/Ca variations in Cretaceous carbonates: Relation to productivity and sea level changes. Palaeogeogr. Palaeoclimatol. Palaeoecol. 168, 311–336. doi:10.1016/S0031-0182(01)00205-X

Stoll, H.M., Schrag, D.P., 2000. High-resolution stable isotope records from the upper cretaceous rocks of Italy and Spain: Glacial episodes in a greenshouse planet? Bull. Geol. Soc. Am. 112, 308–319. doi:10.1130/0016-7606(2000)112<308:HSIRFT>2.0.CO;2

Tarduno, J.A., Brinkman, D.B., Renne, P.R., Cottrell, R.D., Scher, H., Castillo, P., 1998. Evidence for extreme climatic warmth from Late Cretaceous Arctic vertebrates. Science. 282, 2241–2243.

Trabucho Alexandre, J., Tuenter, E., Henstra, G.A., van der Zwan, K.J., van de Wal, R.S.W., Dijkstra, H.A., de Boer, P.L., 2010. The mid-Cretaceous North Atlantic nutrient trap: Black shales and OAEs. Paleoceanography 25.

Turgeon, S., Creaser, R., 2008. Cretaceous oceanic anoxic event 2 triggered by a massive magmatic episode. Nature 454, 323–326.

Uramoto, G.I., Fujita, T., Takahashi, A., Hirano, H., 2007. Cenomanian (Upper Cretaceous) carbon isotope stratigraphy of terrestrial organic matter for the Yezo Group, Hokkaido, Japan. Isl. Arc 16, 465–478. doi:10.1111/j.1440-1738.2007.00580.x

van Bentum, E.C., Hetzel, A., Brumsack, H.J., Forster, A., Reichart, G.J., Sinninghe Damsté, J.S., 2009. Reconstruction of water column anoxia in the equatorial Atlantic during the Cenomanian-Turonian oceanic anoxic event using biomarker and trace metal proxies. Palaeogeogr. Palaeoclimatol. Palaeoecol. 280, 489–498. doi:10.1016/j.palaeo.2009.07.003

van Bentum, E.C., Reichart, G.J., Forster, A., Sinninghe Damsté, J.S., 2012. Latitudinal differences in the amplitude of the OAE-2 carbon isotopic excursion: pCO_2 and paleo productivity. Biogeosciences 9, 717–731. doi:10.5194/bg-9-717-2012

van Helmond, N.A.G.M., Sluijs, A., Papadomanolaki, N.M., Plint, A.G., Gröcke, D.R., Pearce, M.A., Eldrett, J.S., Trabucho-Alexandre, J., Walaszczyk, I., van De Schootbrugge, B., Brinkhuis, H., 2016. Equatorward phytoplankton migration during a cold spell within the Late Cretaceous super-greenhouse. Biogeosciences 13, 2859. doi:10.5194/bg-13-2859-2016

van Helmond, N.A.G.M., Sluijs, A., Reichart, G.-J., Sinninghe Damste, J.S., Slomp, C.P., Brinkhuis, H., 2014. A perturbed hydrological cycle during Oceanic Anoxic Event 2. Geology 42, 123–126. doi:10.1130/G34929.1

Voigt, S., Gale, A.S., Flögel, S., 2004. Midlatitude shelf seas in the Cenomanian-Turonian greenhouse world: Temperature evolution and North Atlantic circulation. Paleoceanography 19, 1–17. doi:10.1029/2004PA001015

Wang, Y., Huang, C., Sun, B., Quan, C., Wu, J., Lin, Z., 2014. Paleo-CO_2 variation trends and the Cretaceous greenhouse climate. Earth-Science Rev. 129, 136–147. doi:10.1016/j.earscirev.2013.11.001

Wendler, J.E., Wendler, I., 2016. What drove sea-level fluctuations during the mid-Cretaceous greenhouse climate? Palaeogeogr. Palaeoclimatol. Palaeoecol. 441, 412–419. doi:10.1016/j.palaeo.2015.08.029

Wilmsen, M., 2003. Sequence stratigraphy and palaeoceanography of the Cenomanian Stage in northern Germany. Cretac. Res. 24, 525–568. doi:10.1016/S0195-6671(03)00069-7

Wilmsen, M., 2007. Integrated stratigraphy of the upper Lower - lower Middle Cenomanian of northern Germany and southern England. Acta Geol. Pol. 57, 263–279.

Wilson, P.A., Norris, R.D., Cooper, M.J., 2002. Testing the Cretaceous greenhouse hypothesis using glassy foraminiferal calcite from the core of the Turonian tropics on Demerara Rise. Geology 30, 607–610. doi:10.1130/0091-7613(2002)030<0607:TTCGHU>2.0.CO

Wohlwend, S., Hart, M., Weissert, H., 2015. Ocean current intensification during the Cretaceous oceanic anoxic event 2 - evidence from the northern Tethys. Terra Nov. 27, 147–155. doi:10.1111/ter.12142

Wright, E.K., 1987. Geological Society of America Bulletin Stratification and paleocirculation of the Late Cretaceous Western Interior Seaway of North America Stratification and paleocirculation of the Late Cretaceous Western Interior Seaway of North America. doi:10.1130/0016-7606(1987)99<480

Zheng, X.-Y., Jenkyns, H., Gale, A., Ward, D., Henderson, G., 2016. A climatic control on reorganization of ocean circulation during the mid-Cenomanian event and Cenomanian-Turonian oceanic anoxic event (OAE 2): Nd isotope evidence. Geology 44, 151–154. doi:10.1130/G37354.1

Chapter 2: Tethyan water mass incursions and orbital control of productivity in the Cenomanian Western Interior Seaway

Sameer Y. Patel, Ian C. Harding, James S. Eldrett, and John E. A. Marshall

This chapter is intended for imminent submission.

Author contributions: S.Y.P collected and analysed the TOC, $\delta^{13}C_{org}$, palynological, XRF, and ICP-MS data, with guidance from I.C.H., J.S.E., and J.E.A.M. J.S.E. assisted in the collection of XRF data. S.Y.P. wrote the manuscript, with editorial input from I.C.H., J.S.E., and J.E.A.M.

2.1 Abstract

Mid-Cenomanian Event I (MCE I), characterized by decreasing water column oxygenation alongside extinctions and reorganizations of marine biota, is thought to be a precursor to the Cenomanian-Turonian boundary event (Oceanic Anoxic Event 2; OAE 2) – a globally significant carbon cycle perturbation. From the early Cenomanian, equatorial Atlantic-sourced Tethyan waters started forming a persistent connection with northerly waters of the Western Interior Seaway of North America (WIS) to create the largest epicontinental sea of the Late Cretaceous. Here, we present a new astronomically–tuned framework for this connection via the analysis of a high-resolution, integrated organic and inorganic palynological, geochemical, and sedimentological dataset from the central-eastern region of the WIS. During MCE I, the Tethyan water mass formed a persistent connection with the northerly-sourced WIS in this region. The strengthening environmental influence of Tethyan waters led to the development of a sustained chemocline at the sediment-water interface, demonstrated by redox-sensitive trace metal enrichments, and vastly increased planktic productivity as seen in organic and carbonate records. We have tuned these Tethyan-diagnostic environmental changes to ~50 kyr obliquity cycles across MCE I. The obliquity maximum coinciding with the deposition of the Thatcher Limestone tempestite indicates enhanced storm activity was driven by increased insolation in this region. Furthermore, our astronomically-tuned environmental record demonstrates insolation variability may have influenced the meridional temperature gradient, periodically enhancing productivity in equatorial Tethyan waters; a similar mechanism to that seen during OAE2. Thus, global, orbitally-paced climate cycles may have driven the regional environmental changes observed during this critical point in the evolution of the WIS.

2.2 Introduction

The Cretaceous "hot greenhouse" interval (~97 Ma – 91 Ma; Friedrich et al., 2012) recorded the development of large epicontinental seas, such as the Western Interior Seaway (WIS) of North America. Shorter-term extreme climatic events upon this geologically persistent climatic state were characterized by periods of worldwide oceanic anoxia which impacted on marine biota and resulted in major global carbon cycle perturbations through burial of vast quantities of organic carbon (Oceanic Anoxic Events; OAEs; Schlanger and Jenkyns, 1976), such as during the Cenomanian-Turonian boundary event (OAE 2; see Jenkyns, 2010). The Mid Cenomanian Event (MCE I; 96.57 Ma - 96.36 Ma; Eldrett et al., 2015a) marked a significant turning point in the global Cenomanian oceanographic system, and is considered a precursor to OAE 2 (Coccioni and Galeotti, 2003). Although not recognized as a global OAE due to the lack of widespread deposition of black shales (Friedrich et al., 2009), MCE I shares many characteristics with Cretaceous OAEs such as global carbon cycle perturbations, extinctions and turnovers of marine biota due to expansions of oxygen minimum zones and oceanic circulation changes (e.g., Coccioni and Galeotti, 2003; Zheng et al., 2016). MCE I has been identified in stable isotope records from marine carbonate and organic carbon records across European, Tethyan, proto-Tropical Atlantic realms (e.g., Coccioni and Galeotti, 2003; Friedrich et al., 2009), and in the WIS (Gale et al., 2008; Joo and Sageman, 2014; Eldrett et al., 2015a) via a characteristic dual positive carbon isotopic excursion (CIE) consisting of two $\delta^{13}C$ maxima of ~+1 ‰ (MCE 1a and MCE 1b, respectively). Ecological, sedimentological, and geochemical variations across MCE I have been studied (e.g., Coccioni and Galeotti, 2003; Friedrich et al., 2009; Zheng et al., 2016), but the majority of these studies either focus on marine carbonate records which have a paucity of organic-rich material (e.g., Wilmsen, 2003, 2007), are limited by low resolution datasets for MCE I, and/or focus on single proxy investigations. Here, we provide the most complete assessment of environmental changes across this climatic event to date in the WIS by integrating high-resolution data derived from organic and inorganic fractions of sediments across MCE I.

The WIS, the largest of the Late Cretaceous epicontinental seas, extended from the Tethys Ocean (present day Gulf of Mexico) northwards to the Arctic Ocean at times of maximum sea level highstand, such as during OAE 2 (Kauffman, 1977). In the early to mid-Cenomanian, the Lower Graneros Shale was deposited in the centre of the basin, across Colorado and Kansas under a southerly-restricted, brackish Western Interior water mass (Eicher, 1965), characterised by a dearth of marine molluscan macrofossils (Cobban and Scott, 1972). Throughout the Cenomanian WIS, incursions of warmer, more saline Tethyan waters changed surface water circulation patterns and influenced environmental conditions leading up to and during OAE 2 across the basin (e.g., Eicher and Diner, 1985; Kauffman, 1988; Eldrett et al., 2017). In the mid-Cenomanian, a fully established Tethyan-WIS connection is evidenced by the "explosion" of foraminiferal, ammonite and inoceramid abundance and species diversity throughout the WIS from the deposition of the

Thatcher Limestone tempestite onwards (Cobban and Scott, 1972; Kauffman, 1986, 1988; Eicher and Diner, 1985; Sageman, 1996; Gale et al., 2008). Previous studies have highlighted the significance of short- and long-term Tethyan water mass interactions in the WIS regarding their regional environmental and oceanographic impacts through foraminiferal and molluscan bivalve bio-event analyses (e.g., Eicher, 1965; Kauffman, 1977, 1985, 1986, 1988; Eicher and Diner, 1985). However, few studies utilise integrated organic (e.g., palynological) and inorganic (e.g., trace metal) data. Here, we construct an orbitally-tuned, high-resolution multiproxy framework to elucidate key driving forces behind profound environmental changes during the central WIS-Tethyan connection, thus furthering our understanding of the basin's oceanographic evolution at this time.

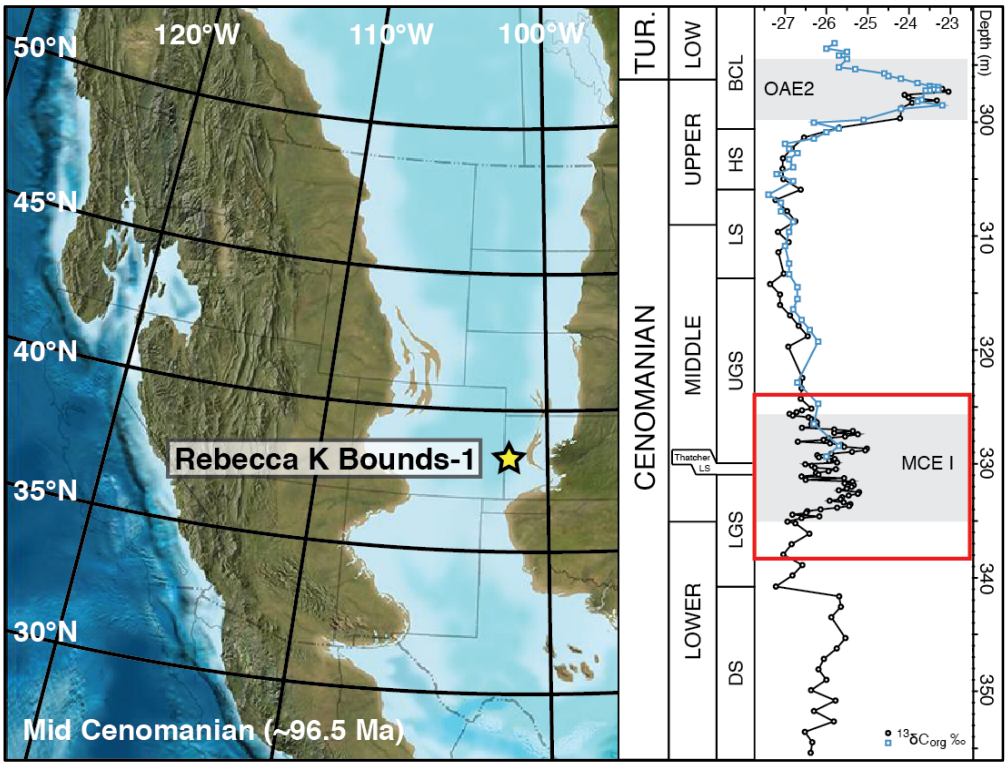

Figure 2.1: Left: Palaeogeographic map of the mid-Cenomanian Western Interior Seaway (used with permission Paleogeography of the Western Interior Seaway of North America © Colorado Plateau Geosystems Inc.), showing the RKB-1 core location (star); Right: Stratigraphy of the RKB-1 core. Red box indicates high resolution study. DS = Dakota Sandstone, LGS = Lower Graneros Shale, UGS = Upper Graneros Shale, LS = Lincoln Shale, HS = Hartland Shale, BCL = Bridge Creek Limestone. Blue carbon isotope record from Dean et al. (1995). WIS age model from Eldrett et al. (2015a).

2.3 Methods

A section of the AMOCO Rebecca K Bounds-1 core (Fig. 2.1; RKB-1; 38°29'26.0"N 101°58'29.7"W) from western Kansas was chosen for its excellent recovery (>90%). The section studied consists of organic-rich mudstones, marls, limestones, and bentonites deposited in near shore/shallow marine shelf settings. Samples were analysed for bulk total organic carbon (TOC

wt. %), organic carbon isotope ratios ($\delta^{13}C_{org}$), palynological data, and trace metal (TM) abundances. The palynological and dinocysts data presented here is from a comprehensive study completed as part of this investigation, the full dataset of which can be found on the U.S. Geological Survey CRC website. Bulk TM concentrations (ppm) were obtained via portable XRF (pXRF), and values were validated with ICP-MS analyses. Trace metals such as molybdenum (Mo) and uranium (U) are used to determine paleoredox conditions as their solubilities vary with oxygen availability, leading to authigenic enrichments in dysoxic/anoxic sedimentary environments (Algeo and Tribovillard, 2009). To determine trace metal enrichments, enrichment factors (TM_{EF}) were calculated by normalizing trace metal concentrations to zirconium and average shale (Brumsack, 2006; Eldrett et al., 2014). Time series analyses were completed through multi-taper method analyses and continuous wavelet transform analyses, following methods outlined by Eldrett et al. (2015b) and references therein. Detailed methodologies are provided in the GSA Data Repository.

2.4 Results and discussion

2.4.1 Water mass evolution across the Tethys-central WIS connection

Palaeoenvironmental changes, such as redox variability, differing water mass sources and related productivity fluctuations were determined by principle component analyses (PCAs) of an integrated geochemical and palynological dataset (see GSA Data Repository). Different dinoflagellate cyst (dinocyst) groups, redox-sensitive trace metals, and major oxides influenced the separation of Lower and Upper Graneros Shale datasets. These variables were analysed in higher resolution to better constrain water mass evolution and subsequent environmental change through RKB-1.

In the Lower Graneros Shale, similar averaged counts of peridinioid dinocysts (P-cysts; ~9,800 counts per gram [c.p.g.]) and gonyaulacoid dinocysts (G-cysts; ~8,700 c.p.g.) alongside a scarcity of calcareous foraminifera recorded in this region (Eicher, 1965) demonstrate organic planktic productivity prevailed. However, G-cyst dominant assemblages in the Lower Graneros Shale, as demonstrated in the P:G dinocyst index (Fig. 2.2F), indicate marine conditions were mostly oligotrophic, rather than sustaining P-cyst assemblages that utilised heterotrophic feeding strategies and are typically found in nutrient rich environments (e.g., Eldrett et al., 2017; see GSA Data Repository). The preservation of fish scales (GSA Data Repository) and abundant benthic arenaceous foraminifera (relative to planktic calcareous species; Eicher, 1965) in sediments characterised by low redox-sensitive trace metal enrichments (Fig. 2.2E; <3 Mo_{EF} & U_{EF}) show this unit was deposited under suboxic conditions (Algeo and Tribovillard, 2009). Occurrences of Tethyan–affiliated *Bosedinia* spp. dinocysts (discussion in Eldrett et al., 2017) throughout the Lower Graneros Shale (Fig. 2.2G), in addition to short-term shifts to P-cyst dominated assemblages and/or increased bulk calcium (Ca_{bulk}) (e.g., Fig 2.2: ~334.5m, ~333m, and ~332m), provide

further evidence that Tethyan waters had established a connection and started to influence environmental conditions in this region of the WIS at this time, expanding upon the observations of Tethyan-affiliated benthic and planktic foraminifera ~5cm below the Thatcher Limestone in Colorado (Eicher and Diner, 1985).

In this record, the high-resolution bulk calcium (Ca_{bulk}) record (Fig. 2.2D) is assumed to primarily represent the biogenic carbonate fraction of the measured bulk $CaCO_3$ contents, as demonstrated by petrological and backscatter SEM analyses of thin sections which reveal numerous calcareous foraminiferal, nannofossil, and inoceramid shell fragments (see GSA Data Repository). From the deposition of the Thatcher Limestone onwards, significant increases in averaged Ca_{bulk} records (Lower Graneros Shale: ~20,800 ppm, Upper Graneros Shale: ~67,600 ppm) and averaged P-cyst abundances (Upper Graneros Shale: ~33,200 c.p.g.), together with an increasingly P-cyst dominated P:G dinocyst index (Fig. 2.2F) indicate environmental conditions promoted substantially enhanced carbonate and organic primary productivity. This interpretation is reinforced by the basin-wide, influx of diverse molluscan macrofossils seen from the Thatcher Limestone depositional event onwards (e.g., Cobban and Scott, 1972; Kauffman 1986), indicating increasingly productive waters promoted the development of more complex ecosystems as Tethyan waters established a stronger connection in this region of the WIS (e.g., Eicher 1965; Cobban and Scott, 1972).

Significantly increased *Bosedinia* spp. abundances in the Upper Graneros Shale (Fig. 2.2G) further evidence the enhanced Tethyan environmental control in the central-eastern WIS. Enrichments of U rose to levels ≥3 (Fig. 2.2E) indicating a chemocline manifested across the sediment water interface (Algeo and Tribovillard, 2009). Substantial enrichments of Mo (≥250; Fig. 2.2E) demonstrate euxnia also periodically prevailed (Algeo and Tribovillard, 2009). However, to discern if these euxinic conditions were limited to the sediment-water interface or if the chemocline migrated to the photic zone at this location, assessments for diagnostic photic zone euxinia biomarkers would need to be completed.

Figure 2.2: Composite data summary for the RKB-1 core section studied. MCE = Mid Cenomanian Event. A) TOC – bulk total organic carbon, in wt%; B) $\delta^{13}C_{org}$ – bulk organic carbon isotope. Red line = 10 point moving average; C) Bandpass filter of interpolated Ca_{log} data, using 0.78 cycles/m frequency discerned from multitaper method (MTM) analyses. Green dashed lines indicate $p > 0.05$ and/or outside cone of influence in CWT analysis. Numbers denote cycles within MCE I and dashed orange horizontal lines show obliquity peaks; D) Ca – bulk calcium (ppm) XRF record. Ca_{log}: interpolated XRF Ca record plotted on log scale; E) U_{EF} & Mo_{EF} – uranium and molybdenum enrichment factors. Purple bars indicate U_{EF} values >3, suggesting anoxic conditions, and elevated Mo_{EF} suggests possible euxinia. All EFs normalized to zirconium and average shale; F); Peridinioid:Gonyaulacoid dinoflagellate cyst ratio. Negative values (dark blue) indicate (oligotrophic) Gonyaulaciod dominant assemblages, and positive values (light blue) indicate (heterotrophic, nutrient-rich) Peridiniod dominant assemblages; G) Tethyan-affiliated *Bosodenia* spp. and Boreal-affiliated *Cyclonephelium compactum–C. membraniphorum* dinocysts (counts per gram); H) Continuous wavelet transform (CWT) of interpolated Ca_{log} data, showing statistically significant cycles/m. Colour range indicates spectral power of frequencies. Thin purple lines signify p=0.05 boundaries, and white shaded area is outside the cone of influence. Black dashed line indicates the 0.78 cycle/m frequency from MTM analyses.

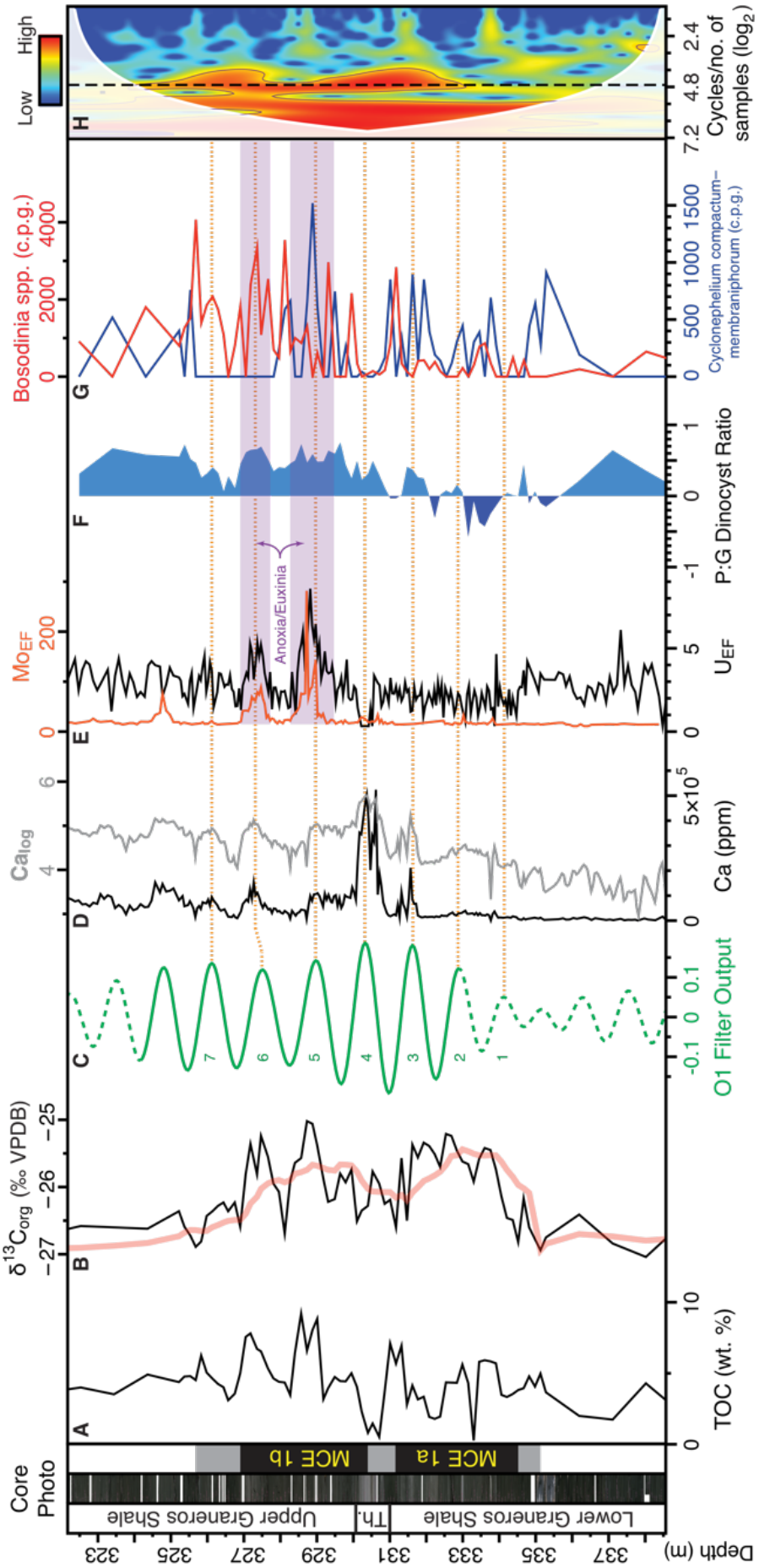
Core Photo
Upper Graneros Shale
Th.
Lower Graneros Shale
MCE 1b
MCE 1a
Depth (m)
323
325
327
329
331
333
335
337
A
TOC (wt. %)
0
10
B
δ13Corg (‰ VPDB)
−27
−26
−25
C
O1 Filter Output
-0.1
0
0.1
7
6
5
4
3
2
1
D
Ca (ppm)
0
5x10^5
Calog
4
6
E
UEF
0
5
MoEF
0
200
Anoxia/Euxinia
F
P:G Dinocyst Ratio
-1
0
1
G
Bosodinia spp. (c.p.g.)
0
2000
4000
Cyclonephelium compactum–membraniphorum (c.p.g.)
0
500
1000
1500
H
Cycles/no. of samples (log2)
7.2
4.8
2.4
Low
High

Increased Tethyan-diagnostic plankton assemblages, elevated planktic productivity, and enrichments of redox-sensitive trace metals demonstrate the environmental influence of Tethyan sourced waters in this region. Thus, the early to mid-Cenomanian incursion of suboxic–anoxic waters from the Tethyan tropical North Atlantic (Demerera Rise; Friedrich et al., 2009) that occurred in the southern WIS (e.g., Eagle Ford Gr., Texas; Eldrett et al., 2017) continued much farther northwards and, at least temporarily, exerted a significant effect on the central-eastern WIS water mass. This northward migration of Tethyan waters must have first been established on the eastern side of the WIS at this latitude, as similar environmental signals are not seen in contemporaneous strata from the centre of the basin (USGS Portland-1 core, Colorado), with the exception of the Thatcher Limestone and towards the end of MCE I (Eldrett et al., 2017). Furthermore, the presence of the Boreal-affiliated *Cyclonephelium compactum–C. membraniphorum* dinocyst complex (Eldrett et al., 2014; van Helmond et al., 2014) across the stratigraphic record in RKB-1 indicates that Tethyan waters did not fully supplant 'native' WIS environmental conditions as evidenced further to the west and south (Eldrett et al. 2017).

To determine the driving forces behind these oceanographic environmental fluctuations, cyclostratigraphic studies were completed on our new records.

2.4.2 Astronomical links between the evolving central WIS connection and MCE I

MCE I is identified in RKB-1 by a complex double-peaked carbon isotope excursion. The first positive excursion in the Lower Graneros Shale is identified as MCE 1a, and the second spanning the Thatcher Limestone and Upper Graneros Shale as MCE 1b (Fig. 2.2B). The event was therefore contemporary with the central WIS-Tethys connection, and so temporally constrains the oceanographic-related environmental changes in this region. This high resolution record refines interpretations of MCE I observed in comparable strata at the Coloradan Pueblo anticline and within the USGS Portland-1 core (Gale et al., 2008; Joo and Sageman, 2014; see GSA Data Repository for correlation discussion), allowing for temporally–constrained, cyclostratigraphic analyses of the RKB-1 sequence to be undertaken.

Geologically short-term climatic and environmental variation is partially influenced by Earth's astronomical cycles, which are modulated by orbital and rotational variances through time (Meyers et al., 2012; Kuiper et al., 2008; Laskar et al., 2011). The expression of these cycles in the sedimentological record have been used to determine durations of climatic events in the WIS through cyclostratigraphic studies (e.g., Meyers et al., 2012b; Eldrett et al. 2015b).

Although MCE I in RKB-1 is not as clearly defined visually by bed-scale sedimentary variations as those recorded in the southern WIS (Eldrett et al., 2015a,b) and in Europe (e.g., Paul et al., 1994; Batenburg et al., 2016), variations in Ca_{bulk} are recorded across the study interval (Fig. 2.2D). Using multitaper method and continuous wavelet transform analyses of Ca_{bulk} in RKB-1, a

statistically significant 0.78 cycle/m signal has been identified through the studied sequence (Fig 2.2H; see GSA Data Repository). A band pass filter of this signal resolved ~7 cycles across MCE I (Fig. 2.2C), similar to that observed in European sections (Folkstone, UK) where bedding couplets across MCE I were counted and attributed to ~20 kyr precession cycles (Paul et al., 1994; Wilmsen, 2007). However, more recently, MCE I has been calculated to have lasted between ~210 and ~450 kyr based on an obliquity-driven astronomical age model from the southern WIS, Texas (Eldrett et al., 2015a), corroborated by a ~300–350 kyr duration determined from an eccentricity derived age model from the Tethyan Umbria-Marche Basin, Italy (Batenburg et al., 2016), suggesting it is unlikely that the cycles recorded in RKB-1 signify precession. The time domain models of Laskar et al. (2004, 2011) have been used to calculate obliquity periodicities of ~48.5 kyr in the mid- to late Cenomanian (Meyers et al., 2012a), and an obliquity signal of 50.23 kyr was resolved in temporally coeval deposits from Texas (Eldrett et al., 2015a). Applying these periodicities to the cycles resolved in RKB-1 provide MCE I durations of ~339.4 kyr to ~351.61 kyr, agreeing with Italian and Texan sections (Eldrett, et al., 2015a; Batenburg et al., 2016), thus resolving a ~50 kyr obliquity signal in RKB-1 (see GSA Data Repository). However, a number of statistically significant higher frequency signals have also been resolved, showing that to be confident of the interpretations, more robust analyses need to be undertaken, such as average spectral misfit or evolutive average spectral misfit methods (Meyers et al., 2012a). Radiometric dating of bentonite layers throughout this section of the record would also further constrain the floating age model.

The obliquity signal is greatest during the deposition the Thatcher Limestone (Fig. 2.2C). As such, this tempestite may represent a time of maximum solar insolation in the WIS (Eldrett et al., 2015b), which would have driven increased wave/storm activity and water column ventilation in shallow waters (see Gale et al., 2008 and Eldrett et al., 2015b), explaining the paradoxical nature of the oxygenated water column (Eicher and Diner, 1985) in an otherwise increasingly oxygen-depleted environment, during the Tethys-central WIS connection.

Peaks in the $CaCO_3$–derived obliquity record are linked to greater intensity of Tethyan water mass mixing in RKB-1, coinciding with P-cyst dominance (Fig. 2.2), indicating periodically increased solar insolation may have heightened productivity. According to Meyers et al. (2012a), obliquity-forced high-latitude insolation variability during OAE 2 could have controlled low-latitude wind strength through changes to the meridional temperature gradient, resulting in periodically enhanced upwelling and thus productivity at the Tethyan equatorial Demerara Rise. When applied to the mid-Cenomanian RKB-1 record, this mechanism could account for the observed Tethyan-related productivity increases in the Lower Graneros Shale (e.g., cycles 2 and 3; Fig. 2.2), ultimately demonstrating that regional environmental changes in the central-eastern WIS might have been principally driven by orbitally-paced changes in the global climatic system. Alternatively, or simultaneously, the significant change in dinoflagellate assemblages before and after the Thatcher

Limestone Member deposition may reflect significant sea-level rise onwards from the deposition of the Upper Graneros Shale in the WIS (e.g., Kauffman, 1988). The smaller fluctuations in carbonate levels recorded in the sedimentary record may also be reflective of carbonate-dilution cycles, as increased runoff from the continent would have led to relatively less carbonate in the system, however the overall productivity may have remained stable. However, increases in organic-walled microplankton during these carbonate maxima (e.g., Lower Graneros Shale) indicate that marine productivity did fluctuate during these times.

2.5 Conclusions

Strengthening intra-basin interactions between Tethyan and WIS waters in the central-eastern region of the basin promoted increasingly anoxic conditions and drastically heightened planktic productivity, leading to the development of a sustained chemocline across the sediment-water interface in this region of the WIS.

These Tethyan-diagnostic environmental indicators are recorded across MCE I, and have been constrained to ~50kyr obliquity–paced cycles. Heightened obliquity-driven insolation and associated increased storm activity may explain the oxygenated Thatcher Limestone depositional event in an otherwise increasingly reducing environment. Furthermore, insolation-driven meridional temperature changes may have increased equatorial Tethyan productivity, as observed during OAE 2. Thus, global, orbitally-paced climate cycles may have been influential in regional environmental fluctuations recorded during this point in the oceanographic evolution of the basin.

2.6 Acknowledgements

This work is supported by an industrial CASE studentship award (NE/L50161X/1) granted by the Natural Environment Research Council UK and Shell International Exploration & Production Inc. We extend our gratitude to the USGS CRC for donating sample material from their collection. In addition, we appreciate the advice Dr. Paul Dodsworth has given us regarding palynological specimen identification.

2.7 References

Algeo, T.J., and Tribovillard, N., 2009, Environmental analysis of paleoceanographic systems based on molybdenum-uranium covariation: Chemical Geology, v. 268, p. 211–225, doi: 10.1016/j.chemgeo.2009.09.001.

Batenburg, S.J., Vleeschouwer, D. De, Sprovieri, M., Hilgen, F.J., Gale, A.S., Singer, B.S., Koeberl, C., Coccioni, R., Claeys, P., and Montanari, A., 2016, Orbital control on the timing

of oceanic anoxia in the Late Cretaceous: Climate of the Past Discussions, doi: 10.5194/cp-2015-182.

Brumsack, H.J., 2006, The trace metal content of recent organic carbon-rich sediments: Implications for Cretaceous black shale formation: Palaeogeography, Palaeoclimatology, Palaeoecology, v. 232, p. 344–361, doi: 10.1016/j.palaeo.2005.05.011.

Cobban, W.A., and Scott, G.R., 1972, Stratigraphy and ammonite fauna of the Graneros Shale and Greenhorn Limestone near Pueblo: Geological Survey Professional Paper 645, p. 1–195.

Coccioni, R., and Galeotti, S., 2003, The mid-Cenomanian Event: Prelude to OAE 2: Palaeogeography, Palaeoclimatology, Palaeoecology, v. 190, p. 427–440, doi: 10.1016/S0031-0182(02)00617-X.

Dean, W.E., Arthur, M.A., Sageman, B.B., and Lewan, M.D., 1995, Core descriptions and preliminary geochemical data for the Amoco Production Company Rebecca K. Bounds# 1 well, Greeley County, Kansas: US Geological Survey.

Eicher, D.L., 1965, Foraminifera and biostratigraphy of the Graneros Shale: Journal of Paleontology, v. 39, p. 875–909.

Eicher, D.L. and Diner, R. 1985, Foraminifera as indicators of water mass in the Cretaceous Greenhorn Sea, Western Interior. In: Pratt, L.M. et al. (eds), Fine grained deposits and biofacies of the Cretaceous Western Interior Seaway: evidence of cyclic sedimentary processes. SEPM Second Annual Midyear Meeting, Golden, Colorado. Field Trip no. 9, August 15th 1985, p. 60-71.

Eldrett, J.S., Dodsworth, P., Bergman, S.C., Wright, M., and Minisini, D., 2017, Water-mass evolution in the Cretaceous Western Interior Seaway of North America and equatorial Atlantic: Climate of the Past, v. 13, p. 1–34, doi: https://doi.org/10.5194/cp-13-1-2017.

Eldrett, J.S., Ma, C., Bergman, S.C., Lutz, B., Gregory, F.J., Dodsworth, P., Phipps, M., Hardas, P., Minisini, D., Ozkan, A., Ramezani, J., Bowring, S.A., Kamo, S.L., Ferguson, K., et al., 2015a, An astronomically calibrated stratigraphy of the Cenomanian, Turonian and earliest Coniacian from the Cretaceous Western Interior Seaway, USA: Implications for global chronostratigraphy: Cretaceous Research, v. 56, p. 316–344, doi: 10.1016/j.cretres.2015.04.010.

Eldrett, J.S., Ma, C., Bergman, S.C., Ozkan, A., Minisini, D., Lutz, B., Jackett, S-J., Macaulay, C., and Kelly, A.E., 2015b, Origin of limestone-marlstone cycles: Astronomic forcing of organic-rich sedimentary rocks from the Cenomanian to early Coniacian of the Cretaceous

Western Interior Seaway, USA: Earth and Planetary Science Letters, v. 423, p. 98–113, doi: 10.1016/j.epsl.2015.04.026.

Eldrett, J.S., Minisini, D., and Bergman, S.C., 2014, Decoupling of the carbon cycle during Ocean Anoxic Event 2: Geology, v. 42, p. 567–570, doi: 10.1130/G35520.1.

Friedrich, O., Erbacher, J., Wilson, P.A., Moriya, K., and Mutterlose, J.J., 2009, Paleoenvironmental changes across the Mid Cenomanian Event in the tropical Atlantic Ocean (Demerara Rise, ODP Leg 207) inferred from benthic foraminiferal assemblages: Marine Micropaleontology, v. 71, p. 28–40, doi: 10.1016/j.marmicro.2009.01.002.

Friedrich, O., Norris, R.D., and Erbacher, J., 2012, Evolution of middle to late Cretaceous oceans-A 55 m.y. Record of Earth's temperature and carbon cycle: Geology, v. 40, p. 107–110, doi: 10.1130/G32701.1.

Gale, A.S., Voigt, S., Sageman, B.B., and Kennedy, W.J., 2008, Eustatic sea-level record for the Cenomanian (Late Cretaceous) - Extension to the Western Interior Basin, USA: Geology, v. 36, p. 859–862, doi: 10.1130/G24838A.1.

Jenkyns, H.C., 2010, Geochemistry of oceanic anoxic events: Geochemistry, Geophysics, Geosystems, v. 11, p. 1–30, doi: 10.1029/2009GC002788.

Joo, Y.J.I., and Sageman, B.B., 2014, Cenomanian to Campanian carbon isotope chemostratigraphy from the Western Interior Basin, USA: Journal of Sedimentary Research, v. 84, p. 529–542, doi: dx.doi.org/10.2110/jsr.2014.38.

Kauffman, E., 1977, Geological and biological overview: Western Interior Cretaceous basin: Mountain Geologist, v. 14, p. 75–99.

Kauffman, E.G., 1985, Paleobiogeography and evolutionary response dynamic in the Cretaceous Western Interior Seaway of North America, in: Jurassic-Cretaceous Biochronology and Paleogeography of North America. Geol. Assoc. Can. Sp. Pap, p. 273–306.

Kauffman, E. G., 1986, High-resolution event stratigraphy: Regional and Global Cretaceous Bio-events, In: O. Walliser, ed., Global Bio-Events, Lecture Notes in Earth History, v. 8, Springer, Berlin, p. 279-335.

Kauffman, E.G., 1988, Concepts and Methods of High-Resolution Event Stratigraphy: Ann. Rev. Earth Planetary Sci, v. 16, p. 605-653.

Kuiper, K.F., Deino, A., Hilgen, F.J., Krijgsman, W., Renne, P.R., and Wijbrans, J.R., 2008, Synchronizing Rock Clocks of Earth History: Science, v. 320, p. 500–504, doi: 10.1126/science.1154339.

Laskar, J., Fienga, A., Gastineau, M., and Manche, H., 2011, La2010: A new orbital solution for the long term motion of the Earth: Astronomy & Astrophysics, v. 4, p. 17, doi: 10.1051/0004-6361/201116836.

Laskar, J., Robutel, P., Joutel, F., Gastineau, M., Correia, a. C.M., and Levrard, B., 2004, A long-term numerical solution for the insolation quantities of the Earth: Astronomy and Astrophysics, v. 428, p. 261–285, doi: 10.1051/0004-6361:20041335.

Meyers, S.R., Sageman, B.B., and Arthur, M.A., 2012a, Obliquity forcing of organic matter accumulation during Oceanic Anoxic Event 2: Paleoceanography, v. 27, p. 1–19, doi: 10.1029/2012PA002286.

Meyers, S.R., Siewert, S.E., Singer, B.S., Sageman, B.B., Condon, D.J., Obradovich, J.D., Jicha, B.R., and Sawyer, D.A., 2012b, Intercalibration of radioisotopic and astrochronologic time scales for the Cenomanian-Turonian boundary interval, western interior Basin, USA: Geology, v. 40, p. 7–10, doi: 10.1130/G32261.1.

Paul, C., Mitchell, S., Marshall, J., and Leafy, P., 1994, Palaeoceanographic events in the Middle Cenomanian of Northwest Europe: Cretaceous Research, v. 15, p. 707–738.

Sageman, B.B., 1996, Lowstand tempestites: Depositional model for Cretaceous skeletal limestones, Western Interior Basin: Geology, v. 24, p. 888-892.

Schlanger, S.O., and Jenkyns, H.C., 1976, Cretaceous oceanic anoxic events: causes and consequences: Netherlands Journal of Geosciences/Geologie en Mijnbouw, v. 55, p. 179–184.

van Helmond, N.A.G.M., Sluijs, A., Reichart, G.-J., Sinninghe Damste, J.S., Slomp, C.P., and Brinkhuis, H., 2014, A perturbed hydrological cycle during Oceanic Anoxic Event 2: Geology, v. 42, p. 123–126, doi: 10.1130/G34929.1.

Wilmsen, M., 2003, Sequence stratigraphy and palaeoceanography of the Cenomanian Stage in northern Germany. Cretac. Res., v. 24, p. 525–568. doi:10.1016/S0195-6671(03)00069-7

Wilmsen, M., 2007, Integrated stratigraphy of the upper Lower - lower Middle Cenomanian of northern Germany and southern England. Acta Geol. Pol., v. 57, p. 263–279.

Zheng, X.-Y., Jenkyns, H., Gale, A., Ward, D., and Henderson, G., 2016, A climatic control on reorganization of ocean circulation during the mid-Cenomanian event and Cenomanian-Turonian oceanic anoxic event (OAE 2): Nd isotope evidence: Geology, v. 44, p. 151–154, doi: 10.1130/G37354.1.

2.8 GSA Data Repository

2.8.1 Analytical methods

Bulk total organic carbon (TOC), organic carbon isotope ($\delta^{13}C_{org}$), and palynological data was collected every 15 cm within MCE I and every 90 cm prior to and after the event in RKB-1. Total carbon (TC) and TOC data was measured by dividing samples into two sets and digesting one half in hydrochloric acid to remove carbonate contents before using a Carlo-Erba EA 1108 Elemental Analyzer (internal analytical precision ± 0.3%) at the National Oceanography Centre, Southampton, following methods described in Forster et al. (2007). Bulk $\delta^{13}C_{org}$ was measured by Iso-Analytical using an Elemental Analyser - Isotope Ratio Mass Spectrometer (EA-IRMS). Standard acid digestion procedures were employed for palynological processing, and each sample was "spiked" with a known amount of exotic *Lycopodium* spores using standardized spore tablets (Batch 124961) to allow for quantitative analyses, as in Eldrett et al. (2015).

2.8.2 Palynological analyses

Core material was broken into small fragments (<1 cm^3) and weighed, with 2-5 g being used for analyses. Samples were then processed for palynology at the Ocean and Earth Science department at the University of Southampton, UK, using the following protocol: treatment in 30% hydrochloric acid (HCl), followed by decanting the acid and washing samples until pH-neutral. This was followed by sample digestion in 60% hydrofluoric acid and subsequent acid decanting and sample neutralization. The resultant organic residue (kerogen) was sieved through a nylon mesh to obtain a ≥15 µm fraction, and spiked with 2-5 *Lycopodium* tablets (Batch 124961) to permit quantitative analysis. Residues were then rapidly boiled in 30% HCl to remove neo-formed flourides and decanted into ~250 ml of water before further sieving. Pyrite was removed by oxidizing samples in 30% nitric acid for 5 minutes, and amorphous organic matter (AOM) was disaggregated using a tunable ultrasonic probe for 40 seconds. After a final sieving, samples were strew-mounted on glass coverslips and left to dry. When dry, the coverslips were inverted and glued onto glass microscope slides using Elvacite 2044. Quantitative palynofacies data were collected by counting 300 marine and continental specimens per sample. The data were normalized to the out-of-count *Lycopodium* spike to obtain counts per gram (c.p.g.). Marine palynomorphs (dinocysts, acritarchs, and prasinophyte algae) were identified to genus or species level using the taxonomic nomenclature catalogued in (Williams et al., 2017), and absolute abundances (c.p.g.) of individual species were recorded by counting 100 marine specimens per sample and normalizing to out-of-count *Lycopodium* occurrences, using similar methods to Eldrett et al. (2015).

2.8.2.1 Peridinioid vs. gonyaulaciod dinocyst ratio

Studies which utilise dinocysts for palaeoproductivity reconstructions primarily rely on the ratio of (proto-) peridinioid dinocysts (P-cysts) versus gonyaulacoid dinocysts (G-cysts; P:G dinocyst ratio) (e.g., Prauss, 2012; Dodsworth, 2015; Eldrett et al., 2017). Modern P-cysts have been found to be linked to nearshore or restricted areas in which terrestrial nutrient input is high, as well as in nutrient-rich upwelling regions, and most are known heterotrophs (review in Sluijs et al., 2005; Dodsworth, 2015). In contrast, G-cysts, are affiliated with oligotrophic and open marine environments and employ an autotrophic feeding strategy (Sluijs et al., 2005; Eldrett et al., 2017). Although the use of modern dinocysts as analogues for ancient species has its limitations (e.g., assuming heterotrophic feeding strategies for fossil P-cysts might be misleading; Dale and Fjellså, 1994), including fossil P-cysts with autotrophic feeding strategies in P:G dinocyst ratios has not significantly altered palaeoenvironmental signals (Sluijs et al., 2005). The P:G ratio can be influenced by the preferential preservation of P-cysts or G-cysts dependant on redox conditions of bottom and pore waters, age of deposition and/or location, and absolute abundances tend to provide more accurate sea surface productivity interpretations (discussion in Eldrett et al., 2017). Furthermore, more reliable palaeoenvironmental and productivity reconstructions from the Cretaceous have been garnered when using the P:G ratio in conjunction with other geochemical, sedimentological, and biological proxies (e.g., Eldrett et al., 2017; Prauss, 2012; van Helmond et al., 2014). In this study, the cumulative total number of respective specimens are used for the P:G ratio. The following equation was used for the P:G ratio, in which values approaching 1 indicate P-cyst dominated assemblages, and values approaching -1 demonstrate G-cyst dominated assemblages:

$$\frac{\Sigma\, peridinioid\ dinocysts - \Sigma\, gonyaulacoid\ dinocysts}{\Sigma\, peridinioid\ dinocysts + \Sigma\, gonyaulacoid\ dinocysts}$$

2.8.3 ICP-MS sample preparation

To remove carbonate contents from samples, ~10 mg of powdered bulk sediment was digested in Teflon pots using a 0.5 ml, 10% solution of 6M hydrochloric acid (HCl). The pots were heated to 130-150°C on hot plates until all acid was evaporated (approx. 1 hour). Samples were further digested in 1 ml of Aqua Regia solution (3:1 HCl:HNO_3) and heated to 80°C for 12 hours to dissolve sulphides and Fe/Mn oxides. Lids were placed on the pots to ensure no acid was lost due to evaporation over this time. The acid was subsequently removed via evaporation by increasing the hot plate temperature to 130-150°C and removing lids. Once dry, hydrofluoric acid (0.25 ml) and perchloric acid (0.25 ml) were added to each sample and heated to 80°C for 12 hours to digest any other minerals and organic matter (with lids kept on). Lids were removed and the temperature was increased to 160°C to evaporate the acids. Samples were dissolved in a 6M HCl solution (filling ~1/3 of a pot) and heated for 48 hours to ensure each sample was in a HCl matrix. Once

samples were fully dissolved, acid was removed by evaporation. The samples were then diluted with 3% HNO_3 in preparation for ICP-MS analysis.

Each sample was diluted to 2000x by emptying pot contents into vials (weighed empty) and filled with 3% HNO_3 (20 ml), then re-weighed. The samples were further diluted to 4000x by taking 2.5ml of 2000x dilution solution and adding 2.5ml 3% HNO_3 in new vials which were weighed empty, with subsample, and once full. Finally, these were diluted to 80000x by taking 0.25ml of 4000x and adding 4.75ml of 3% HNO_3 in new vials which were weighed empty, with subsample, and once full.

Standards were also prepared. 2 ml of each standard, in solution, (BAS 206, JA2, JB1A, BHVD2, JGB1, JB3, BRR1, and BIR1) was pipetted into Teflon pots, and the sample bottle was weighed before/after (standards start at 400x dilution). The standards were placed on a hot plate and evaporated overnight before being made up with 3% HNO_3 so they were also in a HCl matrix. These were then diluted to 4000x by weighing: empty vials; vial + standard in; vial + standard + 20 ml 3% HNO_3 and re-weighing. These were then diluted to 80000x by taking 0.25ml of 4000x solution and adding 4.75ml of 3% HNO_3 in new vials. Each vial was weighed empty, with subsample, and when full. Finally, these were then diluted to 320000x by taking 1ml of 80000x and adding 3ml of 3% HNO_3 in new vials. Each vial was weighed empty, with subsample, and when full.

The samples were run on an Thermo Fisher Scientific ELEMENT 2XR ICP-MS at the University of Southampton (National Ocenaography Centre) and results were obtained for major elements: Na, Mg, Al, K, Ca, V, Cr, Mn, and Fe; and trace elements: Li, Sc, V, Cr, Co, Ni, Cu, Zn, Rb, Sr, Y, Zr, Nb, Mo, Sn, Cs, Ba, La, Ce, Pr, Nd, Sm, Eu, Gd, Tb, Dy, Ho, Er, Tm, Yb, Lu, Hf, Ta, Pb, Th, and U. The reader is referred to the linked online dataset for analytical error margins (% RSD).

ICP-MS data: http://data.usgs.gov/crc-data/core/12001/core_analysis_73303_E006Data17.xlsx

2.8.4 Portable XRF data acquisition

At the USGS Core Research Centre (Denver, Colorado), the RKB-1 core was analysed using a handheld Thermo Scientific Nikon XL3t GOLDD+ XRF Analyzer. This allowed the collection of elemental compositional data of the core in high resolution, in a non-destructive analysis. The following steps were taken to obtain data for the following elements: Mo, Zr, Sr, U, Rb, Th, Pb, As, Zn, Cu, Ni, Co, Fe, Mn, Cr, V, Ti, Sc, Ca, K, S, Ba, and Cs.

The core was marked at 10 cm intervals from the base of the X-Bentonite down to the end of the Mid Cenomanian Event (MCE I) positive isotope excursion (CIE), from where the intervals were shortened to 5cm across MCE I. Below MCE I, sample resolution was increased back to 10cm. The handheld analyser was set to take readings over 120 seconds, and was calibrated by taking a reading of a factory standard (NIST LOW 2709). A reading was taken before and after each data recording session. Once calibrated, readings were taken for each interval, ensuring that no air gap was present between the analyser and the core, and that the analyser was not moved during three 120 second analysis.

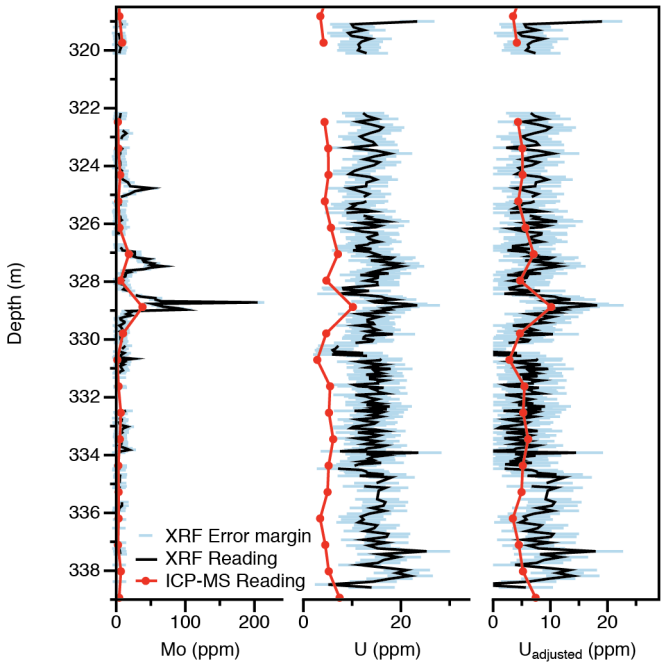

Figure 2.3: Comparisons between portable XRF and ICP-MS elemental counts, before and after adjusting for measurement drift during XRF data acquisition.

To calibrate for elemental measurement drift during sampling sessions, the difference between NIST LOW 2709 measurements and factory values from the beginning and end of each session was calculated for each element used. A linear positive or negative drift was assumed, and so interpolated drift coefficient values were calculated, based on number of readings taken per session. The interpolated coefficient values were then added to each sample reading to produce an adjusted elemental count (ppm). These adjusted records were validated by comparing to ICP-MS readings (e.g., Fig. 2.3).

2.8.4.1 Redox-sensitive trace element enrichments

Before palaeoenvironmental reconstructions using redox sensitive trace elements can be undertaken, it must first be determined if the trace element contents within sediments are controlled by the flux of detrital material into the marine system, or are authigenic. By comparing trace

element accumulations against titanium (Ti) concentrations, correlative checks can be used to determine the main sources for these elements (see Tribovillard et al., 2006). As Ti is predominantly immobile during diagenesis and of terrigenous origin, a strong correlation would infer it is mainly controlled by detrital sources and, thus, would not be useful for paleoenvironmental analysis (Tribovillard et al., 2006). In this study, no redox-sensitive elements correlate with Ti, denoting their authigenic nature.

Trace element accumulation was determined by comparing values to average values in the Earth's crust or using "average shale" values (see Wedepohl, 1991) and determining whether they are relatively enriched or depleted, which infers reducing or oxidising conditions, respectively (Calvert and Pedersen, 1993). The only source of zirconium (Zr) in pelagic sediments is from terrigenous input, and so normalising to this element removes the effect of variable terrigenous input in these sediments (Milnes and Fitzpatrick, 1989). Furthermore, normalising elemental data to Zr has been used in previously WIS studies (e.g., Eldrett et al., 2014), as it corrects for highly variable carbonate contents (Snow et al., 2005). An enrichment factor of >3 represents a detectable enrichment of said element over crustal averages, and a value of >10 suggests a moderate to strong degree of enrichment (Algeo and Tribovillard, 2009). The following equation was used to obtain enrichment factors for each element:

$$Enrichement\ Factor\ (EF) = \frac{\left(\frac{\text{Element}}{\text{Zr}}\right) sample}{\left(\frac{\text{Element}}{\text{Zr}}\right) avg.shale}$$

2.8.5 Determining the biogenic nature of the $CaCO_3$ signal

The bulk Ca (ppm) record obtained via pXRF (Ca_{bulk}) was compared to $CaCO_3$ (wt. %) concentrations (Fig. 2.4) calculated from the TOC (wt. %) measurements obtained for RKB-1, using the following formula, where TOC = Total Organic Carbon and AC = Acidified Carbon (de-carbonated fraction of sample analysed for TOC):

$$Calcite = 100 * 1 - TOC / AC$$

The two records correlate well, allowing use of the high resolution Ca_{bulk} record to be used for further analyses. Although XRD analyses and/or elemental maps using SEM-EDS would need to be completed in order to discern exact mineralogy within the sedimentary matrices, we follow similar assumptions as other studies from the Cretaceous WIS in that most of the wt.% bulk $CaCO_3$ signal is from coccolith, foraminiferal, and molluscan shell material, even though it is likely that there is some diagenetic $CaCO_3$ as well.

Previous microfossil analyses established the whole Kansan Graneros Shale section was equivalent to the *Trochamminiodes apricarius* biozone of the Coloradan Graneros Shale (Eicher, 1965). At Rock Canyon, CO., abundant calcareous benthic and planktonic species were observed, in the *T. apricarius* biozone (Eicher, 1965).

In RKB-1, low Ca_{bulk} counts in the Lower Graneros Shale (LGS) indicate there was less calcareous productivity in this section of RKB-1. However, identification of biogenic apatite using SEM-EDS (Fig. 2.5A) gives evidence of productive pelagic waters, as this is associated with fossilized fish scales, which are also found in the Coloradan Graneros Shale (Cobban and Scott, 1972).

Polished thin sections from horizons of low Ca_{bulk} concentrations correlate with sparse occurrences of dwarfed *Heterohelix* calcareous foraminiferal tests in clay- and organic-rich sedimentary matrices (Fig. 2.5B). Conversely, high Ca_{bulk} counts in the Upper Graneros Shale (UGS) represent diverse and abundant foraminifera of varying size (Fig. 2.5C). Many foraminiferal tests are clay filled, and minor recrystallization was observed in some tests and the surrounding sedimentary matrix, which was expected due to the age of the sediment. As such, this alteration not thought to alter the primary environmental signal.

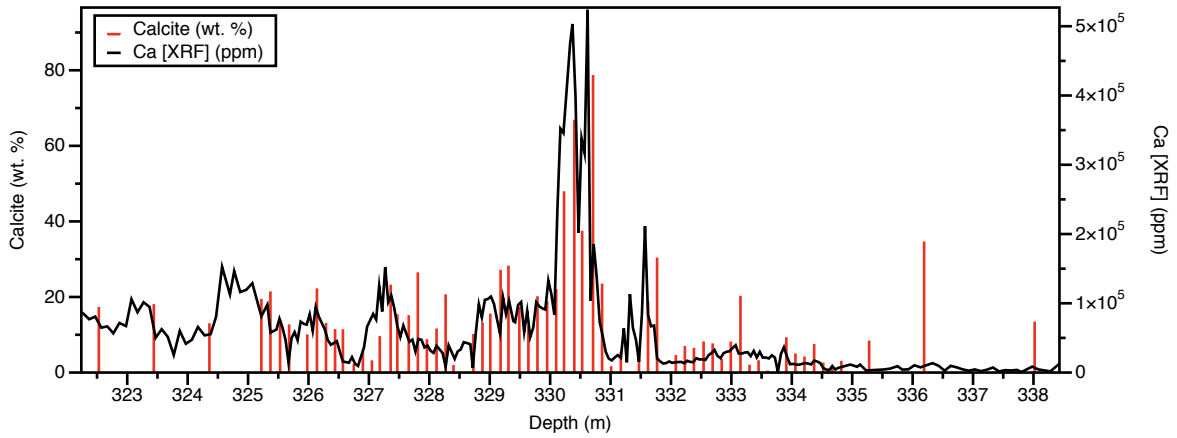

Figure 2.4: Comparison of measured Ca (ppm) data from pXRF to $CaCO_3$ concentrations calculated with TOC measurement data show strong correlation.

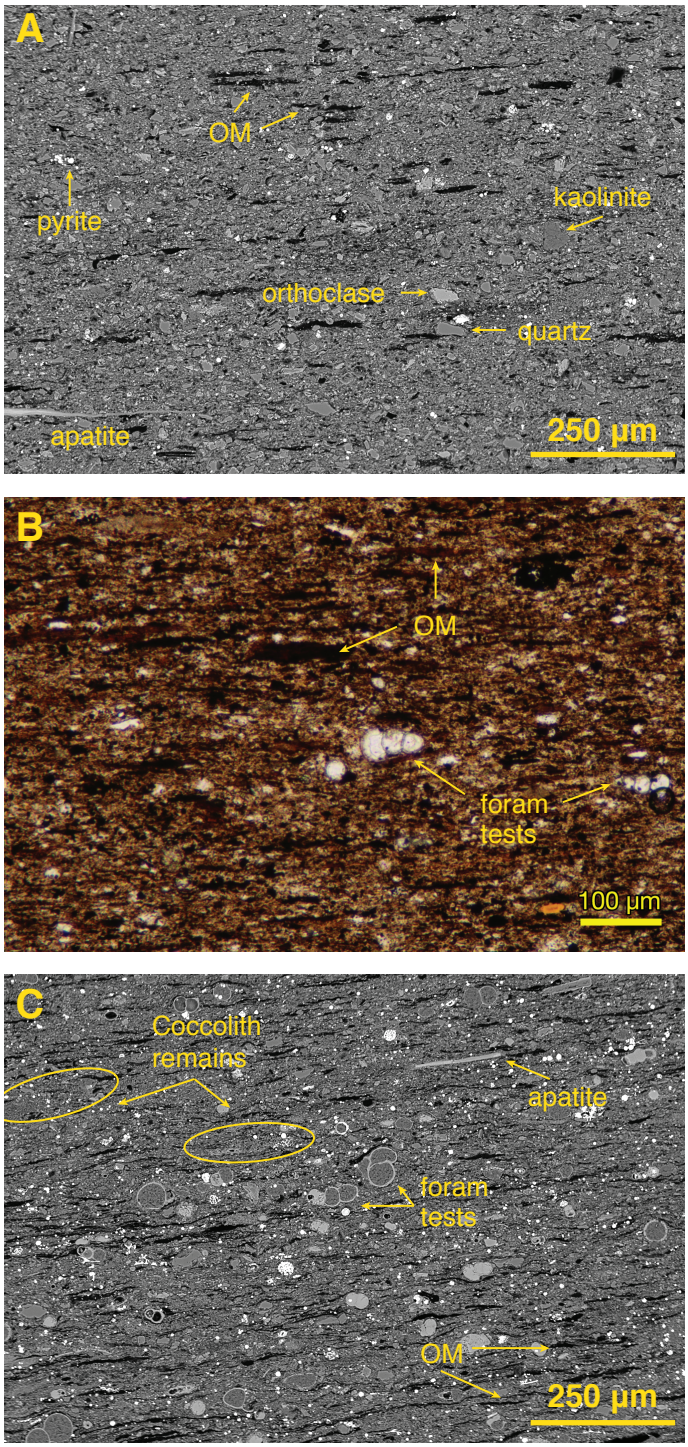

Figure 2.5: A) Backscatter SEM image of Lower Graneros Shale sample (TOC: 5.9%; $CaCO_3$: 3.2%). Sedimentary matrix contains elongate biogenic apatite, clay minerals, and organic matter. B) Transmitted light microscopy image of a low $CaCO_3$ section of the Upper Graneros Shale shows well preserved foram tests. Test walls and chambers show clear boundaries, suggesting only minor recrystallization. Surrounding matrix is predominantly comprised of clay and/or organic material suggesting little/no calcite secondary environmental signal. C) Backscatter SEM image of highest TOC section in Upper Graneros Shale, characterised with anoxia/euxinia and >25 wt. % $CaCO_3$. Numerous foraminiferal tests may be main source of $CaCO_3$. Minor recrystallization suggests minimal diagenetic alteration; however, most chambers are clay filled.

2.8.6 Correlating RKB-1 & MCE I to other sites

The dual peaked carbon isotope excursion (CIE) characterizing MCE I has been recorded in the WIS from samples from Coloradan Pueblo anticline (Gale et al., 2008), and in the Portland-1 core (Joo and Sageman, 2014). At both sites, MCE I initiated in the Lower Graneros Shale, extended across the Thatcher Limestone, and culminated in the Upper Graneros Shale, below the basin-wide "x-bentonite". Thus, MCE I can be confidently identified within the RKB-1 $\delta^{13}C_{org}$ record as it is expressed in similar strata to the lithostratigraphically correlated USGS Portland-1 core (Scott et al., 1998; Joo and Sageman, 2014). However, the high resolution $\delta^{13}C_{org}$ data obtained for RKB-1 resolves a much more complex isotopic record than that of Portland-1, with an excursion in the Lower Graneros Shale culminating below the Thatcher Limestone and two well-defined maxima manifesting in the Upper Graneros Shale. Joo and Sageman (2014) identified MCE 1a and MCE 1b via carbon isotope maxima within the Upper Graneros Shale in the Portland-1 core. Additional data points integrated into the Portland-1 record resolve a more complex CIE during MCE I with additional isotope maxima in both Graneros units (Fig. 2.6A; Eldrett et al., 2017).

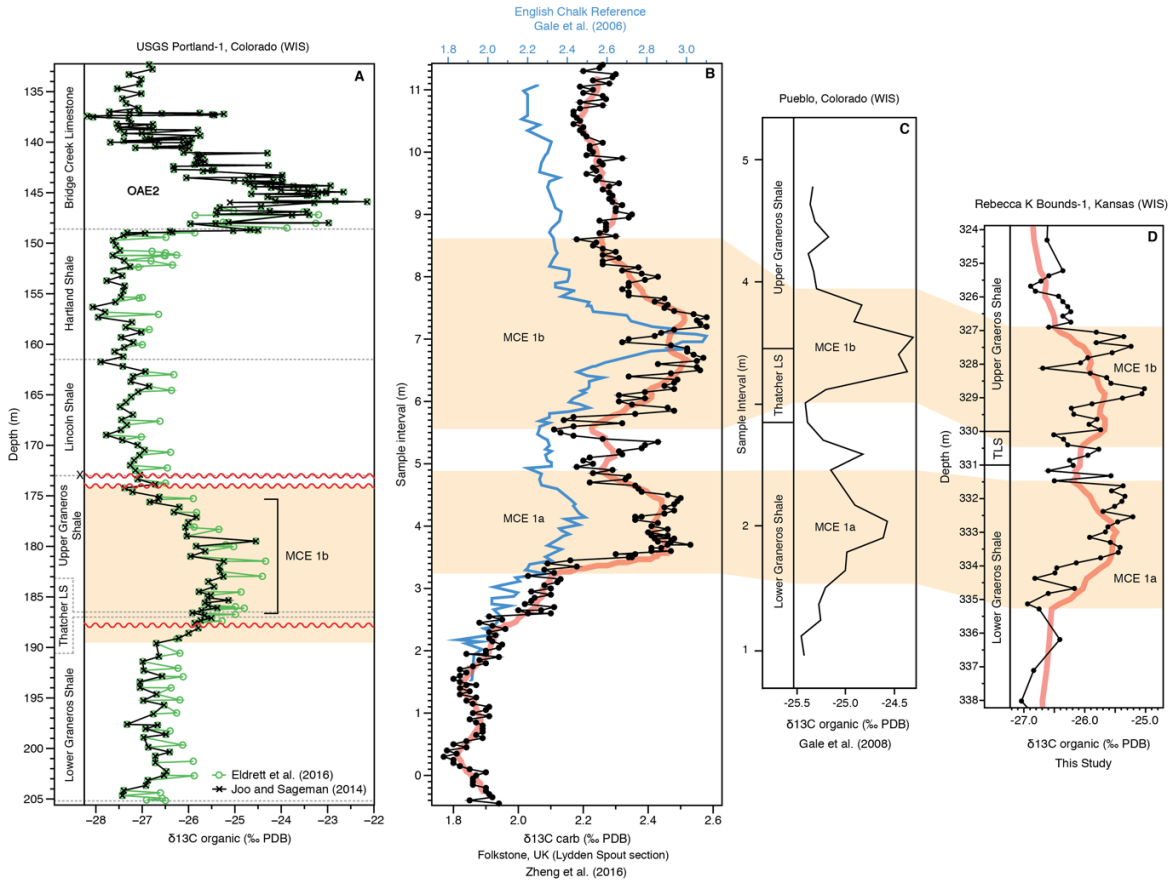

Figure 2.6: Organic carbon and carbonate isotope records for MCE I in European and WIS sites. A) USGS Portland-1 $\delta^{13}C_{org}$ record of Joo and Sageman, 2014 (black), and Eldrett et al., 2017 (green). Red lines denote hiatuses identified in this study, and yellow bar shows extent of MCE I isotope excursion; B) $\delta^{13}C_{carb}$ records from the English Chalk reference curve (blue; Jarvis et al., 2006), and Folkestone, UK (black; Gale et al., 2008; Zheng et al., 2016). Red line is 10 point moving average of Folkestone data; C) Pueblo anticline MCE I $\delta^{13}C$ record (Gale et al., 2008); D) RKB-1 $\delta^{13}C$ record for MCE I. Red line is 10 point moving average of data. Orange bars correlate MCE 1a and MCE 1b across European and WIS sections.

Gale et al. (2008) correlated the Pueblo anticline CIE to one they produced from Folkestone, UK, where previous outcrop studies in close vicinity resolved the MCE I CIE in sufficient enough resolution separate MCE 1a and MCE 1b (Jenkyns et al., 1994; Paul et al., 1994; Mitchell, 1996). The Folkestone CIE of Gale et al. (2008) was subsequently correlated to the English Chalk reference curve (Jarvis et al., 2006; Zheng et al., 2016) which utilized the original Folkestone MCE I carbon isotope studies of Jenkyns et al. (1994) and Paul et al. (1994) (Fig. 2.6B). This correlative study discerned that at the Pueblo anticline, MCE 1a occurred within the Lower Graneros Shale and MCE 1b in the Upper Graneros Shale, with the Thatcher Limestone separating the two stages (Figs. 2.6B & C).

The RKB-1 MCE I carbon isotope record is remarkably similar those reported at the Pueblo anticline and Folkestone (Figs. 2.6B, C, & D). At both WIS sites, a positive isotopic excursion occurs in the Lower Graneros Shale culminating prior to the Thatcher Limestone, and this trend is reflected in contemporaneous stratigraphic units at Folkestone. Furthermore, in all three records, a smaller positive CIE is seen prior to the MCE 1b isotope excursion. Finally, the Folkestone and RKB-1 isotope records express two distinct positive excursions during MCE 1b. This trend is also reflected in the Pueblo anticline record, albeit not as pronounced as in RKB-1.

When comparing the RKB-1 MCE I carbon isotope excursion to that of Portland-1, it is clear that MCE 1a is not fully recorded in latter core. Discrepancies between the extent and nature of the CIEs suggest there was a hiatus prior to the Thatcher Limestone in Portland-1 (Fig. 2.6A). The MCE 1b interval is more expanded in Portland-1 than in RKB-1. However, the Upper Graneros Shale interval between the end of MCE 1b and the x-bentonite is more condensed than in RKB-1. As such, another hiatus between MCE I and the x-bentonite in Portland-1 can be identified, assuming the respective sedimentation rates remained constant at these two sites. Finally, a third hiatus is identified at the x-bentonite in Portland-1, as the Upper Graneros Shale continued to be deposited in RKB-1 after this basin-wide volcanic event, whereas a sharp change in lithology is observed in Portland-1.

For these reasons, the interpretation of the placement of MCE 1a and MCE 1b within the WIS isotope record by Gale et al. (2008) has been applied to the RKB-1 carbon isotope record, rather than that of Joo and Sageman (2014).

2.8.7 Integrated geochemical and palynological principal component analyses

Eldrett et al. (2017) completed principal component analyses (PCAs) on an integrated geochemical and palynological dataset from numerous sites in the Late Cretaceous WIS, and two sites from the Tropical North Atlantic (Demerara Rise) to determine controls on organic matter composition and environmental drivers. Data from the RKB-1 core was integrated into the dataset of Eldrett et al. (2017) to determine the wider environmental trends recorded in RKB-1. It is that discerned

Graneros Shale samples from RKB-1 and Portland-1 cores are influenced by similar variables when mid-Cenomanian RKB-1 data are incorporated into the study (Fig. 2.7). RKB-1 and Portland-1 data plots positively along Component 1, and neutrally (~0) along Component 2, showing environmental conditions did not change drastically from the centre of the seaway to the eastern margin. The Lower Graneros Shale in RKB-1 plots slightly negatively along Component 2, whereas the Upper Graneros Shale in RKB-1 plots slightly positively. As both sites from the Demerara Rise plot positively along Component 2, and were deposited in Tethyan waters (Friedrich et al., 2008), the PCA shows the Upper Graneros Shale in RKB-1 may have been deposited during times of heightened Tethyan and WIS water mass mixing.

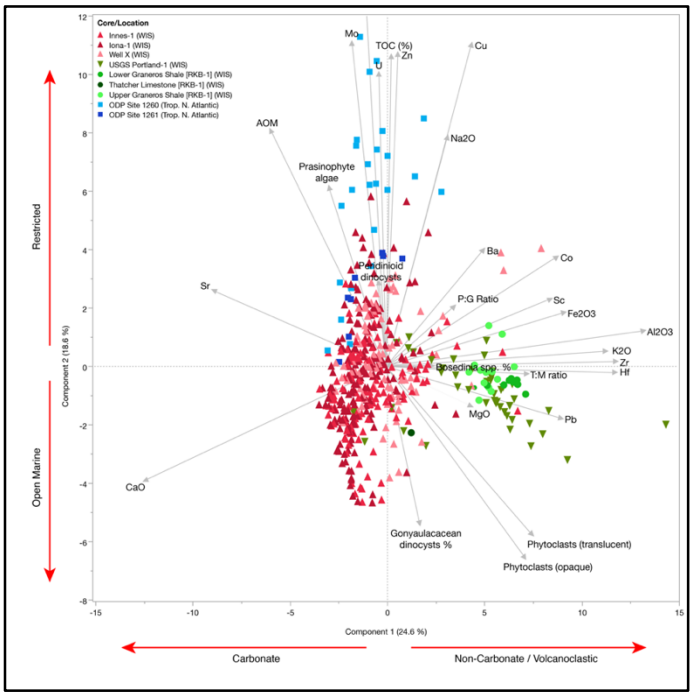

Figure 2.7: Principal component analysis of geochemical and palynological data from numerous Cenomanian sites in the WIS and Tropical North Atlantic, showing palaeoenvironmental controls on sediment deposition and correlations between RKB-1 and other studies.

A second PCA of isolated RKB-1 data shows the regional environmental influences that characterise the three units (Fig. 2.8). The separation of the two Graneros Shale units are seen in greater detail, with the Lower Graneros Shale plotting negatively along the Component 2 axis, and the Upper Graneros Shale plotting positively along this axis. The variables influencing this axis (e.g., redox-sensitive TMs) show the Upper Graneros Shale is characterised more by reducing conditions than its Lower counterpart. Clear separation of peridinioid vs. gonyaulacoid dinocyst grouping is observed for the two Graneros Shale units, suggesting environmental variability between these units influenced changes in the type of dinoflagellate productivity across this sequence.

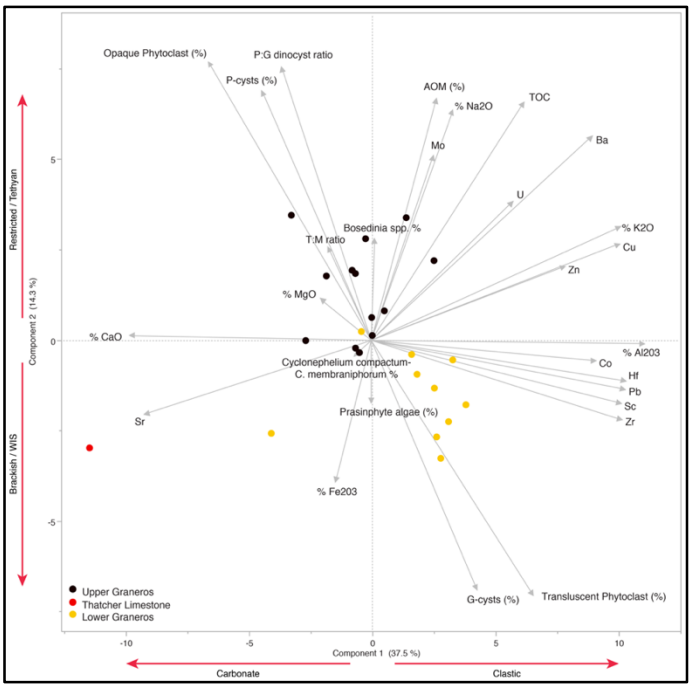

Figure 2.8: Principal component analysis of Lower Graneros (yellow), Thatcher Limestone Member (red), and Upper Graneros Shale (black) RKB-1 palynological and geochemical data.

2.8.8 Cyclostratigraphy methods

Time series analyses were conducted on the carbonate (Ca_{bulk}) record, which was interpolated, logarithmically scaled, and detrended (Ca_{log}). An initial study and signal filtering was completed using Analyseries (version 2.0.8) (Paillard et al., 1996). Multitaper method (MTM) spectral analyses were accomplished using Astrochron (version 0.6; Meyers, 2014) using three 3-π discrete prolate spheroidal sequences (DPSS) tapers to determine statistically significant cycle frequencies. Continuous Wavelet Transform (CWT) analyses of the interpolated Ca_{log} dataset were also run to discern cycle frequencies using PAST (version 3.12; Hammer et al., 2001). The following methods for the time series analyses were used:

1. Ca (ppm) XRF data was converted to a logarithmic scale (hereby referred to as "CaLog").
2. In *Analyseries* (version 2.0.8), Piecewise linear interpolation was used to create a uniformly spaced CaLog dataset (hereby referred to as "CaLogInt") using the following settings:
    a. Evenly sampled between 322.17m – 338.57m at 0.05m intervals.
    b. Linear interpolation (mean values between mid-points).
3. Multitaper method (MTM) spectral analysis via *Astrochron* (version 0.6) was conducted on CaLogInt using the following settings:

   a. mtm(CaLogInt,tbw=3,ntap=3,padfac=5,demean=T,detrend=T,siglevel=0.9,ar1=T, output=3,CLpwr=T,pl=1,sigID=F,genplot=T,verbose=T)
   b. See *Astrochron* R package (Meyers, 2014) for input definitions.

4. The largest statistically significant peak (>90% AR1 confidence level) via the MTM analysis identified indicated that a cyclic signal within the CaLog record was present at a frequency of 0.78 cycles/meter.
5. In *Analyseries*, the interpolated dataset was filtered using the identified frequency from the MTM analysis, with a Gaussian bandwidth of 0.1.
6. The number of cycles through the MCE I interval within the Ca dataset was counted and based on the calculated duration of MCE I, the cyclicity of the CaLogInt data was compared to theoretical orbital cycles.
   a. Meyers et al. (2012) determined theoretical Late Cenomanian target orbital periods based on the orbital solutions of Laskar et al. (2004; 2011) are (E = Eccentricity; O = Obliquity; P = Precession): E1 = 405.47 kyr, E2 = 126.98 kyr, E3 = 96.91 kyr, O1= 48.54 kyr, O2= 37.66 kyr, P1= 22.42 kyr, P2= 18.33 kyr.
   b. Through Piecewise linear interpolation of data from Berger et al. (1992) (via *Astrochron*), O1= 50.352 kyr, O2= 38.888 kyr, P1= 22.324 kyr, P2= 18.524 kyr at 96 Ma, approximately when MCE I occurred.
   c. ~7 cycles across MCE I are identified in the RKB-1 record.
   d. Using the cyclostratigraphic records of Batenburg et al. (2016) we determine that the duration of MCE I = ~350 kyr. Thus, 350/7 = 50 kyr/cycle.
   e. Eldrett et al. (2015) resolved a similar obliquity signal (50.23 kyr) in contemporaneous deposits from Texas, supporting these results.
7. Using O1 = 48.5 kyr, which has a frequency of 0.78 cycles/meter in the CaLogInt dataset, orbital periodicity targets for E1, E2, E3, O2, P1, and P2 orbital targets have been calculated to see if they were resolved in the MTM analysis (Fig. 2.9).
   a. If 48.5 kyr = 0.78 cycles/m
      then 48.5 kyr = (1/0.78) meters
      so 1 kyr = (1/0.78) / 48.5

E1	=	1 / (405.5 * ((1/0.78) / 48.5))	=	0.093 cycles/m
E2	=	1 / (127.0 * ((1/0.78) / 48.5))	=	0.298 cycles/m
E3	=	1 / (96.9 * ((1/0.78) / 48.5))	=	0.390 cycles/m
O2	=	1 / (37.7 * ((1/0.78) / 48.5))	=	1.003 cycles/m
P1	=	1 / (22.4 * ((1/0.78) / 48.5))	=	1.689 cycles/m
P2	=	1 / (18.3 * (91/0.78) / 48.5))	=	2.067 cycles/m

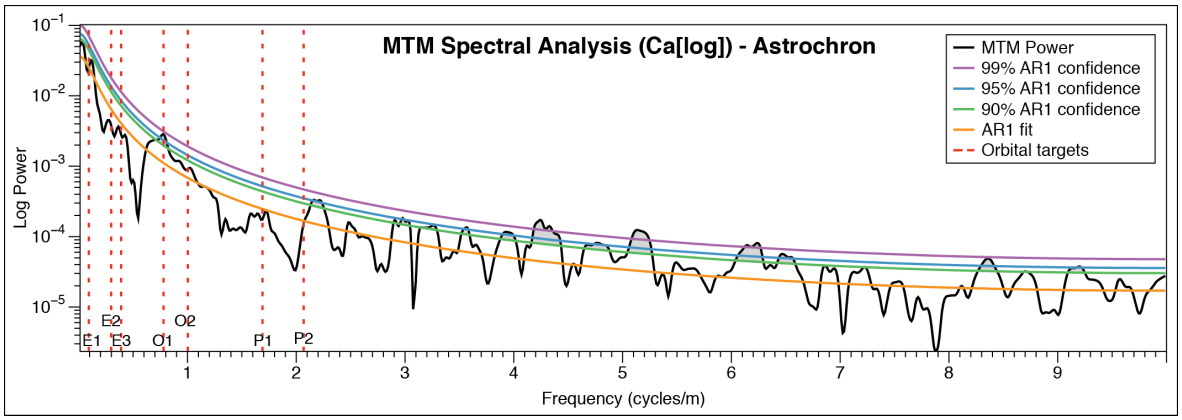

Figure 2.9: Multitaper method analysis of interpolated logarithmic Ca XRF data, with calculated orbital targets shown. Grey shaded areas indicate MTM power spectra at >90% confidence levels.

8. The LogCaInt dataset was loaded into *PAST* (version 3.12) for a Continuous Wavelet Transform (CWT) analysis (Hammer et al., 2001).
    a. Power, Cone of Influence, and p=0.05 significance levels options were all chosen, with lag=0 and a sampling interval of 1.
9. A statistically significant strong spectral power is seen from ~$2^{4.4}$ to ~$2^{4.8}$ cycles/no. of sample.
    a. As data are loaded in as number of samples rather than sample depth (in meters), data was converted using the following equation, where x = spectral power and, y = 0.05 (the interpolated sampling frequency):

$$1 / (x * y) = \text{cycle/meter}$$

    b. Using this equation, the cycle frequency of the statistically significant spectral power range is 0.72 to 0.94, which agrees with the MTM analysis, suggesting the cyclicity discerned between these analyses are robust enough to infer a conclusion from.
    c. The spectral powers of the theoretical orbital frequencies obtained in Step 7 were calculated to see if the CWT analysis resolved these periodicities (Fig. 2.10) using the following equation, where OF = orbital frequency, and y = 0.05 (the sampling frequency):

$$\log_2[((1 / OF) / y)] = \text{spectral power for CWT analysis}$$

$$E1 = 2^{7.75}; E2 = 2^{6.07}; E3 = 2^{5.68}; O1 = 2^{4.68}; O2 = 2^{4.31}; P1 = 2^{3.57}; P2 = 2^{3.27}$$

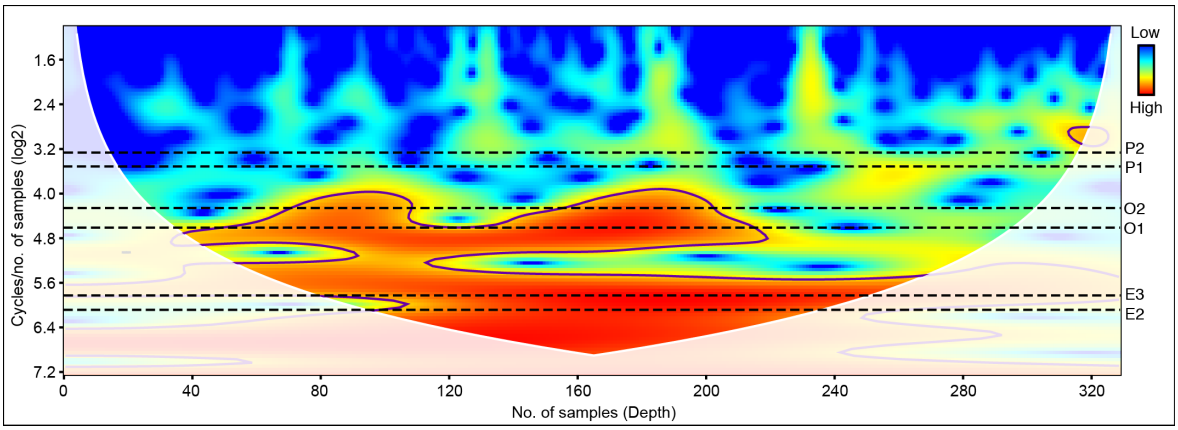

Figure 2.10: Continuous Wavelet Transform (CWT) analysis of interpolated logarithmic Ca XRF data, with calculated orbital targets shown (black dashed lines). White shaded area is the cone of influence, and purple line signifies p=0.05 boundary. Colour spectrum signifies spectral power.

2.8.9 References

Algeo, T.J., Tribovillard, N., 2009, Environmental analysis of paleoceanographic systems based on molybdenum-uranium covariation: Chemical Geology no. 268, p. 211–225. doi:10.1016/j.chemgeo.2009.09.001

Batenburg, S.J., Vleeschouwer, D. De, Sprovieri, M., Hilgen, F.J., Gale, A.S., Singer, B.S., Koeberl, C., Coccioni, R., Claeys, P., and Montanari, A., 2016, Orbital control on the timing of oceanic anoxia in the Late Cretaceous: Climate of the Past Discussions, doi: 10.5194/cp-2015-182.

Berger, A., Loutre, M.-F., and Laskar, J., 1992, Stability of the astronomical frequencies over the Earth's history for paleoclimate studies: Science, v. 255, p. 560.

Calvert, S., Pedersen, T., 1993, Geochemistry of recent oxic and anoxic marine sediments: implications for the geological record: Marine. Geology, no. 1-2, p. 67-88.

Cobban, W.A., and Scott, G.R., 1972, Stratigraphy and Ammonite Fauna of the Graneros Shale and Greenhorn Limestone Near Pueblo , Colorado Stratigraphy and Ammonite Fauna of the Graneros Shale and Greenhorn Limestone Near Pueblo , Colorado: Geological Survey Professional Paper 645, p. 1–195.

Dale, B., Fjellså, A., 1994, Dinoflagellate cysts as paleoproductivity indicators: state of the art, potential, and limits, in: Carbon Cycling in the Glacial Ocean: Constraints on the Ocean's Role in Global Change. Springer, p. 521–537.

Dodsworth, P., 2015, Palynostratigraphy and palaeoenvironments of the Eagle Ford Group (Upper Cretaceous) at the Lozier Canyon outcrop reference section, west Texas, USA: Palynology, no. 40(3), p. 357-378. doi:10.1080/01916122.2015.1073188

Eicher, D.L., 1965, Foraminifera and biostratigraphy of the Graneros Shale: Journal of Paleontology, p. 875–909.

Eldrett, J.S., Dodsworth, P., Bergman, S.C., Wright, M., and Minisini, D., 2017, Water-mass evolution in the Cretaceous Western Interior Seaway of North America and equatorial Atlantic: Climate of the Past, v. 13, p. 1–34, doi: https://doi.org/10.5194/cp-13-1-2017.

Eldrett, J.S., Ma, C., Bergman, S.C., Lutz, B., Gregory, F.J., Dodsworth, P., Phipps, M., Hardas, P., Minisini, D., Ozkan, A., Ramezani, J., Bowring, S.A., Kamo, S.L., Ferguson, K., et al., 2015, An astronomically calibrated stratigraphy of the Cenomanian, Turonian and earliest Coniacian from the Cretaceous Western Interior Seaway, USA: Implications for global chronostratigraphy: Cretaceous Research, v. 56, p. 316–344, doi: 10.1016/j.cretres.2015.04.010.

Eldrett, J.S., Minisini, D., and Bergman, S.C., 2014, Decoupling of the carbon cycle during Ocean Anoxic Event 2: Geology, v. 42, p. 567–570, doi: 10.1130/G35520.1.

Forster, A., Schouten, S., Moriya, K., Wilson, P.A., and Damsté, J.S.S., 2007, Tropical warming and intermittent cooling during the Cenomanian/Turonian oceanic anoxic event 2: Sea surface temperature records from the equatorial Atlantic: Paleoceanography, v. 22, p. 1–14, doi: 10.1029/2006PA001349.

Friedrich, O., Erbacher, J., Moriya, K., Wilson, P.A., and Kuhnert, H., 2008, Warm saline intermediate waters in the Cretaceous tropical Atlantic Ocean: Nature Geoscience, v. 1, p. 453–457, doi: 10.1038/ngeo217.

Gale, A.S., Voigt, S., Sageman, B.B., and Kennedy, W.J., 2008, Eustatic sea-level record for the Cenomanian (Late Cretaceous) - Extension to the Western Interior Basin, USA: Geology, v. 36, p. 859–862, doi: 10.1130/G24838A.1.

Hammer, Ø., Harper, D.A.T., and Ryan, P.D., 2001, Paleontological statistics software package for education and data analysis: Palaeontologia Electronica, v. 4, p. 9–18, doi: 10.1016/j.bcp.2008.05.025.

Jarvis, I., Gale, A.S., Jenkyns, H.C., and Pearce, M.A., 2006, Secular variation in Late Cretaceous carbon isotopes: a new delta C-13 carbonate reference curve for the Cenomanian-Campanian (99.6-70.6 Ma): Geological Magazine, v. 143, p. 561–608, doi: 10.1017/S0016756806002421.

Jenkyns, H.C., Gale, A. S., and Corfield, R.M., 1994, Carbon- and oxygen-isotope stratigraphy of the English Chalk and Italian Scaglia and its palaeoclimatic significance: Geological Magazine, v. 131, p. 1, doi: 10.1017/S0016756800010451.

Joo, Y.J.I., and Sageman, B.B., 2014, Cenomanian To Campanian Carbon Isotope Chemostratigraphy From the Western Interior Basin, USA: Journal of Sedimentary Research, v. 84, p. 529–542, doi: dx.doi.org/10.2110/jsr.2014.38.

Laskar, J., Fienga, A., Gastineau, M., and Manche, H., 2011, La2010: A new orbital solution for the long term motion of the Earth: Astronomy & Astrophysics, v. 4, p. 17, doi: 10.1051/0004-6361/201116836.

Laskar, J., Robutel, P., Joutel, F., Gastineau, M., Correia, a. C.M., and Levrard, B., 2004, A long-term numerical solution for the insolation quantities of the Earth: Astronomy and Astrophysics, v. 428, p. 261–285, doi: 10.1051/0004-6361:20041335.

Meyers, S.R., 2014, Astrochron: An R package for astrochronology: Available at c ran. rproject. org/web/packages/astrochron/index. html,.

Meyers, S.R., Sageman, B.B., and Arthur, M.A., 2012, Obliquity forcing of organic matter accumulation during Oceanic Anoxic Event 2: Paleoceanography, v. 27, p. 1–19, doi: 10.1029/2012PA002286.

Milnes, A.R., Fitzpatrick, R.W., 1989. Titanium and zirconium minerals. Miner. soil Environ. 1131–1205.

Mitchell, S.F., 1996, Foraminiferal assemblages from the late Lower and Middle Cenomanian of Speeton (North Yorkshire, UK): relationships with sea-level fluctuations and watermass distribution: Journal of Micropalaeontology, v. 15, p. 37–54.

Paillard, D., Labeyrie, L., and Yiou, P., 1996, Macintosh Program performs time-series analysis: Eos, Transactions American Geophysical Union, v. 77, p. 379, doi: 10.1029/96EO00259.

Paul, C., Mitchell, S., Marshall, J., and Leafy, P., 1994, Palaeoceanographic events in the Middle Cenomanian of Northwest Europe: Cretaceous Research, v. 15, p. 707–738, http://www.sciencedirect.com/science/article/pii/S0195667184710391 (accessed June 2016).

Scott, R.W., Franks, P.C., Evetts, M.J., Bergen, J.A., and Stein, J.A., 1998, Timing of mid-Cretaceous relative sea level changes in the Western Interior: Amoco No. 1 Bounds Core, *in* Stratigraphy and Paleoenvironments of the Cretaceous Western Interior Seaway, USA, Special Publications of SEPM, p. 35–58.

Sluijs, A., Pross, J., Brinkhuis, H., 2005. From greenhouse to icehouse; organic-walled dinoflagellate cysts as paleoenvironmental indicators in the Paleogene. Earth-Science Rev. 68, 281–315. doi:10.1016/j.earscirev.2004.06.001

Snow, L.J., Duncan, R.A., Bralower, T.J., 2005. Trace element abundances in the Rock Canyon Anticline, Pueblo, Colorado, marine sedimentary section and their relationship to Caribbean plateau construction and ocean anoxic event 2. Paleoceanography 20, 1–14. doi:10.1029/2004PA001093

Tribovillard, N., Algeo, T.J., Lyons, T., Riboulleau, A., 2006. Trace metals as paleoredox and paleoproductivity proxies: An update. Chem. Geol. 232, 12–32. doi:10.1016/j.chemgeo.2006.02.012

van Helmond, N.A.G.M., Sluijs, A., Reichart, G.-J., Sinninghe Damste, J.S., Slomp, C.P., Brinkhuis, H., 2014. A perturbed hydrological cycle during Oceanic Anoxic Event 2. Geology 42, 123–126. doi:10.1130/G34929.1

Wedepohl, K., 1991. The composition of the upper earth's crust and the natural cycles of selected metals. Metals in natural raw materials, in: Merian, E., Clarkson, T.W. (Eds.), Metals and Their Compounds in the Environment. VCH. 3-17.

Zheng, X.-Y., Jenkyns, H., Gale, A., Ward, D., and Henderson, G., 2016, A climatic control on reorganization of ocean circulation during the mid-Cenomanian event and Cenomanian-Turonian oceanic anoxic event (OAE 2): Nd isotope evidence: Geology, v. 44, p. 151–154, doi: 10.1130/G37354.1.

Chapter 3: Oceanographic and environmental influence on the Mid-Cenomanian Event in the Western Interior Seaway of North America

Sameer Y. Patel, Ian C. Harding, Jessica H. Whiteside, James S. Eldrett, Sargent Bray, and John E. A. Marshall

This chapter will be submitted to *Geology*.

Author contributions: S.Y.P collected and analysed the lipid biomarker and palynofacies data, with guidance from J.H.W., I.C.H., and J.S.E. Six samples were processed for lipid biomarker analyses by S.B., who also ran the GC-MS. S.Y.P. wrote the manuscript, with editorial input from I.C.H., J.H.W., J.S.E., and J.E.A.M.

3.1 Abstract

The Mid Cenomanian Event (MCE I) is considered a precursor to one of the largest magnitude carbon cycle perturbations of the Late Cretaceous, Oceanic Anoxic Event (OAE) 2. However, MCE I, itself, is not considered an OAE because it lacks global black shale deposition. Nevertheless, a diagnostic positive carbon isotope excursion (CIE) denoting the event is observed globally in carbonate sequences and organic carbon-rich mudrocks, such as in the central-eastern portion of the Western Interior Seaway (WIS) in North America. Here, we conduct the first lipid biomarker analysis of MCE I, and integrate trace metal and palynological data to resolve the nature of organic matter (OM) accumulation and preservation in the WIS at this time. We determine the close proximity of a large deltaic complex to our study site was pivotal in the formation of salinity-stratified waters during MCE I. Enhanced insolation-driven storm activity increased surface runoff and ventilated surface waters, and photic zone euxinia prevailed in the water column, allowing green sulphur bacteria to utilize OM under a sulfidic chemocline. Furthermore, enhanced Tethyan water mass influence on the environment promoted increased eukaryotic productivity, causing greater OM fluxes to the sediment-water interface, where refractory OM was preserved in bacterially-induced suboxic-anoxic conditions. Enhanced photosynthetic marine productivity during MCE I, as evidenced at this site, may have been a key driver of enhanced preservation of ^{13}C-enriched OM, ultimately contributing to the global nature of the positive CIE denoting this climatic event.

3.2 Introduction

The Late Cretaceous Epoch was punctuated by short-term extreme climatic events during which widespread marine anoxia led to the extensive deposition of organic-rich black shale deposits (oceanic anoxic events; OAEs; Schlanger and Jenkyns, 1976). The Cenomanian-Turonian boundary event (CTBE), also known as OAE 2, was one of the most significant Cretaceous OAEs, recording profound perturbations in the global carbon cycle (e.g., Jarvis et al., 2011) at a time when the epicontinental Western Interior Seaway (WIS) of North America extended from the proto-Gulf of Mexico to the Arctic Ocean (Kauffman, 1985). Prior to this, the Mid Cenomanian Event (MCE I) marked the beginning of a transitionary period in the Cenomanian oceanographic system as increasingly oxygen-depleted conditions were established in basins on a global scale, eventually leading into OAE 2 (Coccioni and Galeotti, 2003; Friedrich et al., 2009). MCE I is not considered an OAE because it lacks globally widespread black shale deposits (Coccioni and Galeotti, 2003). Nevertheless, positive carbon isotope excursions ($\delta^{13}C$ CIEs) identified in black shale deposits from the proto-Atlantic Tethyan realm (e.g., Friedrich et al., 2009), organic-rich mudrocks and marls in the WIS (e.g., Joo and Sageman, 2014; Eldrett et al., 2017) and carbonate-rich successions across Europe (review in Jarvis et al., 2006), demonstrate the global extent of this carbon cycle perturbation across anoxic and oxygenated marine settings. Positive $\delta^{13}C$ CIEs associated with OAEs are the result of enhanced photosynthetic productivity as this led to enrichments of ^{13}C in atmospheric and oceanic carbon reservoirs, which was subsequently mobilized, buried, and preserved (Jenkyns and Clayton, 1986). Therefore, reconciling environmental and climatic driving forces behind organic matter (OM) production and preservation in mid-Cenomanian times is key to understanding the global nature of MCE I.

During the Cenomanian, reorganizations of oceanographic circulation patterns, amongst other factors such as climatic changes, significantly influenced environmental conditions across global basins (Zheng et al., 2016). Oxygen-depleted Tethyan waters (Friedrich et al., 2009) migrated northward into the southern WIS in the early Cenomanian (Eldrett et al., 2017), before mixing with the Boreal-sourced central-WIS water mass during MCE I; when heightened solar insolation-driven storm activity prevailed (Chapter 2). This central WIS-Tethyan water mass connection significantly enhanced primary productivity (Chapter 2) and promoted the proliferation of diverse molluscan species across the basin (Cobban, 1993; Kauffman, 1985), signaling profound oceanographic and climatic changes influenced environmental conditions in WIS at this time.

In this paper, we conduct the first lipid biomarker analyses of mid-Cenomanian organic-rich mudrocks to determine how environmental and oceanographic changes influenced organic matter (OM) accumulation in the WIS, and in turn demonstrate this basin's role as an important organic carbon sink during MCE I.

3.3 Materials and methods

The AMOCO Rebecca K Bounds-1 core (Fig. 3.1; RKB-1; 38°29'26.0"N 101°58'29.7"W) from western Kansas, U.S.A., was deposited in the eastern-central region of the Cretaceous WIS and consists of organic-rich mudrocks, marls, and limestones. Lipid biomarker analyses were conducted on eighteen samples spanning MCE I between core depths 318.82 m and 338.02 m (Fig. 3.1), with TOC contents of 2.0-6.6 wt.% (Fig. 3.2). Aliphatic and aromatic fractions of samples obtained via standard lipid extraction and separation techniques were analysed by GC-MS (see GSA Data Repository). The GC-MS temperature program of Koopmans et al. (1996) was used for all samples to assess the presence of isorenieratene and its derivatives. Compounds were identified by comparison to North Sea Oil standards, and quantified by integration of appropriate peaks in specific ion chromatograms (e.g., *m/z* 57 for *n*-alkanes (*n*-C_x; x = carbon number), *m/z* 191 for hopanes, and *m/z* 217 for steranes). Lipid biomarker analyses were completed to elucidate OM sources, providing a comprehensive overview of paleoenvironmental conditions when combined with our earlier palynological and geochemical results (Chapter 2). Biomarker ratios used for palaeoenvironmental analyses can be found in the GSA Data Repository.

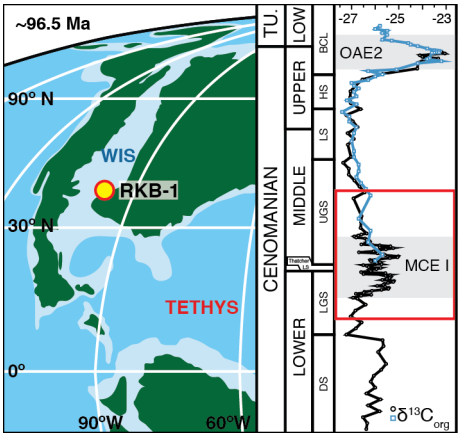

Figure 3.1: Left: Palaeogeographic map of the mid-Cenomanian Western Interior Seaway (modified after Blakey, 2014), showing the RKB-1 core location (star); Right: Carbon isotope stratigraphy of RKB-1 core (Chapter 2). Red box denotes study interval. DS = Dakota Sandstone, LGS = Lower Graneros Shale, UGS = Upper Graneros Shale, LS = Lincoln Shale, HS = Hartland Shale, BCL = Bridge Creek Limestone.

Total organic carbon (TOC), bulk organic carbon isotopes, and palynological data were obtained from Chapter 2. Amorphous organic matter content (AOM %) was estimated by visually scanning palynological slides, and additional palynomorph abundances (e.g., terrigenous organic matter) were obtained following standard methods (see GSA Data Repository).

The integrated dataset was divided into stages (pre-MCE, MCE 1a, MCE 1b, and post-MCE) based on CIE subdivisions of Chapter 2 to investigate environmental changes prior to, during, and after a persistent central WIS-Tethyan water mass connection was established during MCE I.

3.4 Results and discussion

3.4.1 Shoreline proximity

Molecular compound distributions (see GSA Data Repository for list of identified compounds) are dominated by short and mid-chain length alkanes (n-C_{17-26}) indicative of predominantly algal and/or bacterial-sourced OM input (review in Peters et al., 2005). However, pristane/n-C_{17} and phytane/n-C_{18} ratios (1.3–2.7 and 1.0–2.3, respectively; GSA Data Repository) demonstrate the low maturity OM was of mixed marine and terrestrial origin (Shanmugam, 1985; Peters et al., 2005). High continental:marine (C:M) palynomorph ratios (≥1) throughout the section (Fig. 3.2) support the biomarker proxy by showing a significant fraction of the visually distinguishable OM is terrigenous, of which phytoclasts are the dominant constituent (example in GSA Data Repository). The odd-even preference index, scaled to n-C_{27-33} (OEP; Scalan et al., 1970) indicates the presence of epicuticular waxes from vascular higher plant leaves (Rieley et al., 1991). All values are ≥1.0 (Fig. 3.2) and follow similar trends to those seen in the C:M record, corroborating the palynological observations. This continentally-derived OM was likely introduced via large deltaic complexes that spanned the latitudinal length of central Kansas as recorded by Hattin et al. (1987), when humid, subtropical climate (references in Arthur and Sageman, 2004) would have promoted enhanced continental runoff, as suggested in the upper Cenomanian in this region (Elderbak et al., 2014). Similar distributions of marine planktic-derived C_{27}-sterols (29-36%) and terrigenous-diagnostic C_{29}-sterols (25-36%) support these conclusions and indicate the Graneros Shale units in RKB-1 were deposited in near-shore estuarine/bay settings (GSA Data Repository; Huang and Meinschein, 1979; Hakimi et al., 2016).

3.4.2 Environmental control on organic matter accumulation across MCE I

Throughout the sampled record, high AOM contents (up to 90% of palynological assemblages) reflect TOC fluctuations (Fig. 3.2), highlighting this as a significant fraction of the preserved OM. Gammacerane indices of >0.1 (Fig. 3.2) indicate moderate water column stratification prevailed (Sinninghe Damsté et al., 1995). This, together with terrigenous-diagnostic OM records, indicates surface waters may have become brackish as a result of surface runoff from the proximal deltaic complex, which is suggested to have maintained its regional environmental influence until at least the earliest Turonian (Elderbak et al., 2014).

Prior to, and during the initial part of MCE 1a, distributions of eukaryotic and terrestrial-diagnostic regular C_{27-29} steranes compared to prokaryotic C_{29-33} hopanes (sterane:hopane ratio; Fig. 3.2; Liu et al., 2017 and references within) show bacterially-derived OM was relatively more dominant, as also reflected by the tricyclic triterpane:hopane ratio (GSA Data Repository; Marynowski et al., 2000). Low homohopane and lycopane indices (<10; modified from Peters and Moldowan, 1991

and <0.3; Sinninghe Damsté et al., 2003, respectively) demonstrate that conditions at the sediment-water interface were not fully anoxic, supported by low enrichment factors (EF) of redox-sensitive trace metals (<3 U_{EF} and Mo_{EF}; Fig. 3.2; Algeo and Tribovillard, 2009). Enhanced bacterial activity could explain the relatively high TOC contents (1-6%) in the prevailing suboxic (Tribovillard et al., 2012; GSA Data Repository), oligotrophic conditions (Chapter 2), as prokaryotic organisms may have utilized labile organic compounds (e.g., from the low levels of planktic productivity and/or from continental sources) to produce refractory organic carbon that was subsequently preserved, analogous to OM accumulation in modern oceans (e.g., Ogawa et al., 2001). Furthermore, the highest TOC-normalized abundances of isorenieratene derivatives are observed throughout the pre-MCE interval (Fig. 3.2). As isorenieratene is a characteristic pigment of anaerobic, photoautotrophic "green sulphur" bacteria that requires free hydrogen sulfide (H_2S) (see Koopmans et al., 1996), the identification of its diagenetic derivatives (Fig. 3.2; GSA Data Repository) indicate photic zone euxinia (PZE) was established as a sulfidic chemocline manifested below oxygenated surface waters throughout the succession (Fig. 3.3; Kump et al., 2005), lending support to enhanced bacterial activity.

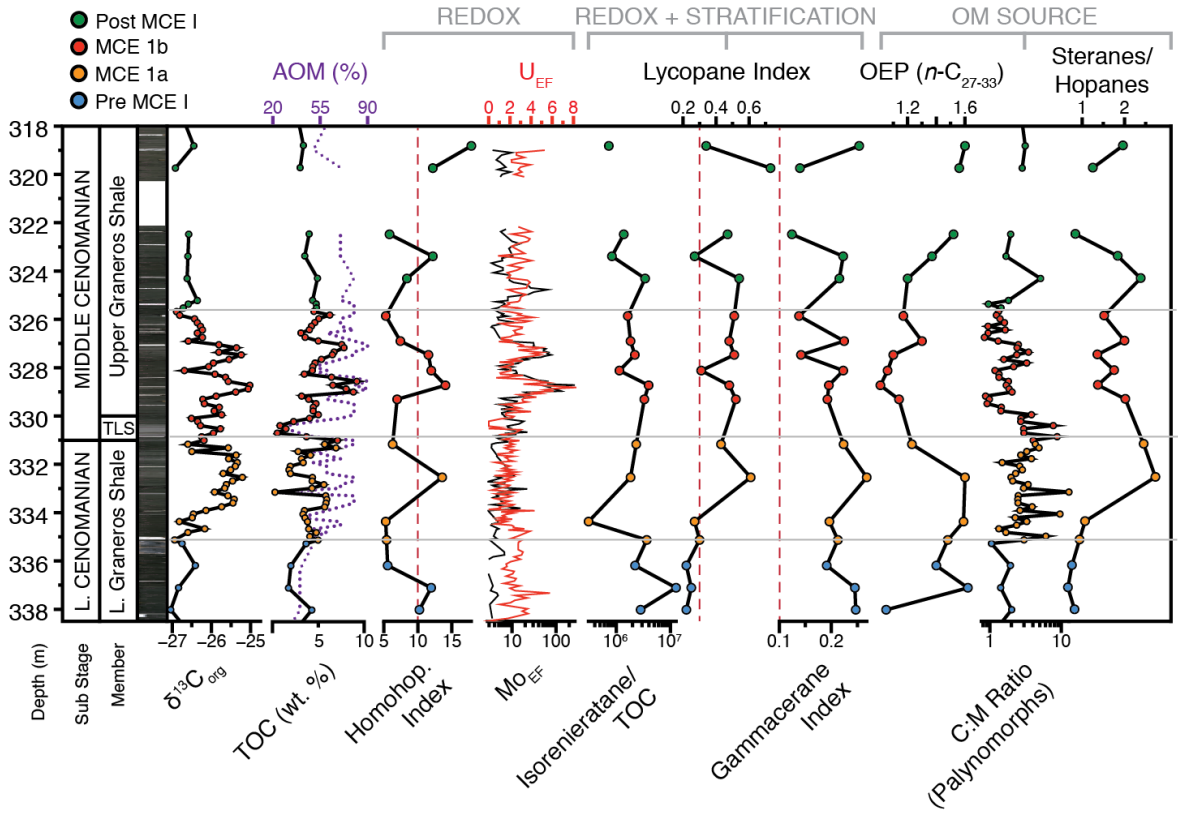

Figure 3.2: Integrated paleoenvironmental record for RKB-1 across MCE I. Bulk organic carbon isotope ($\delta^{13}C_{org}$), total organic carbon (TOC), uranium and molybdenum enrichment factors (U_{EF} and Mo_{EF}) from Chapter 2. AOM: amorphous organic matter (visual estimate). Homohop. Index: homohopane index = (100 × [C_{35}/(ΣC_{31-35}) αβ hopanes]); >10 = anoxia; (Peters and Moldowan, 1991). Lycopane Index: (Lycopane+*n*-C_{35})/*n*-C_{31}; >0.3 = bottom water anoxia in present day Black Sea (Sinninghe Damsté et al., 2003). Gammacerane Index: Gammacerane/C_{30}-17α-hopane; >0.1 = anoxia/salinity driven stratification (Sinninghe Damsté et al., 1995). OEP: Odd-even preference of C_{27-33} *n*-alkanes (Scalan et al., 1970). C:M Ratio: continental vs. marine palynomorph ratio. Steranes/Hopanes: Σ ((C_{27-29}ααα[S+R]) + (C_{27-29}αββ[S+R])) steranes) / (ΣC_{29-33}-17α-hopanes) (Liu et al., 2017).

MCE 1a records the lowest relative isorenieratene abundances before they steadily rise across this interval (Fig. 3.2), demonstrating PZE weakened as MCE I initiated, but then strengthened as Tethyan-influenced enhanced eukaryotic productivity prevailed (Fig. 3.2: sterane:hopane ratio). During MCE 1a, lycopane indices increase to values >0.3 (Fig. 3.2) demonstrating that OM was being preserved in increasingly oxygen-depleted, suboxic conditions (GSA Data Repository) at the sediment-water interface (Tribovillard et al., 2012; Sinninghe Damsté et al., 2003). Heightened C:M and OEP values illustrate there was also greater terrigenous input during this time, which may have been the result of heightened insolation-driven storm activity across this interval (Chapter 2). We suggest this might have resulted in increasingly nutrient-rich, oxygenated surface waters that could sustain the enhanced Tethyan-influenced planktic activity (Fig. 3.3), as reflected by heightened sterane:hopane ratios (see Liu et al., 2017).

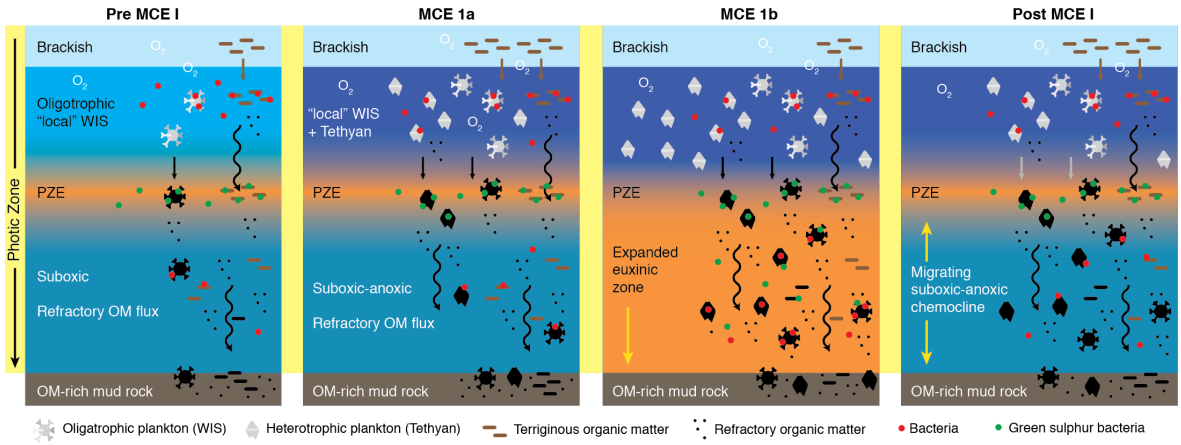

Figure 3.3: Conceptual mid-Cenomanian water column model for RKB-1. PZE = photic zone euxinia.

From the onset of MCE 1b, the decreasing C:M ratio and OEP index (Fig. 3.2) illustrate enhanced Tethyan-related marine productivity (Chapter 2) exerted a stronger influence on OM accumulation than freshwater runoff. However, terrigenous OM input was still substantial, as shown by C:M values ≥1, indicating surface waters were still well mixed and thus ventilated. Decreases in the sterane:hopane ratio coincident with TOC, U_{EF} and $Mo_{EF,}$ and homohopane index maxima during MCE 1b (Fig. 3.2; GSA Data Repository) may be evidence of enhanced bacterial activity below oxygenated surface waters that utilized large fluxes of organic-rich detritus, resulting from heightened eukaryotic productivity. Additionally, relative increases in the isorenieratene record coincide with Mo_{EF} maxima (Fig. 3.2), indicating PZE may have temporarily extended down to the sediment-water interface, further signifying increased prokaryotic activity relative to eukaryotic productivity (Fig. 3.3). These intervals might also have been associated with a strong metal-oxyhydroxide particulate shuttle mechanism (GSA Data Repository; Tribovillard et al., 2012), explaining the manifestation of strongly euxinic conditions in a basin that was, at the same time, becoming progressively less restricted as the Tethyan-central WIS connection became established. Alongside the lowest isorenieratene/TOC values across MCE 1b, the lycopane index falls below 0.3, coincident with the TOC and trace metal enrichment minima (Fig. 3.2; ~328m), indicating a

brief period of increasingly oxygenated conditions (Algeo and Tribovillard, 2009; Sinninghe Damsté et al., 2003). Relatively heightened sterane:hopane, OEP, and C:M values than those for the TOC maximum lower in this stage, indicate conditions were similar to those observed during MCE 1a; thus increased storm activity may have driven this time of enhanced oxygenation.

Post-MCE I, environmental conditions fluctuated between those observed during MCE 1a and MCE 1b (Figs. 3.2 and 3.3). Increases in the OEP and C:M indices, and decreases in the sterane:hopanes index indicate planktic productivity decreased after MCE I, suggesting the environmental influence of Tethyan waters reduced. Mo_{EF} and U_{EF} show the sediment-water interface returned to suboxic-anoxic conditions (GSA Data Repository) corroborating this interpretation. However, lycopane and homohopane indices display inverse relationships regarding anoxia-thresholds (Fig. 3.2), showing the chemocline may have been intermittently migrating from the sediment-water interface into water column (Fig. 3.3).

Together, these records demonstrate that basin-wide oceanographic changes and regional climatic conditions promoted enhanced photosynthetic bacterial and eukaryotic productivity at this site, resulting in notable ^{12}C-enriched OM accumulations. Furthermore, conditions conducive to OM preservation are observed across the WIS in this interval (e.g., Texas: Eldrett et al., 2017; Colorado: Joo and Sageman, 2014; Canada: Schröder-Adams et al., 2001). As such, the WIS served as an important organic carbon sink during MCE I, which together with other regionally extensive TOC-rich reservoirs (e.g., western Atlantic margin: Demerera Rise: Friedrich et al., 2009; Blake Nose: Ando et al., 2009) could help explain the global nature of the positive MCE I CIE at a time when globally widespread organic-rich mudrock deposition did not occur.

3.5 Conclusions

We determine that a stratified water column prevailed in the central-eastern WIS, as insolation-driven storm activity led to increased surface runoff from a large deltaic complex to the east, leading to the development of ventilated, brackish surface waters. Persistent photic zone euxinia through this record was symptomatic of enhanced productivity in these surface waters, under which a sulfidic chemocline developed. Bacteria within this zone and lower in the oxygen-starved water column utilized organic carbon fluxes, producing refractory organic carbon, which was subsequently preserved in suboxic-anoxic conditions across the sediment-water interface. Marine OM derived from enhanced photosynthetic-driven productivity at this site helps explain the global nature of the MCE I CIE, as this process would have resulted in enriched ^{13}C in the oceanic and atmospheric reservoirs. As such, environmental and oceanographic conditions at this site, together with extensive OM accumulations across the WIS played an intrinsic role in influencing the global carbon cycle during the mid-Cenomanian.

3.6 Acknowledgments

This work is supported by an industrial CASE studentship award (NE/L50161X/1) granted by the Natural Environment Research Council UK and Shell International Exploration & Production Inc. We extend our gratitude to the USGS CRC for donating sample material from their collection.

3.7 References

Algeo, T.J., and Tribovillard, N., 2009, Environmental analysis of paleoceanographic systems based on molybdenum-uranium covariation: Chemical Geology, v. 268, p. 211–225, doi: 10.1016/j.chemgeo.2009.09.001.

Ando, A., Huber, B.T., MacLeod, K.G., Ohta, T., and Khim, B.K., 2009, Blake Nose stable isotopic evidence against the mid-Cenomanian glaciation hypothesis: Geology, v. 37, p. 451–454, doi: 10.1130/G25580A.1.

Arthur, M.A., and Sageman, B.B., 2004, Sea-level control on source-rock development: Perspectives from the Holocene Black Sea, the Mid-Cretaceous Western Interior Basin of North America, and the Late Devonian Appalachian Basin: SEPM Special Publication, v. 82, p. 35–59.

Cobban, W.A., 1993, Diversity and distribution of Late Cretaceous ammonites, Western Interior, United States: Evolution of the Western Interior Basin: Geological Association of Canada Special Paper, v. 39, p. 435–451.

Coccioni, R., and Galeotti, S., 2003, The mid-Cenomanian Event: Prelude to OAE 2, *in* Palaeogeography, Palaeoclimatology, Palaeoecology, v. 190, p. 427–440, doi: 10.1016/S0031-0182(02)00617-X.

Elderbak, K., Leckie, R.M., and Tibert, N.E., 2014, Paleoenvironmental and paleoceanographic changes across the Cenomanian-Turonian Boundary Event (Oceanic Anoxic Event 2) as indicated by foraminiferal assemblages from the eastern margin of the Cretaceous Western Interior Sea: Palaeogeography, Palaeoclimatology, Palaeoecology, v. 413, p. 29–48, doi: 10.1016/j.palaeo.2014.07.002.

Eldrett, J.S., Dodsworth, P., Bergman, S.C., Wright, M., and Minisini, D., 2017, Water-mass evolution in the Cretaceous Western Interior Seaway of North America and equatorial Atlantic: Climate of the Past, v. 13, p. 1–34, doi: https://doi.org/10.5194/cp-13-1-2017.

Friedrich, O., Erbacher, J., Wilson, P.A., Moriya, K., and Mutterlose, J.J., 2009, Paleoenvironmental changes across the Mid Cenomanian Event in the tropical Atlantic

Ocean (Demerara Rise, ODP Leg 207) inferred from benthic foraminiferal assemblages: Marine Micropaleontology, v. 71, p. 28–40, doi: 10.1016/j.marmicro.2009.01.002.

Hakimi, M.H., Abdullah, W.H., Alqudah, M., Makeen, Y.M., and Mustapha, K.A., 2016, Reducing marine and warm climate conditions during the Late Cretaceous, and their influence on organic matter enrichment in the oil shale deposits of North Jordan: International Journal of Coal Geology, v. 165, p. 173–189, doi: 10.1016/j.coal.2016.08.015.

Hattin, D.E., Siemers, C.T., and Stewart, G.F., 1987, Upper Cretaceous stratigraphy and depositional environments of western Kansas: Guidebook of the Kansas Geological Survey, v. 3, p. 1–30, http://archives.datapages.com/data/kgs/data/039/039001/1_kgs0390001.htm.

Huang, W.-Y., and Meinschein, W.G., 1979, Sterols as ecological indicators: Geochimica et cosmochimica acta, v. 43, p. 739–745.

Jarvis, I., Gale, A.S., Jenkyns, H.C., and Pearce, M.A., 2006, Secular variation in Late Cretaceous carbon isotopes: a new delta C-13 carbonate reference curve for the Cenomanian-Campanian (99.6-70.6 Ma): Geological Magazine, v. 143, p. 561–608, doi: 10.1017/S0016756806002421.

Jarvis, I., Lignum, J.S., Gröcke, D.R., Jenkyns, H.C., and Pearce, M.A., 2011, Black shale deposition, atmospheric CO 2 drawdown, and cooling during the Cenomanian-Turonian Oceanic Anoxic Event: Paleoceanography, v. 26, p. 1–17, doi: 10.1029/2010PA002081.

Jenkyns, H.C., and Clayton, C.J., 1986, Black shales and carbon isotopes in pelagic sediments from the Tethyan Lower Jurassic: Sedimentology, v. 33, p. 87–106.

Joo, Y.J.I., and Sageman, B.B., 2014, Cenomanian to Campanian carbon isotope chemostratigraphy from the Western Interior Basin, USA: Journal of Sedimentary Research, v. 84, p. 529–542, doi: dx.doi.org/10.2110/jsr.2014.38.

Kauffman, E.G., 1985, Paleobiogeography and evolutionary response dynamic in the Cretaceous Western Interior Seaway of North America, *in* Jurassic-Cretaceous biochronology and paleogeography of North America, Geol. Assoc. Can. Sp. Pap, v. 27, p. 273–306.

Koopmans, M.P., Köster, J., Van Kaam-Peters, H.M.E., Kenig, F., Schouten, S., Hartgers, W.A., De Leeuw, J.W., and Sinninghe Damsté, J.S., 1996, Diagenetic and catagenetic products of isorenieratene: Molecular indicators for photic zone anoxia: Geochimica et Cosmochimica Acta, v. 60, p. 4467–4496, doi: 10.1016/S0016-7037(96)00238-4.

Kump, L.R., Pavlov, A., and Arthur, M.A., 2005, Massive release of hydrogen sulfide to the surface ocean and atmosphere during intervals of oceanic anoxia: Geology, v. 33, p. 397–400, doi: 10.1130/G21295.1.

Liu, B., Zhang, G., Mao, F., Liu, J., and Lü, M., 2017, Geochemistry and origin of Upper Cretaceous oils from the Termit Basin, Niger: Journal of Petroleum Geology, v. 40, p. 195–207, doi: 10.1111/jpg.12672.

Marynowski, L., Narkiewicz, M., and Grelowski, C., 2000, Biomakers as environmental indicators in a carbonate complex, example from the Middle to Upper Devonian, Holy Cross mountains, Poland: Sedimentary Geology, v. 137, p. 187–212, doi: 10.1016/S0037-0738(00)00157-3.

Ogawa, H., Amagai, Y., Koike, I., Kaiser, K., and Benner, R., 2001, Production of refractory dissolved organic matter by bacteria: Science, v. 292, p. 917–920, doi: 10.1126/science.1057627.

Peters, K.E., and Moldowan, J.M., 1991, Effects of source, thermal maturity, and biodegradation on the distribution and isomerization of homohopanes in petroleum: Organic Geochemistry, v. 17, p. 47–61, doi: 10.1016/0146-6380(91)90039-M.

Peters, K.E., Walters, C.C., and Moldowan, J.M., 2005, The biomarker guide: Cambridge University Press, v. 1.

Rieley, G., Collier, R.J., Jones, D.M., Eglinton, G., Eakin, P.A., and Fallick, A.E., 1991, Sources of sedimentary lipids deduced from stable carbon-isotope analyses of individual compounds: Nature, v. 352, p. 425.

Scalan, E.S., Smith, J.E., Melanogaster, D., and Dawood, M.M., 1970, An improved measure of the odd-even predominance in the normal alkanes of sediment extracts and petroleum: Geochimica et Cosmochimica Acta, v. 34, p. 611–620.

Schlanger, S.O., and Jenkyns, H.C., 1976, Cretaceous oceanic anoxic events: causes and consequences: Geologie en Mijnbouw, v. 55, p. 179–184.

Schröder-Adams, C.J., Cumbaa, S.L., Bloch, J., Leckie, D.A., Craig, J., Seif El-Dein, S.A., Simons, D.J.H.A.E., and Kenig, F., 2001, Late Cretaceous (Cenomanian to Campanian) paleoenvironmental history of the Eastern Canadian margin of the Western Interior Seaway: Bonebeds and anoxic events: Palaeogeography, Palaeoclimatology, Palaeoecology, v. 170, p. 261–289, doi: 10.1016/S0031-0182(01)00259-0.

Shanmugam, G., 1985, Significance of coniferous rain forests and related organic matter in generating commercial quantities of oil, Gippsland Basin, Australia: American Association of Petroleum Geologists Bulletin, v. 69, p. 1241–1254, doi: 10.1306/AD462BC3-16F7-11D7-8645000102C1865D.

Sinninghe Damsté, J.S., Kenig, F., Koopmans, M.P., Köster, J., Schouten, S., Hayes, J.M., and de Leeuw, J.W., 1995, Evidence for gammacerane as an indicator of water column stratification: Geochimica et Cosmochimica Acta, v. 59, p. 1895–1900, doi: 10.1016/0016-7037(95)00073-9.

Sinninghe Damsté, J.S., Kuypers, M.M.M., Schouten, S., Schulte, S., and Rullkötter, J., 2003, The lycopane/C31 n-alkane ratio as a proxy to assess palaeoxicity during sediment deposition: Earth and Planetary Science Letters, v. 209, p. 215–226, doi: 10.1016/S0012-821X(03)00066-9.

Tribovillard, N., Algeo, T.J., Baudin, F., and Riboulleau, A., 2012, Analysis of marine environmental conditions based on molybdenum-uranium covariation-Applications to Mesozoic paleoceanography: Chemical Geology, v. 324–325, p. 46–58, doi: 10.1016/j.chemgeo.2011.09.009.

Zheng, X.-Y., Jenkyns, H., Gale, A., Ward, D., and Henderson, G., 2016, A climatic control on reorganization of ocean circulation during the mid-Cenomanian event and Cenomanian-Turonian oceanic anoxic event (OAE 2): Nd isotope evidence: Geology, v. 44, p. 151–154, doi: 10.1130/G37354.1.

3.8 GSA Data Repository

3.8.1 Methods

3.8.1.1 Biomarkers

Lipid extractions from powdered, freeze-dried rock core samples (~1-3 g) were completed using a Thermo 250 Accelerated Solvent Extractor with dichloromethane:methanol (DCM:MeOH; 9:1 v/v), using the following program: preheat: 5 minutes; heat: 5 minutes; static: 5 minutes; pressure: 1,500 psi; flush: 70%; purge: 300 seconds; cycles: 3.

Solvent extracts were passed through activated copper columns to remove elemental sulphur and then reduced to dry residues with a Genevac EZ-2 vacuum centrifuge, and resultant total lipid extractions (TLEs) were quantified gravimetrically (Table 3.1). TLEs were loaded onto small silica gel columns to separate aliphatic, aromatic, and polar fractions using hexane, hexane:DCM (4:1), and DCM:MeOH (1:1), respectively.

Aliphatic and aromatic fractions were analyzed in full scan using a Thermo Trace 1310 gas chromatograph (DB-5 column; 30m x 0.25 mm internal diameter; 0.25 μm film thickness) coupled to a Thermo TSQ8000 mass spectrometer at the National Oceanography Centre Southampton, using the oven program detailed by Koopmans et al. (1996).

Depth (m)	TOC (wt. %)	$\delta^{13}C_{org}$	TLE (mg/g)
318.82	3.37	-26.45	2.7
319.74	3.01	-26.92	2.5
322.48	4.00	-26.58	3.4
323.39	3.52	-26.60	2.7
324.36	4.91	-26.62	3.9
325.68	4.52	-26.89	3.0
326.90	5.00	-26.59	3.2
327.47	6.54	-25.24	11.8
328.12	4.35	-26.69	4.6
328.73	6.59	-25.02	7.2
329.31	3.95	-26.22	3.7
331.17	5.69	-26.60	4.2
332.54	4.36	-25.21	13.3
334.37	3.82	-26.82	4.1
335.13	4.97	-26.94	2.3
336.19	2.00	-26.41	1.5
337.11	1.74	-26.84	2.8
338.02	4.29	-27.04	2.4

Table 3.1: Total lipid extract (TLE) quantities for each sample after solvent extraction. Total organic carbon (TOC) and bulk organic carbon isotope ($\delta^{13}C_{org}$) values from Chapter 2.

3.8.1.1.1 Palynology

Core material was broken into small fragments (<1 cm^3) and weighed, with 2-5 g being used for analyses. Samples were then processed for palynology at the National Ocenaography Centre in Southampton, UK, using the following protocol: treatment in 30% hydrochloric acid (HCl), followed by decanting the acid and washing samples until pH-neutral. This was followed by sample digestion in 60% hydrofluoric acid and subsequent acid decanting and sample neutralization. The resultant organic residue (kerogen) was sieved through a nylon mesh to obtain a ≥15 µm fraction, and spiked with 2-5 *Lycopodium* tablets (batch: 124961) to permit quantitative analysis. Residues were then rapidly boiled in 30% HCl to remove neo-formed flourides and decanted into ~250 ml of water before further sieving. Pyrite was removed by oxidizing samples in 30% nitric acid for 5 minutes, and amorphous organic matter (AOM) was disaggregated using a tunable ultrasonic probe for 40 seconds. After a final sieving, samples were strew-mounted on glass coverslips and left to dry. When dry, the coverslips were inverted and glued onto glass microscope slides using Elvacite 2044. Quantitative palynofacies data were collected by counting 300 marine and continental specimens per sample. The data were normalized to the out-of-count *Lycopodium* spike to obtain counts per gram (c.p.g.). AOM abundance was recorded by scanning palynofacies slides and visually estimating a relative percentage cover of each slide compared to the other palynomacerals present (see Fig. 3.4 example palynofacies slide). Marine palynomorphs

(dinocysts, acritarchs, and prasinophyte algae) were identified to genus or species level using the taxonomic nomenclature catalogued in (Williams et al., 2017).

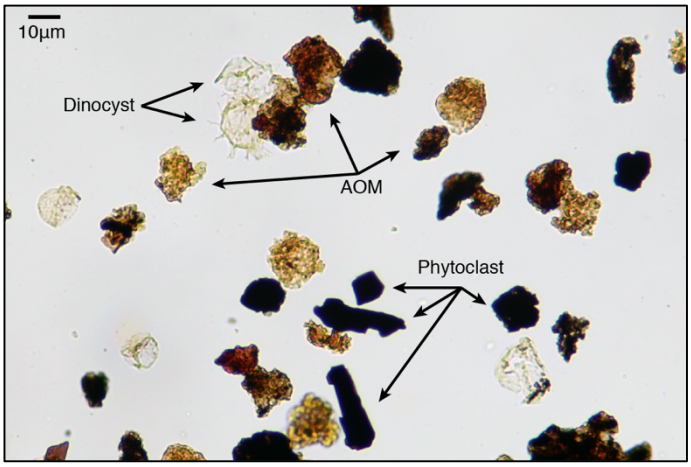

Figure 3.4: Example palynofacies assemblage from Lower Graneros Shale. AOM: amorphous organic matter.

3.8.1.2 Biomarker identification

Compounds were identified (Fig 3.5; Table 3.2) by correlating molecular peak retention times to those from the Norwegian Geochemical Standard North Sea Oil (NGS NSO-1; Patience et al., 2003), which was analyzed alongside samples in this study. Volatile, low molecular weight *n*-alkanes (< *n*-C_{17}) were not resolved due to the starting temperature of the GC-MS oven program used. The aromatic fraction of sample 319.74 m was not analyzed due to laboratory complications.

Elevated fragment ions (*m/z* 133 and 134) are used to determine the presence of isorenieratene and its diagenetic and catagenetic derivatives (aryl-isoprenoids; Koopmans et al., 1996). Although isorenieratene nor its diagenetic product isorenieratane was identified in any samples, isorenieratene derivatives were identified (Fig. 3.6) by scanning mass chromatograms filtered for *m/z* 133. It is possible isorenieratene and other derivatives, including isorenieratane, might be present in the polar fraction as organically-bound sulphur compounds (e.g., Sinninghe Damsté et al., 1993); however, Raney nickel desulphurization of this fraction would be needed in order to resolve these compounds (see Peters et al., 2005). Summed peak areas were normalized to TOC contents to compare relative intensities of photic zone euxinia (PZE) across the record.

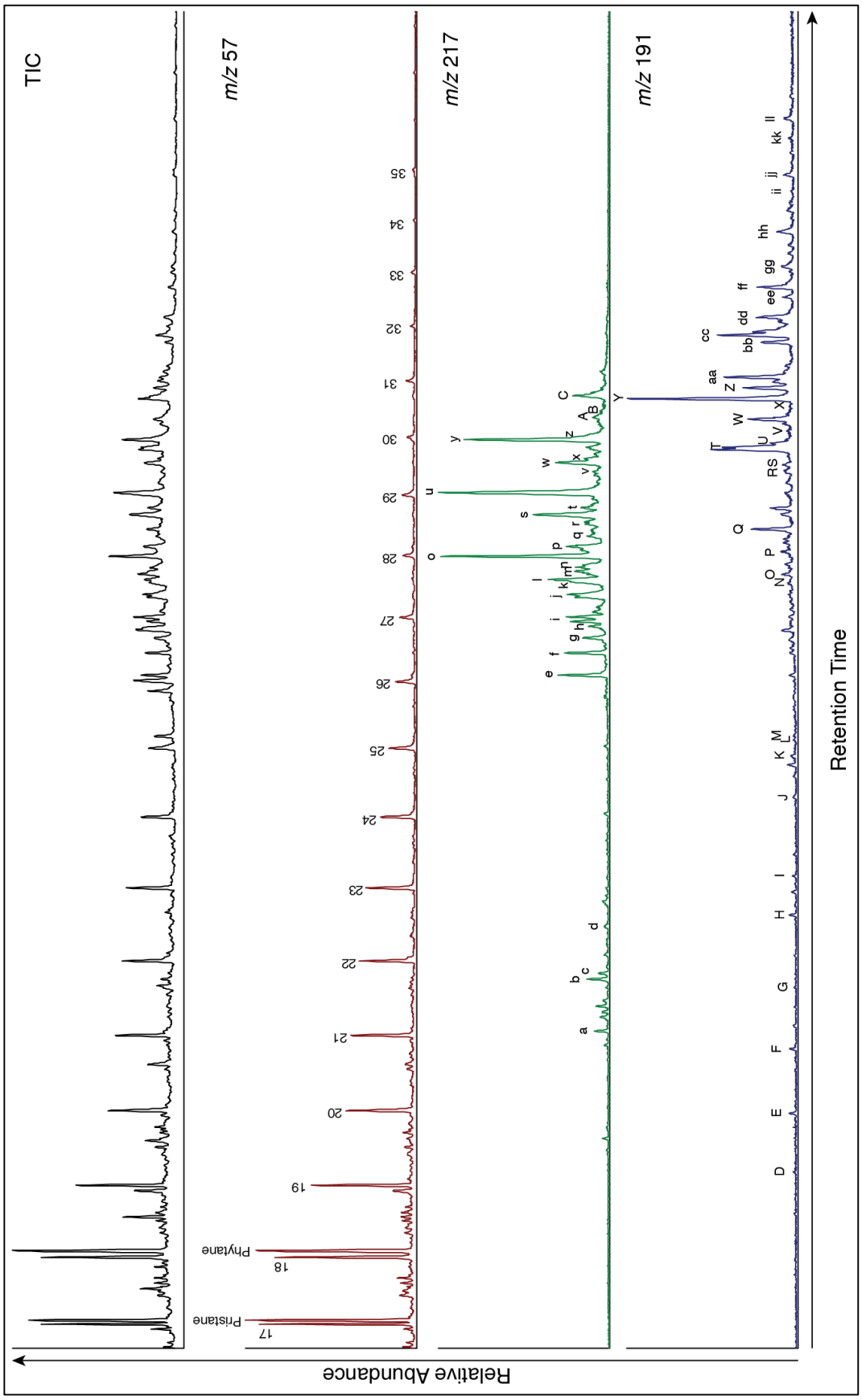

Figure 3.5: Example aliphatic fraction total ion chromatogram (TIC) and mass chromatograms used to identify alkanes (*m/z* 57), steranes (*m/z* 217) and hopanes (*m/z* 191) from sample 328.12m. Numbers in *m/z* 57 mass chromatogram refer to *n*-alkane carbon number, and letters in *m/z* 217 and *m/z* 191 mass chromatograms illustrate identified compounds and are defined in Table 3.2.

Steranes (m/z 217)		Hopanes (m/z 191)	
a	C_{21} diasterane	D	C_{19} tricyclic triterpane
b	C_{21} αββ diasterane	E	C_{20} tricyclic triterpane
c	C_{22} diasterane	F	C_{21} tricyclic triterpane
d	C_{22} αββ diasterane	G	C_{22} tricyclic triterpane
e	C_{27} dia β S	H	C_{23} tricyclic triterpane
f	C_{27} dia β R	I	C_{24} tricyclic triterpane
g	C_{27} diaα S	J	C_{25} tricyclic triterpane
h	C_{27} diaα R	K	C_{24} tetracyclic terpane
i	C_{28} dia β S	L	C_{26} tricyclic triterpane R
j	C_{28} dia β R	M	C_{26} tricyclic triterpane S
k	C_{28} dia α R	N	C_{29} tricyclic triterpane 22R
l	C_{27} ααα 20S	O	C_{29} tricyclic triterpane 22S
m	C_{29} dia β S	P	C_{27}-18α-22,29,30-trisnorhopane; Ts
n	C_{27} αββ 20S	Q	C_{27}-17α-22,29,30-trisnorhopane; Tm
o	C_{27} ααα 20R	R	C_{28} αβ (bisnorhopane)
p	C_{29} dia β R	S	C_{29}-25-nor-30αβ
q	C_{29} dia α R	T	C_{29} αβ (norhopane)
r	C_{28} ααα 20S	U	C_{29} Ts
s	C_{29} dia α S	V	C_{30} d (diahopane)
t	C_{28} αββ 20S	W	C_{29} βα (normoretane)
u	C_{28} ααα 20R	X	C_{30} oleanane
v	C_{29} ααα 20S	Y	C_{30} αβ hopane
w	C_{29} αββ 20R	Z	C_{30} 30-nor-29-homo-17aH-hopane
x	C_{29} αββ 20S	aa	C_{30} βα (moretane)
y	C_{29} ααα 20R	bb	C_{31} αβ S hopanes
z	C_{30} ααα 20S	cc	C_{31} αβ R hopane
A	C_{30} αββ 20R	dd	C_{30} Gammacerane
B	C_{30} αββ 20S	ee	C_{32} αβ S hopane
C	C_{30} ααα 20R	ff	C_{32} αβ R hopane
		gg	C_{33} αβ S hopane
		hh	C_{33} αβ R hopane
		ii	C_{34} αβ S hopane
		jj	C_{34} αβ R hopane
		kk	C_{35} αβ S hopane
		ll	C_{35} αβ R hopane

Table 3.2: Identified hopanes and sterane compounds within samples using Norwegian Geochemical Standard North Sea Oil as reference material. Letters refer to identified peaks in Figure 3.5.

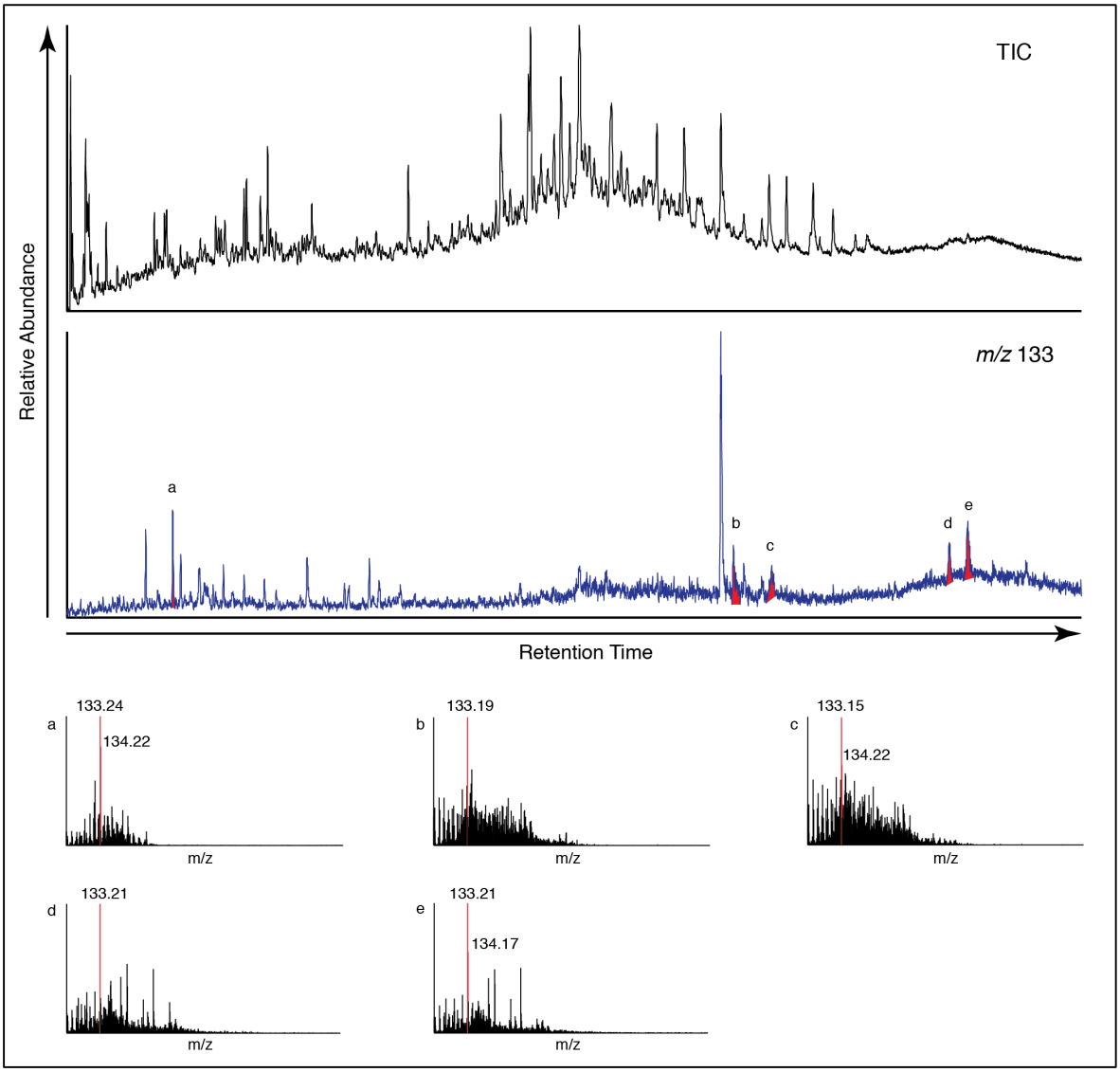

Figure 3.6: Example aromatic fraction total ion chromatogram (TIC) and mass chromatogram (*m/z* 133) for sample 332.54 m, used to identify isorenieratene derivatives (red peaks). Letters refer to mass spectra shown at bottom of figure. Red lines in mass spectra highlight characteristic elevated fragment ions of isorenieratene derivatives (e.g., Koopmans et al., 1996).

3.8.2 Biodegradation and thermal maturity

All total ion chromatograms (TICs) had small unresolved complex mixtures under slightly elevated chromatographic baselines (e.g., Fig. 3.5), indicating samples were subjected to little biodegradation (Peters et al., 2005). However, to remove potential bias from varying degrees of biodegradation across samples, biomarker ratios were used rather than absolute abundances.

During burial, isomerization of biologically unstable hopanes and steranes to geologically stable derivatives allow for the assessment of thermal maturity of samples. The degrees of isomerization of various hopanes and steranes have different equilibrium end values (Table 3.3), and so these indices are used in conjunction to obtain more robust assessments (Peters et al., 2005). Low values across all indices indicate samples are thermally immature, as supported by the identification of numerous well-preserved dinoflagellates (Chapter 2). Thus, biomarkers in this study should not be significantly affected by thermal degradation, allowing for their use as environmental indicators.

Thermal Maturity Index	Range of Utility	Averaged Sample Values	Reference
100 * Ts/(Ts+Tm)	0% (immature) to 100% (late oil generation)	26% (immature)	Peters et al., 2005
100 * C_{30} βα/(βα+αβ) hopanes	100% (immature) to 5% (early peak oil generation)	26% (immature)	Peters et al., 2005
100 * C_{32} αβ 22S/(22S + 22R) hopanes	0% (immature) to 60% (early oil generation)	23% (immature)	Peters et al., 2005
100 * C_{27} ααα 20S/(20S + 20R) steranes	0% (immature) to 55% (early oil generation)	24% (immature)	Cao et al., 2009

Table 3.3: Thermal maturity indices. Ts = C_{27} 18α-22,29,30-trisnorhopane; Tm = C_{27} 17α-22,29,30-trisnorhopane.

3.8.3 Environmental reconstructions

Equations for indices and ratios used in this study are given in Table 3.4.

3.8.3.1 Redox and water column stratification

Lycopane index: Lycopane is more readily degraded in oxic conditions within the sediment-water interface than long-chain *n*-alkanes and thus can be used as a redox indicator (Sinninghe Damsté et al., 2003). The lycopane index was found to increase in oxygen minimum zones within the sediment-water interface to levels >0.3, in modern settings (Arabian Sea), and heightened values have also been discerned in paleoenvironmental studies (e.g., Cenomanian-Turonian boundary samples; Sinninghe Damsté et al., 2003).

Homohopane index: C_{31-35} homohopanes are derived from functionalized C_{35} bacteriohopanepolyols in the lipid membranes of many bacteria (Peters and Moldowan, 1991). Under reducing conditions C_{35} homohopanes are preferentially preserved due to sulfurization reactions (Peters et al., 2005). Thus, the relative abundance of C_{35} to other homohopanes can be indicative depositonal redox conditions.

Gammacerane index: Gammacerane is derived from bacterivorous, anaerobic ciliates residing at/below the chemocline in highly stratified marine and non-marine settings, and so can used to indicate water column stratification (Sinninghe Damsté et al., 1995; Peters et al., 2005).

Pristane/Phytane ratio: Reducing/anoxic conditions promote the cleavage of the phytyl side chain in chlorophyll to produce phytol, which is subsequently converted to phytane. In oxic conditions, phytol is converted to pristane (Peters et al., 2005), and thus the ratio of these can be used to determine the redox potential in depositional settings. Low values (<1) indicate anoxic conditions, intermediate values (1-3) suggest suboxic conditions, and >3 values are indicative of terrestrial (oxic) settings (see Hakimi and Abdullah, 2013).

3.8.3.2 Sources of organic matter

Continental/Marine palynomorph ratio: The ratio of terrestrial palynodebris counts (phytoclasts, pollen, spores) against marine palynomorphs (dinoflagellates, prasinophytes, acritarchs) allows for the assessment of relative distributions of organic matter from marine and continental realms (adapted from Pross, 2001).

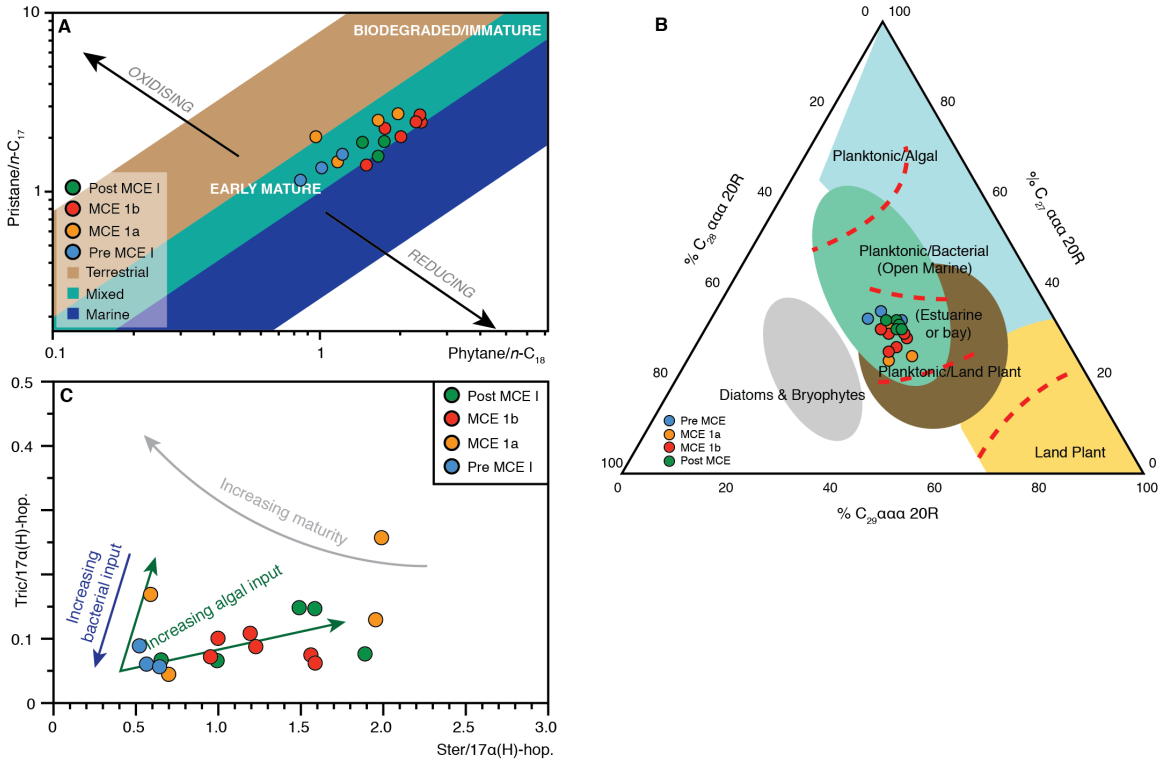

Figure 3.7: Pristane/*n*-C_{17} vs. Phytane/*n*-c_{18} plot showing redox conditions, organic matter sources, and maturity; adapted after Shanmugam (1985). Figure 5B: Distribution of C_{27-29} regular steranes showing organic matter source input; modified after Huang and Meinschein (1979) and Hakimi et al. (2016). Figure 5C: Cross plot of ΣC_{28-29} [20S+R] tricyclic triterpanes/C_{30}-17α-hopane vs. (ΣC_{27-29}ααα[S+R]+C_{27-29}αββ[S+R] steranes)/(ΣC_{29-33}-17α-hopanes), showing organic matter source variations; modified after Marynowski et al. (2000).

Sterane/Hopane ratio: Used to assess the relative contributions of eukaryotic (mainly algal and higher plant) vs. prokaryotic (bacterial) organic matter (Chakhmakhchev et al., 1996). Values generally approach unity or higher in marine organic matter, and lower values are indicative of microbially reworked and/or terrigenous organic matter (Chakhmakhchev et al., 1996).

Tricyclic Triterpane/Hopane ratio: Cyclisation of algal-derived regular hexaprenoles leads to the formation of tricyclic triterpanes (see Marynowski et al., 2000). Thus, the ratio of tricyclic triterpanoids to hopanes can indicate algal vs. bacterial organic matter input (Fig. 3.8C).

C_{29}/C_{27} Sterane ratio: C_{27} sterols are more abundant in red algae, and thus are indicative of marine organic matter (Peters et al., 2005). C_{29} sterols have been linked to green algae and terrigenous input, and so could be tentatively used as a continental organic matter source indicator (Huang and Meinschein, 1979).

BT/PHEN vs. Pr/Ph cross plots have been utilized to determine paleo-depositional environments (Fig. 3.9; Hughes et al., 1995). DBT and PHEN are products of geological degradation rather than direct organic matter input, and thus are controlled by the nature of the depositional environments rather than types of organic matter (Hughes et al., 1995). The origin of DBT can ultimately be correlated with the amount of H_2S available to interact with an organic substrate, thus increased

DBT/PHEN values reflect increases in reduced sulphur availability in the depositional environment (Hughes et al., 1995).

Free H_2S within the sediment was persistent across the record, as indicated by the presence of DBT. However, low DBT values may be resultant of H_2S being utilised in the water column by Chlorobiaceae, as indicated by the aryl-isoprenoid record. Although some samples plot in the lacustrine zone (Fig. 3.9), caution for this interpretation was given by Hughes et al. (1995) and palynological observations (Chapter 2) in conjunction with biomarker proxies demonstrate this lacustrine interpretation is not accurate, but rather marine conditions persisted across the record.

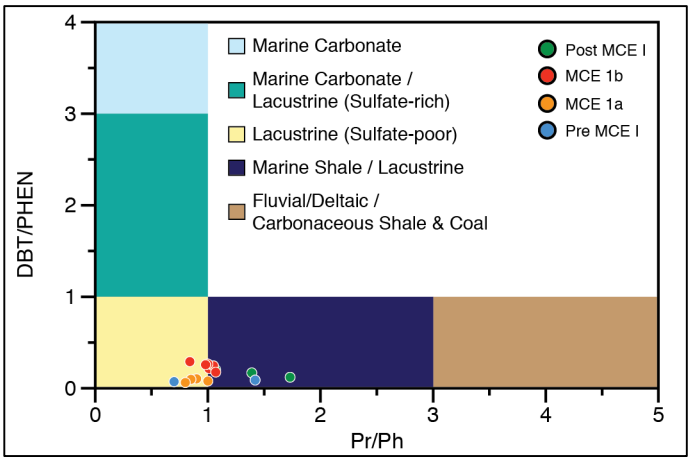

Figure 3.8: Dibenzothiophene/Phenanthene vs. Pristane/Phytane depositional environment cross plot (adapted after Hughes et al., 1995).

Index	Equation	Interpretations	Reference
Lycopane Index	$\frac{Lycopane + nC_{35}}{nC_{31}}$	>0.3 = sediment water interface anoxia	Sinninghe Damsté et al., 2003
Homohopane Index	$\frac{C_{35}\alpha\beta\ S + R}{\Sigma\ (C_{31-35}\alpha\beta\ S + R)} \times 100$	Increasing values = more reducing	Peters and Moldowan, 1991; Peters et al., 2005
Gammacerane Index	$\frac{Gammacerane}{C_{30}\ \alpha\beta\ hopane}$	>0.1 = stratified, anoxic waters	Sinninghe Damsté et al., 1995
Pristane/Phytane ratio	$\frac{Pristane}{Phytane}$	Lower values = more reducing; >3 = oxic	Peters et al., 2005
Continental/Marine palynomorph ratio	$\frac{Terrestrial\ counts}{Marine\ counts}$	Increasing values = more continental input	Pross, 2001
Sterane/Hopane ratio	$\frac{\Sigma\ [(C_{27-29}\ \alpha\alpha\alpha\ S + R) + (C_{27-29}\ \alpha\beta\beta\ S + R)]}{\Sigma\ (C_{29-33}\text{-}17\alpha\text{-}hopanes)}$	≥1 = marine organic matter; lower values indicate terrigenous input and/or bacterial reworking	Chakhmakhchev et al., 1996; Marynowski et al., 2000; Liu et al., 2017
Tricyclic Triterpane/Hopane ratio	$\frac{\Sigma\ (C_{28-29}\ S + R)\ Tricyclic\ Terpanes}{\Sigma\ (C_{30}\text{-}17\alpha\text{-}hopane)}$	Lower values = increasing bacterial input	Marynowski et al., 2000
C_{29}/C_{27} Sterane ratio	$\frac{(C_{29}\ \alpha\alpha\alpha\ S + R)}{(C_{27}\ \alpha\alpha\alpha\ S + R)}$	Higher values = more terrestrial input	Huang and Meinschein, 1979; Liu et al., 2017

Table 3.4: Biomarker and palynological indices used in this study.

Sample	Pr/Ph	Pr/nc17	Ph/nc18	OEP (C27-33)	Homohop. Index	Isoren/TOC	Lycopane Index	C29/C27 Steranes
318.82	1.39	1.75	1.45	1.60	17.87	727428	0.34	0.93
319.74	1.31	2.00	1.99	1.56	12.20	No Data	0.73	0.91
322.48	1.73	1.89	1.45	1.52	5.83	1373661	0.47	0.93
323.39	1.39	1.91	1.75	1.37	12.21	830741	0.27	0.89
324.31	1.07	1.58	1.66	1.20	8.39	3408431	0.54	0.89
325.86	1.01	2.03	2.02	1.17	5.29	1630314	0.51	0.81
326.90	0.84	1.41	1.50	1.30	7.43	1830996	0.48	0.83
327.47	1.05	2.45	2.41	1.10	11.56	2201670	0.51	0.66
328.12	1.00	2.26	1.76	1.06	11.98	1140679	0.31	0.83
328.73	1.07	2.69	2.38	1.01	14.06	3954845	0.48	0.64
329.31	0.98	2.46	2.30	1.14	6.95	3296186	0.52	0.80
331.17	1.00	2.73	1.97	1.23	6.30	2332761	0.43	0.61
332.54	0.90	2.51	1.66	1.60	13.58	1835108	0.61	0.69
334.37	0.85	2.03	0.97	1.59	8.11	307484	0.27	0.80
335.13	0.80	1.47	1.17	1.48	5.40	3653545	0.30	0.81
336.19	0.70	1.16	0.85	1.40	5.56	2224369	0.22	0.77
337.11	1.42	1.62	1.22	1.62	11.97	12704689	0.25	0.93
338.02	1.54	1.36	1.02	1.05	10.23	2815778	0.22	0.99

Sample	Gammacerane Index	Sterane/Hopane Ratio	Tric/17a(H)-hop.	%27aaaR	%28aaaR	%29aaaR	DBT/PHEN
318.82	0.25	2.17	0.15	30	36	34	0.15
319.74	0.14	1.35	0.07	30	37	33	No Data
322.48	0.12	0.89	0.07	32	34	34	0.15
323.39	0.22	2.03	0.15	31	37	32	0.12
324.31	0.22	2.47	0.08	30	38	32	0.17
325.86	0.14	1.59	0.09	33	36	31	0.20
326.90	0.22	2.15	0.07	30	40	30	0.22
327.47	0.14	1.23	0.07	33	39	28	0.29
328.12	0.22	1.62	0.11	30	39	31	0.25
328.73	0.20	1.30	0.10	35	38	27	0.27
329.31	0.19	2.10	0.06	34	34	32	0.18
331.17	0.22	2.57	0.13	36	39	25	0.26
332.54	0.27	2.69	0.26	31	43	26	0.08
334.37	0.21	0.84	0.17	34	34	32	0.10
335.13	0.21	0.92	0.04	32	35	33	0.10
336.19	0.19	0.76	0.06	35	30	34	0.06
337.11	0.25	0.71	0.09	32	32	36	0.07
338.02	0.25	0.87	0.06	29	37	34	0.09

Table 3.5: Values of biomarker indices for redox and organic matter source interpretations. All indices are described in text and Table 3.4.

3.8.4 References

Cao, C., Love, G.D., Hays, L.E., Wang, W., Shen, S., and Summons, R.E., 2009, Biogeochemical evidence for euxinic oceans and ecological disturbance presaging the end-Permian mass extinction event: Earth and Planetary Science Letters, v. 281, p. 188–201.

Chakhmakhchev, A., Suzuki, N., Suzuki, M., and Takayama, K., 1996, Biomarker distributions in oils from the Akita and Niigata Basins, Japan: Chemical geology, v. 133, p. 1–14.

Eldrett, J.S., Ma, C., Bergman, S.C., Lutz, B., Gregory, F.J., Dodsworth, P., Phipps, M., Hardas, P., Minisini, D., Ozkan, A., Ramezani, J., Bowring, S.A., Kamo, S.L., Ferguson, K., et al., 2015, An astronomically calibrated stratigraphy of the Cenomanian, Turonian and earliest Coniacian from the Cretaceous Western Interior Seaway, USA: Implications for global chronostratigraphy: Cretaceous Research, v. 56, p. 316–344, doi: 10.1016/j.cretres.2015.04.010.

Eldrett, J.S., Minisini, D., and Bergman, S.C., 2014, Decoupling of the carbon cycle during ocean anoxic event 2: Geology, v. 42, p. 567–570, doi: 10.1130/G35520.1.

Hakimi, M.H., and Abdullah, W.H., 2013, Geochemical characteristics of some crude oils from Alif Field in the Marib-Shabowah Basin, and source-related types: Marine and Petroleum Geology, v. 45, p. 304–314, doi: 10.1016/j.marpetgeo.2013.05.008.

Huang, W.-Y., and Meinschein, W.G., 1979, Sterols as ecological indicators: Geochimica et cosmochimica acta, v. 43, p. 739–745.

Hughes, W.B., Holba, A.G., and Dzou, L.I.P., 1995, the Ratios of Dibenzothiophene To Phenanthrene and Pristane To Phytane As Indicators of Depositional Environment and Lithology of Petroleum Source Rocks: Geochimica et Cosmochimica Acta, v. 59, no. 17, p. 3581–3598.

Koopmans, M.P., Köster, J., Van Kaam-Peters, H.M.E., Kenig, F., Schouten, S., Hartgers, W.A., De Leeuw, J.W., and Sinninghe Damsté, J.S., 1996, Diagenetic and catagenetic products of isorenieratene: Molecular indicators for photic zone anoxia: Geochimica et Cosmochimica Acta, v. 60, p. 4467–4496, doi: 10.1016/S0016-7037(96)00238-4.

Liu, B., Zhang, G., Mao, F., Liu, J., and Lü, M., 2017, Geochemistry and origin of Upper Cretaceous oils from the Termit Basin, Niger: Journal of Petroleum Geology, v. 40, p. 195–207, doi: 10.1111/jpg.12672.

Marynowski, L., Narkiewicz, M., and Grelowski, C., 2000, Biomakers as environmental indicators in a carbonate complex, example from the Middle to Upper Devonian, Holy Cross mountains, Poland: Sedimentary Geology, v. 137, p. 187–212, doi: 10.1016/S0037-0738(00)00157-3.

Peters, K.E., and Moldowan, J.M., 1991, Effects of source, thermal maturity, and biodegradation on the distribution and isomerization of homohopanes in petroleum: Organic Geochemistry, v. 17, p. 47–61, doi: 10.1016/0146-6380(91)90039-M.

Peters, K.E., Walters, C.C., and Moldowan, J.M., 2005a, The biomarker guide: Cambridge University Press.

Peters, K.E., Walters, C.C., and Moldowan, J.M., 2005b, The biomarker guide: Volume 2: Biomarkers and isotopes in petroleum systems and earth history: Cambridge University Press.

Pross, J., 2001, Paleo-oxygenation in Tertiary epeiric seas: evidence from dinoflagellate cysts: Palaeogeography, Palaeoclimatology, Palaeoecology, v. 166, p. 369–381.

Shanmugam, G., 1985, Significance of coniferous rain forests and related organic matter in generating commercial quantities of oil, Gippsland Basin, Australia: American Association of Petroleum Geologists Bulletin, v. 69, no. 8, p. 1241–1254, doi: 10.1306/AD462BC3-16F7-11D7-8645000102C1865D.

Sinninghe Damsté, J.S., Kenig, F., Koopmans, M.P., Köster, J., Schouten, S., Hayes, J.M., and de Leeuw, J.W., 1995, Evidence for gammacerane as an indicator of water column stratification: Geochimica et Cosmochimica Acta, v. 59, no. 9, p. 1895–1900, doi: 10.1016/0016-7037(95)00073-9.

Sinninghe Damsté, J.S., Kuypers, M.M.M., Schouten, S., Schulte, S., and Rullkötter, J., 2003, The lycopane/C31 n-alkane ratio as a proxy to assess palaeoxicity during sediment deposition: Earth and Planetary Science Letters, v. 209, no. 1–2, p. 215–226, doi: 10.1016/S0012-821X(03)00066-9.

Sinninghe Damsté, J.S., Wakeham, S.G., Kohnen, M.E., Hayes, J.M., and de Leeuw, J.W., 1993, A 6,000-year sedimentary molecular record of chemocline excursions in the Black Sea.: Nature, v. 362, no. 6423, p. 827.

Tribovillard, N., Algeo, T.J., Baudin, F., and Riboulleau, A., 2012, Analysis of marine environmental conditions based on molybdenum-uranium covariation-Applications to Mesozoic paleoceanography: Chemical Geology, v. 324–325, p. 46–58, doi: 10.1016/j.chemgeo.2011.09.009.

Chapter 4: Environmental evolution of the central-eastern margin of the Cenomanian Western Interior Seaway

Sameer Y. Patel, Ian C. Harding, James S. Eldrett, and John E. A. Marshall

This chapter will be submitted to *Cretaceous Research*.

Author contributions: S.Y.P collected and analysed the TOC, $\delta^{13}C_{org}$, palynological, XRF, and ICP-MS data, with guidance from I.C.H., J.S.E., and J.E.A.M. J.S.E. assisted in the collection of XRF data. S.Y.P. wrote the manuscript, with editorial input from I.C.H., J.S.E., and J.E.A.M.

4.1 Abstract

The Cretaceous Western Interior Seaway of North America (WIS) offers a unique insight into environmental responses to oceanographic changes during times of stressed global climates, such as during oceanic anoxic events (OAEs). Of these, OAE 2 (marking the Cenomanian-Turonian boundary), and more recently, the Mid-Cenomanian Event (MCE I), have been the focus of numerous studies as they represent two significant global carbon cycle perturbations. However, limited datasets for this interval in the central-eastern region of the WIS has meant that environmental and oceanographic reconstructions are not fully constrained on this side of the basin. Here, by completing an integrated palynological, geochemical, and sedimentological investigation of the Rebecca K Bounds-1 core from western Kansas, we demonstrate how dynamic water mass interactions across the basin influenced the environmental evolution of this section of the WIS.

We determine that the "local-WIS" watermass, which consisted of mixed Boreal and Tethyan waters eventually flooded terrestrial regions of central North America (e.g., central Colorado to western Kansas) during the early to mid-Cenomanian. At the start of MCE I, we record a short-lived southward incursion of Boreal waters, mirroring contemporaneous migrations documented from European sites, and thus demonstrate the global nature of this short-lived oceanic reorganisation. Following MCE I, local-WIS waters re-established until the Greenhorn Cyclothem, when a basin-wide Tethyan oceanic front migrated northwards into the central WIS. By the mid-late Cenomanian, Tethyan waters fully supplanted the local-WIS water mass, leading to intensely stratified, anoxic conditions that continued until the onset of OAE 2 in the latest Cenomanian. From the onset of OAE 2, we record a major oceanographic reorganisation in which the water column became increasingly ventilated and mixed. We attribute this to a second southward migration of Boreal waters and due to the rapid and widespread nature of this incursion, we

determine the conceptual cyclonic surface water gyre model put forward for the late Cenomanian-early Turonian was not the dominant driver of oceanic circulation during this interval.

4.2 Introduction

Well preserved Late Cretaceous strata from the Western Interior Seaway of North America (WIS) have been the subject of many palaeoceanographic and environmental studies (e.g., Siemers, 1976; Kauffman, 1977, 1985; Hattin et al., 1987; Eicher and Diner, 1989; Cobban, 1993; Dean et al., 1995; Schröder-Adams et al., 1996; Leckie et al., 1998; Sageman et al., 1998; Scott et al., 1998; Arthur and Sageman, 2004; Keller and Pardo, 2004; Meyers et al., 2012; Corbett et al., 2014; Eldrett et al., 2014, 2015a,b; Joo and Sageman, 2014). These analyses have contributed to the current holistic understanding of watermass circulation and oceanographic evolution across the basin, in particular from the late Cenomanian to the early Turonian when the most pronounced global carbon cycle perturbation of the Late Cretaceous occurred (Oceanic Anoxic Event 2; OAE 2) (e.g., Eicher, 1965; Kauffman, 1986, 1988; Hay et al., 1993; Slingerland et al., 1996; Gale et al., 2008; Elderbak et al., 2014; Elderbak and Leckie, 2016; Eldrett et al., 2017).

During the Cenomanian, an epeiric seaway extended across central North America as equatorial Tethyan waters reconnected to the Boreal-derived Mowry Sea during the third-order marine transgressive event formalised as the Greenhorn Cyclothem (Kauffman, 1977). The development of this fully connected seaway is believed to have impacted upon global climate and oceanic circulation patterns by: (1) creating a meridional oceanic "gateway" through which oxygenated, low salinity northern Boreal waters and stratified, normal-saline equatorial Tethyan waters could freely flow (Kauffman, 1985; Arthur and Sageman, 2004; Elderbak and Leckie, 2016; Eldrett et al., 2017); and (2) connecting high-latitude warm, humid regions to equatorial hot, arid zones (see Arthur and Sageman, 2004; Hay and Floegel, 2012).

This incursion of Tethyan waters into the WIS is thought to have allowed for the proliferation of calcareous plankton and molluscan macrofauna across the basin, as recorded in lithologic changes from organic-rich mudrocks to predominantly fossiliferous carbonate-rich facies leading up to and during OAE 2 (e.g., Eicher, 1965; Kauffman, 1985, 1986, 1988; Cobban, 1993; Fisher et al., 1994; Corbett et al., 2014). In the centre of the basin, today located in Colorado, this incursion is represented by the deposition of the mid-Cenomanian skeletal limestone tempestite marker bed, the Thatcher Limestone (Eicher, 1965; Cobban and Scott, 1972; Sageman, 1996; Gale et al., 2008). However, higher-resolution studies of the mid-Cenomanian global carbon cycle anomaly (the Mid-Cenomanian Event; MCE I) from western Kansas (Fig. 4.1) that encompass the Thatcher Limestone, demonstrate that the environmental influence of Tethyan waters occurred *prior* to the deposition of the tempestite (e.g., Kauffman, 1986; Chapters 2 and 3), leading to the development of a mixed Boreal and Tethyan "local-WIS" water mass. MCE I is considered a turning point in the

Cenomanian oceanographic system and a precursor to OAE 2, as it marks the beginning of a ~2 Myr transitionary period in many global basins towards increasingly stratified, oligotrophic surface and dysaerobic intermediate-bottom waters, which in turn led to stepwise extinctions of marine biota leading up to OAE 2 (Coccioni and Galeotti, 2003; Friedrich et al., 2009; Hardas et al., 2012; Gambacorta et al., 2016). However, from the onset of OAE 2 in the WIS, relatively well-oxygenated bottom waters from the central to southern regions of the basin (Leckie et al., 1998; Eldrett et al., 2014; Elderbak and Leckie, 2016), and the occurrences of Boreal-affiliated fossil dinoflagellate cyst (dinocyst) species (Eldrett et al., 2014, 2017; van Helmond et al., 2014), imply that changes in biodiversity may have been driven by a rapid southward Boreal incursion into the WIS, rather than being due to an enhanced Tethyan water mass influence during the late Cenomanian to early Turonian (Eldrett et al., 2017).

These findings demonstrate that our understanding of the complex, dynamic water-mass evolution in the WIS is still uncertain. Here we reconstruct Cenomanian palaeoenvironmental conditions in this section of the WIS by analysing a newly acquired multiproxy (palynological, geochemical, and sedimentological) dataset from western Kansas to reconstruct Cenomanian palaeoenvironmental conditions, and subsequently assess the evolution of the Cenomanian WIS water mass by integrating this dataset with those from the central and southern regions of the seaway.

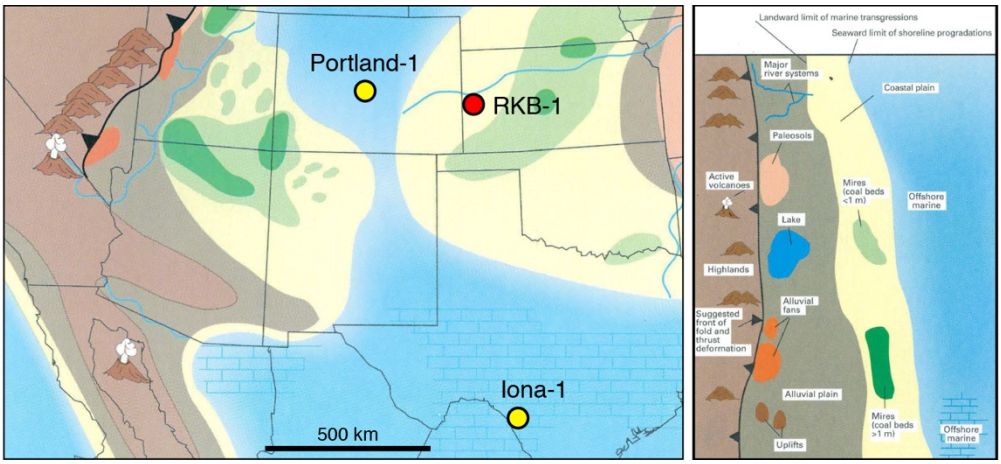

Figure 4.1: Early to mid-Cenomanian palaeogeographic reconstruction of the mid-southern Western Interior Seaway, with study location (RKB-1) shown in red. Adapted from Roberts and Kirschbaum (1995), courtesy of the U.S. Geological Survey.

4.3 Methods

4.3.1 Study Location

The Cenomanian WIS was contained within a north-south orientated asymmetric, retroarc foreland basin that developed during the late Jurassic to late Cretaceous Sevier Orogeny (Armstrong, 1968).

Continued thrusting and subsidence ultimately led the western side of the basin to form much deeper and consist of a thicker sediment fill than the stable eastern cratonic platform (Kauffman and Caldwell, 1993). Samples were acquired from the Rebecca K Bounds-1 (RKB-1) core by U.S. Geological Survey staff at the Core Research Centre in Denver, Colorado. RKB-1 was drilled by the AMOCO Production Company in central-western Kansas (38°29'26.0"N 101°58'29.7"W), and represents a site from the central-eastern margin of the Cenomanian WIS (Fig. 4.1).

The study interval extends from the Dakota Sandstone Formation (DS); through the Graneros Shale (comprising the Lower Graneros Shale [LGS], Thatcher Limestone [TL], and the Upper Graneros Shale [UGS] members); and into the Greenhorn Formation (consisting of the Lincoln Limestone [LL], Hartland Shale [HS], and Bridge Creek Limestone [BCL] members), spanning the early Cenomanian to early Turonian epochs (Dean et al., 1995; Scott et al., 1998). Sampling resolution was 90 cm across this interval, and higher resolution data from the Graneros Shale (Chapter 2) were integrated into the dataset.

4.3.2 Palynological analyses

Core material from the same sample intervals as for TOC was broken into small fragments (<1 cm^3) and weighed, with 2-5 g being used for analyses. Samples were then processed for palynology at the Ocean and Earth Science department at the University of Southampton, UK, using the following protocol: treatment in 30% hydrochloric acid (HCl), followed by decanting the acid and washing samples with de-ionised water until pH-neutral. This was followed by sample digestion in 60% hydrofluoric acid and subsequent acid decanting and sample neutralization. The resultant organic residue (kerogen) was sieved through a nylon mesh to obtain a ≥15 µm fraction, and spiked with 2-5 *Lycopodium* tablets (batch: 124961) to permit quantitative analysis. Residues were then rapidly boiled in 30% HCl to remove neo-formed flourides and decanted into ~250 ml of water before further sieving. Pyrite was removed by oxidizing samples in 30% nitric acid for 5 minutes, and amorphous organic matter (AOM) was disaggregated using a tunable ultrasonic probe for 40 seconds. After a final sieving, samples were strew-mounted on glass coverslips and left to dry. When dry, the coverslips were inverted and glued onto glass microscope slides using Elvacite 2044. Quantitative palynofacies data were collected by counting 300 marine and continental specimens per sample. The data were normalized to the out-of-count *Lycopodium* spike to obtain counts per gram (c.p.g.). AOM abundance was recorded by scanning palynofacies slides and visually estimating a relative percentage cover of each slide compared to the other palynomacerals present. Marine palynomorphs (dinocysts, acritarchs, and prasinophyte algae) were identified to genus or species level using the taxonomic nomenclature catalogued in (Williams et al., 2017), and absolute abundances (c.p.g.) of individual species were recorded by counting 100 marine specimens per sample and normalizing to out-of-count *Lycopodium* occurrences, using similar methods to Eldrett et al. (2015a).

4.3.2.1 Peridinioid vs. gonyaulaciod dinocyst ratio

Studies that utilise dinocysts for palaeoproductivity reconstructions primarily rely on the ratio of (proto-) peridinioid dinocysts (P-cysts) versus gonyaulacoid dinocysts (G-cysts; P:G dinocyst ratio) (e.g., Prauss, 2012; Dodsworth, 2015; Eldrett et al., 2017). Modern P-cysts have been found to be linked to nearshore or restricted areas in which terrestrial nutrient input is high, as well as in nutrient-rich upwelling regions, and most are known heterotrophs (review in Sluijs et al., 2005; Dodsworth, 2015). In contrast, G-cysts, are affiliated with oligotrophic and open marine environments and employ an autotrophic feeding strategy (Sluijs et al., 2005; Eldrett et al., 2017). Although the use of modern dinocysts as analogues for ancient species has its limitations (e.g., assuming heterotrophic feeding strategies for fossil P-cysts might be misleading; Dale and Fjellså, 1994), including fossil P-cysts with autotrophic feeding strategies in P:G dinocyst ratios should not significantly alter palaeoenvironmental signals (Sluijs et al., 2005). Furthermore, more reliable palaeoenvironmental and productivity reconstructions from the Cretaceous have been garnered when using the P:G ratio in conjunction with other geochemical, sedimentological, and biological proxies (e.g., Eldrett et al., 2017; Prauss, 2012; van Helmond et al., 2014). In this study, the cumulative total number of respective specimens are used for the P:G ratio. Further discussion on palynofacies ratios used in this study is found in the Supplementary Information.

4.3.2.2 Simpsons index of diversity

The Simpson's index of diversity (SID) was calculated for all samples in which marine palynomorphs were present using *PAST* (version 3.0; Hammer et al., 2001) to assess for ecological changes across the study interval, with higher values indicative of more diverse palynological assemblages (Simpson, 1949).

4.3.3 Total organic carbon, carbonate, and carbon isotope analyses

The bulk organic carbon isotope record ($\delta^{13}C_{org}$) of Dean et al. (1995) extending from the Upper Graneros Shale to the Bridge Creek Limestone members, and that from Chapter 2, which spans from the Dakota Sandstone to the Bridge Creek Limestone are used in this study. Bulk total organic carbon contents (TOC wt. %) and subsequent bulk carbonate content estimates ($CaCO_3$ wt. %) were obtained on sample splits following methods outlined by Forster et al. (2007). Additional TOC, $CaCO_3$, and $\delta^{13}C_{org}$ data for RKB-1 were integrated from the studies by Bojesen-Koefoed and Nytoft (2003) (spanning the Hartland Shale and Bridge Creek Limestone), Dean et al. (1995) and Chapter 2.

4.3.4 Trace metal analyses

Major and trace metal (TM) data were collected by both handheld XRF and ICP-MS methods from the Lower Graneros Shale, through the Thatcher Limestone, and into the Upper Graneros Shale. Additional records spanning the Hartland Shale and Bridge Creek Limestone (Bojesen-Koefoed and Nytoft, 2003), and from the Upper Graneros Shale to the Bridge Creek Limestone (Dean et al., 1995; Nakamura, 2015) were integrated into the dataset. All data (originally reported in parts per million, ppm) were normalised to zirconium (Eldrett et al., 2014) and enrichment factors relative to crustal averages were calculated (TM_{EF}) following methods used by (Brumsack, 2006) (see Supplementary Information for XRF and ICP-MS methods, and TM calibration discussion).

When assessing palaeo-redox conditions via TM analyses, uranium/thorium (U/Th) ratios were used as Th is predominantly detrital and relatively immobile in low-temperature surface conditions, whereas U in its 6+ valence state is readily soluble and so is lost during weathering. In contrast, U is insoluble in its 4+ valence state and so can be fixed in reducing conditions, leading to increased U supply via diffusion from seawater (see Jones and Manning, 1994), ultimately increasing U/Th values. Through factor analyses, Jones and Manning (1994) determined the U/Th ratio to be a reliable index for palaeoredox bottom water conditions, with values ≤ 0.75 indicating oxic settings, $0.75 \leq 1.25$ representative of dysoxic settings, and ≥ 1.25 showing suboxic and anoxic conditions prevailed. However, the geological context of sediments must be considered when using this ratio as U and Th are also enriched in volcanogenic material, and thus reworking of bentonitic layers may influence this index.

4.3.5 Bioturbation index

The degree of bioturbation (bioturbation index; BI) at each sample horizon was evaluated using a classification scheme adapted from Taylor and Goldring (1993). The grades used in this index range from 1 (no bioturbation) to 6 (complete bioturbation/completely homogenous), and were assigned from visual reviews of the RKB-1 core. BI 1 represents no bioturbation with clearly visible, undisturbed sub-millimetre laminations. Low levels of bioturbation, in which laminated layers are slightly disturbed and/or have "soft/hazy" boundaries are classified as grade BI 2. Moderately bioturbated sediments (BI 3) are classified by having frequently disrupted laminations and some evidence of vertical or horizontal burrowing. Clearly defined biotic structures cutting across a sedimentary fabric that is primarily destroyed through biotic reworking has been assigned BI 4 grade. Intense bioturbation (BI 5) is represented by complete biotic reworking of sediments, in which the original physical sedimentary structures have been obscured. BI 6 refers to completely homogenous sediments, which are the product of intense bioturbation. Examples for each grade can be found in the Supplementary Information.

4.4 Results and interpretations

4.4.1 WIS chronostratigraphic constraints on RKB-1

RKB-1 has been constrained to the astronomically-calibrated southern-WIS age model of Eldrett et al. (2015a) by correlating the $\delta^{13}C_{org}$ record to that of the Shell Iona-1 core (Texas; Eldrett et al., 2014) and the USGS Portland-1 core (Colorado; Joo and Sageman, 2014; Eldrett et al., 2017) (Fig. 4.2). In the absence of ammonite and inoceramid biostratigraphic constraints for RKB-1, other identifiable tie-points common to all cores have been used. These include the Albian-Cenomanian boundary (~100.5 Ma; Gradstein et al., 2012), which has previously been interpreted to lie within a hiatus in the Dakota Formation at 357.25 m in RKB-1 (Scott et al., 1998). Within the early Cenomanian, the beginning of the MCE I CIE (~96.57 Ma; Eldrett et al., 2015a) as identified in Chapter 2 in RKB-1 was used, and the base of the Thatcher Limestone marks the boundary between the early and mid-Cenomanian (~96.5 Ma; Eldrett et al., 2015a; Gale et al., 2008; Hook and Cobban, 2007). The end of the MCE I CIE (~96.36 Ma; Eldrett et al., 2015a), and the base of the basin-wide x-bentonite (~318.97 m; ~95.7 Ma Eldrett et al., 2015a) were used for mid-Cenomanian tie-points. Finally, for the late Cenomanian and early Turonian, three of four basin-wide bentonites (Elder, 1985) were identified: A-bentonite (299.62 m): ~94.57 Ma; B-bentonite (297.58 m): ~94.34 Ma; C-bentonite (294.73 m): ~93.67 Ma; (Dean et al., 1995; Sageman et al., 1998; Eldrett et al., 2015a).

Constant sedimentation rates between these tie points were assumed, other than between the Albian-Cenomanian boundary and the start of the MCE I as a distinct terrestrial-marine lithologic change is observed within this interval. Relatively consistent Fe_2O_3 and K_2O values across the Lower Graneros Shale (see Supplementary Information), extending from the basal Thatcher Limestone to the upper Dakota Formation contact indicate terrestrially derived sediment input was constant for this section. Thus, the calculated sedimentation rate between the basal Thatcher Limestone Member and the start of MCE I was extrapolated down to the Lower Graneros Shale-Dakota Formation contact. The resultant interpolated age at this contact was subsequently used to complete the age model for that part of the stratigraphy from the upper Dakota Sandstone/Lower Graneros Shale contact to the Albian-Cenomanian boundary interval (see Supplementary Information for interpolated age model using calculated sedimentation rates).

Figure 4.2: Bulk organic carbon isotope record ($\delta^{13}C_{org}$) and lithostratigraphic correlation of the RKB-1 to chronostratigraphically constrained $\delta^{13}C_{org}$ records of the Portland-1 and Iona-1 cores. Portland-1 $\delta^{13}C_{org}$ records from Joo and Sageman (2014) and Eldrett et al. (2017), and Iona-1 $\delta^{13}C_{org}$ record from Eldrett et al. (2015a). Age model from Eldrett et al. (2015a). Portland-1 ammonite biostratigraphy from Sageman et al. (1998) and Joo and Sageman (2014). RKB-1 lithostratigraphic boundaries and additional RKB-1 $\delta^{13}C_{org}$ data (blue) from Dean et al. (1995). Purple bar shows range of Boreal, early-Cenomanian *Cribroperidinium edwardsii* dinocyst in RKB-1. RKB-1 core photos courtesy of the U.S. Geological Survey.

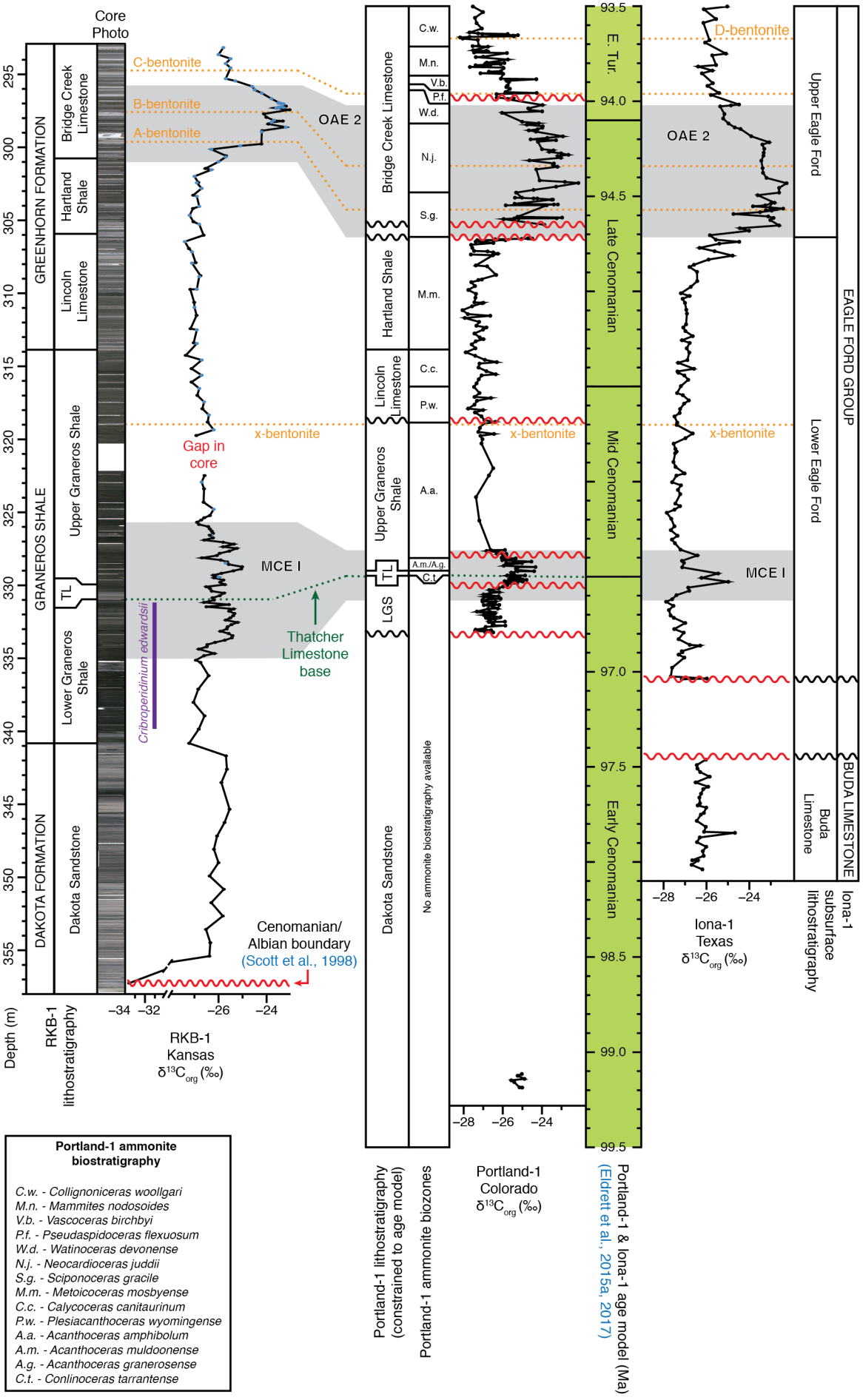

Portland-1 ammonite biostratigraphy

C.w. - Collignoniceras woollgari
M.n. - Mammites nodosoides
V.b. - Vascoceras birchbyi
P.f. - Pseudaspidoceras flexuosum
W.d. - Watinoceras devonense
N.j. - Neocardioceras juddii
S.g. - Sciponoceras gracile
M.m. - Metoicoceras mosbyense
C.c. - Calycoceras canitaurinum
P.w. - Plesiacanthoceras wyomingense
A.a. - Acanthoceras amphibolum
A.m. - Acanthoceras muldoonense
A.g. - Acanthoceras granerosense
C.t. - Conlinoceras tarrantense

4.4.2 Depositional environmental conditions (RKB-1)

4.4.2.1 Dakota Sandstone Formation

The studied Dakota Sandstone interval comprises of fine-grained sandstones, claystones and siltstones, and contains only continentally-derived palynomacerals, consisting of phytoclasts, higher plant tissues and cuticles, pollen, and spores (Figs. 4.3 and 4.4). Small-scale sedimentary structures (<1-10 cm) including lenticular- and flaser bedding, as well as ripple laminations are observed throughout the section, with relatively thicker mudstone beds often separating the sandstone-mudstone packages (e.g., Fig. 4.3). These sedimentary structures are interpreted to represent tidal rhythmites, which form when slackwater conditions and currents capable of bedload transports alternate in tidally-influenced, low-energy environments such as lagoons, estuaries, or bays (Kvale and Archer, 1991; Archer, 1995; Terwindt, 2009; Saeed and Evans, 2012). The upper section of the studied Dakota Sandstone interval contains increased TOC contents within darker coloured, finer grained beds, relative increases in phytoclasts, spores and pollen (e.g., ~341-346 m; Fig. 4.4), and numerous coal beds and rootlets (see Supplementary Information for visual example). Together, these are indicative of an organic-rich facies representative of either freshwater to brackish swamps in fluviodeltaic settings (Siemers, 1976), or lagoons/marshes near coastal margins of large deltaic complexes (Hattin et al., 1987). No freshwater palynomorphs were identified, indicating it is unlikely that deposition occurred in a freshwater swamp. However, the presence of *Monosulcites* angiosperm pollen and *Classopollis* gymnosperm pollen, typically found in subtropical swamps and lowlands that occupy coastal plains (Srivastava, 1976; Schrank, 2010; Akyuz et al., 2016), demonstrate deposition occurred within, or in close proximity to, a brackish coastal swamp. Alongside these observations, sedimentary structures within the upper Dakota Sandstone from central Kansas have previously been interpreted to represent active fills of fluvial channels (Hattin et al., 1987). Together, these observations suggest that a large central-Kansan deltaic complex (Hattin et al., 1987) extended westward to the RKB-1 site, which was situated in a tidally-influenced, marginal lagoon/marsh, corroborating the Cenomanian WIS palaeogeographic reconstruction of Roberts and Kirschbaum (1995) (Fig. 4.1).

4.4.2.2 Graneros Shale

Upwards from the Dakota Sandstone-Lower Graneros Shale boundary (~341 m), a significant change in the environmental regime is recorded, as the sedimentary matrix transitions from predominantly fine grained sandstones to mudstones and siltstones (Figs. 4.2 and 4.3). Decreasing bioturbation indices, increasing TOC and AOM contents, a distinct negative shift in $\delta^{13}C_{org}$ values, significant decreases in terrestrial palynomorphs (Fig. 4.4), and the first occurrence of dinocysts (Fig. 4.5), demonstrate oxygen-depleted, marine settings prevailed. This change to marine conditions signals a precursory regional transgressive event to the WIS 3rd order Greenhorn transgressive cyclothem (Kauffman, 1977).

In RKB-1, marine palynomorph assemblages across the Graneros Shale (314 - 341 m) are generally dominated by P-cysts (Fig. 4.5) indicating conditions mostly favoured heterotrophic productivity, and are interpreted to reflect the influence of southerly-sourced Tethyan waters that increased nutrient supply in surface and intermediate waters (Chapter 2; Chapter 3). However, within this interval, co-occurrences of the Boreal-affiliated *Cyclonephelium compactum–C. membraniphorum* dinocyst complex (Eldrett et al., 2014; van Helmond et al., 2014, 2016) alongside Tethyan-affiliated *Bosedinia* spp. dinocysts (Eldrett et al., 2017; Chapter 2) demonstrate a mixed water mass was present at this study site (Fig. 4.5). SID values remain consistent around ~0.8 (Fig. 4.5), denoting that this sequence contains the most diverse range of marine organic-walled planktic taxa in the study interval (Simpson, 1949), which in turn suggests environmental conditions were not stressed (Wall et al., 1977). This interpretation is corroborated by relatively low enrichments of redox-sensitive TMs (Figs. 4.5 and 4.6; MO_{EF}: ~1-10; V_{EF}: <3; U/Th: <1.25), which illustrate that water column conditions were mostly oxic-suboxic (Jones and Manning, 1994; Tribovillard et al., 2006; Algeo and Tribovillard, 2009). However, the presence of the photic zone euxinia (PZE)-indicative isorenieratene biomarker and its associated diagenetic products (e.g., Simons and Kenig, 2001; Chapter 3) demonstrate that the anoxic-euxinic conditions prevailed at least on a seasonal basis below productive surface waters (Sinninghe Damsté et al., 1993; Kump et al., 2005; Sun et al., 2016).

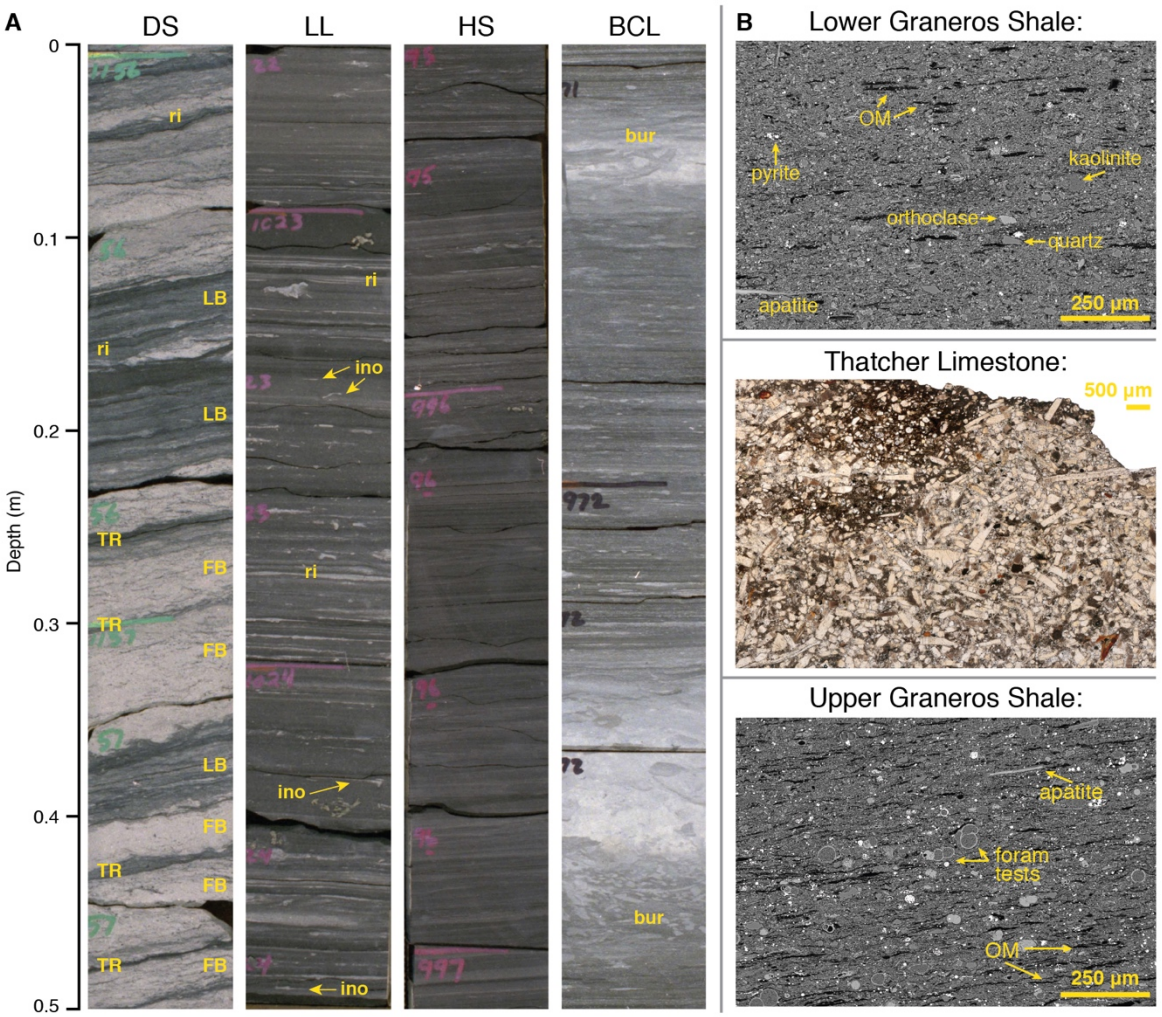

Figure 4.3: Example facies and microfacies/fabric of RKB-1 members in study interval. DS: Dakota Sandstone; LL: Lincoln Limestone; HS: Hartland Shale; BCL: Bridge Creek Limestone. DS, LL, HS, and BCL core photographs (A) courtesy of U.S. Geological Survey; (downwards depositional direction). FB: flaser bedding; TR: tidal rhythmites; LB: lenticular bedding; ri: ripple beds; ino: inoceramid shell fragments; bur: burrows; OM: organic matter. B) Lower Graneros Shale and Upper Graneros Shale: backscatter scanning electron microscope photographs. Thatcher Limestone: transmitted light microscope composite photograph showing disaggregated inoceramid shell fragments.

The presence of the dinocyst *Cribroperidinium edwardsii* throughout the Lower Graneros Shale, (Fig. 4.2; see Supplementary Information for full dinocyst records), also present in the Boreal-influenced, early Cenomanian Fish Scales Formation in south-eastern Alberta, Canada (Schröder-Adams et al., 1996), further support the characterisation of a mixed Boreal-Tethyan water mass at the RKB-1 site. Maximum absolute abundances of *C. edwardsii* alongside relative increases in *C. compactum–C. membraniphorum* just prior to the initiation of MCE I (represented by the dual-peaked positive CIE from ~335m to 326m; Mitchell, 1996; Chapter 2), and G-cyst dominated assemblages during the initial phase of MCE I (331-334 m; Fig. 4.4) show oligotrophic conditions temporarily prevailed (Chapter 2), indicating a strengthened Boreal water mass influence at this time. Microfacies analyses of the Lower Graneros Shale reveal a lack of preserved foraminiferal tests and inoceramid shell fragments within this unit (Fig. 4.3). However, these fossils do appear in the overlying Thatcher Limestone and Upper Graneros Shale (Fig. 4.3), and together with the absence of *C. edwardsii* from the Lower Graneros Shale-Thatcher Limestone boundary upwards, these records corroborate that a distinct change in environmental conditions is evident in the mid-Cenomanian (Gale et al., 2008; Chapter 2; Chapter 3). Furthermore, the composition of the Thatcher Limestone consists primarily of disaggregated inoceramid shell fragments within a calcite cement, interpreted as a tempestite (Sageman, 1996), and demonstrates a change to enhanced nutrient-rich conditions in which these molluscan bivalves could thrive.

In the Upper Graneros Shale, palynofacies assemblages across the second phase of MCE I (MCE 1b) are characterised by a marked increase of large (>500 µm), elongate, as-yet unclassified crescentic palynomacerals (Fig. 4.4; see Supplementary Information). This influx is coincident with periods of enhanced anoxic-euxinic conditions, as shown by elevated U/Th values and Mo enrichments (Fig. 4.5: 327-329 m; Fig. 4.6). During this interval, Tethyan waters exerted a stronger environmental influence on the mixed WIS water mass (Patel et al., in prep; Chapter 3), and may have even fully supplanted the local waters, as supported by a marked increase in *Bosedinia* spp. dinocysts alongside an absence of the *Cyclonophelium compactum–C. membraniphorum* dinocyst complex (Fig. 4.5).

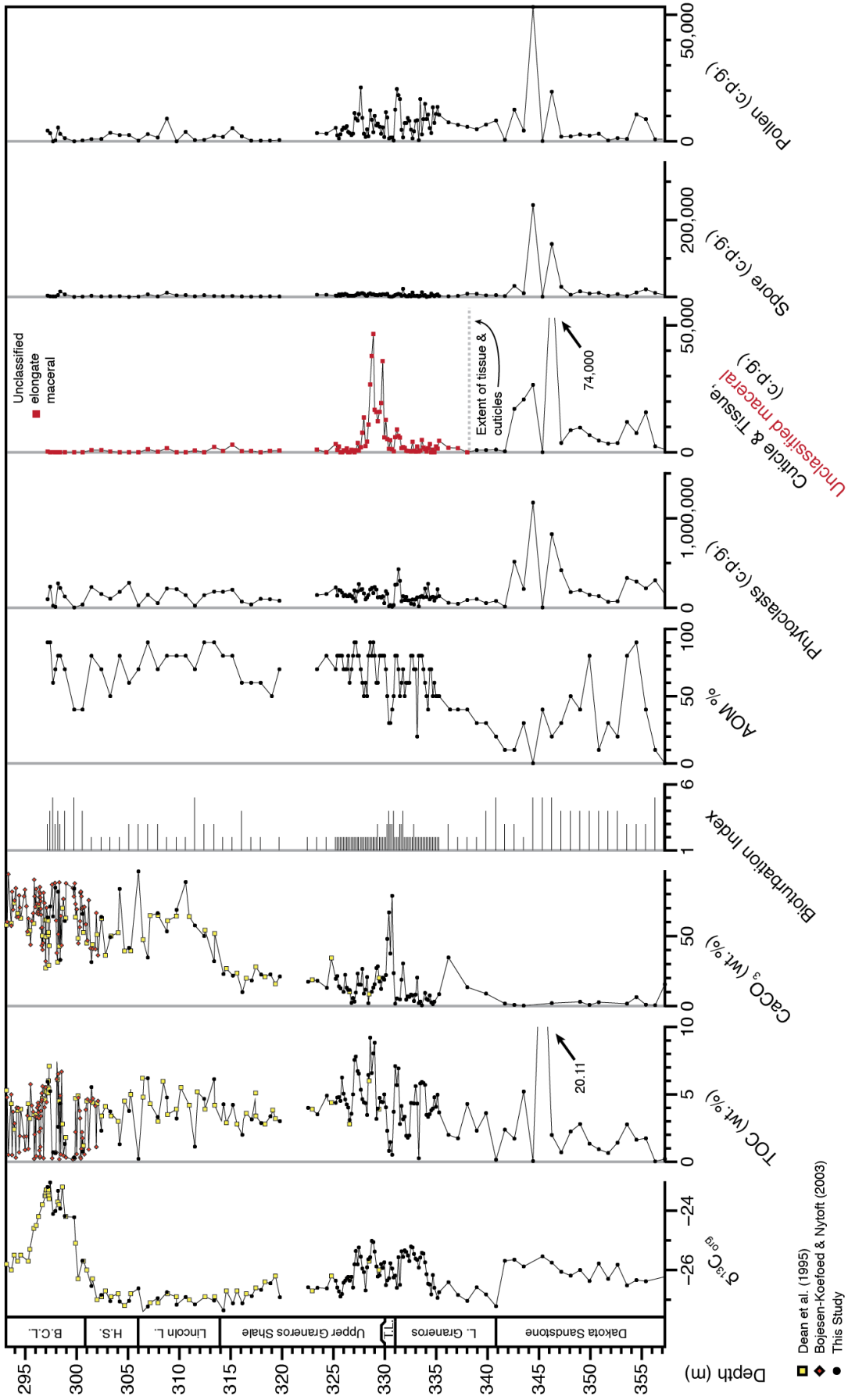

Figure 4.4: Geochemical and terrigenous palynofacies record for whole RKB-1 study interval. TOC: total organic carbon; AOM: amorphous organic matter; c.p.g.: counts per gram.

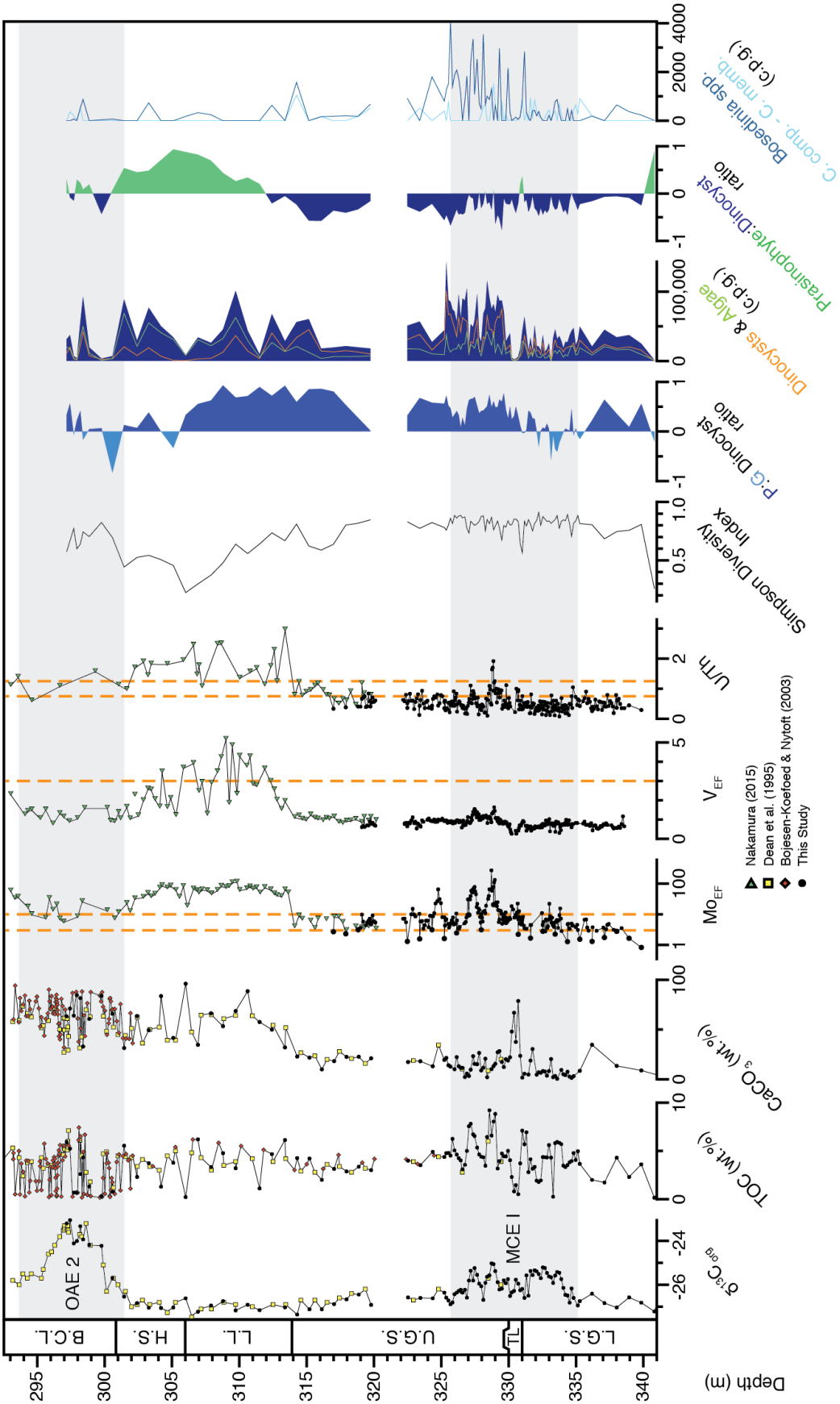

Figure 4.5: Geochemical and marine palynomorph record for the Greenhorn cyclothem in RKB-1 study interval. TOC: total organic carbon; EF: enrichment factor; P:G: peridinioid:gonyaulacoid dinocysts; C. comp – C. memb: *Cyclonephelium compactum–membraniphorum* Boreal-affiliated dinocyst complex; *Bosedinia* spp.: Tethyan-affiliated dinocysts; c.p.g.: counts per gram.

4.4.2.3 Lincoln Limestone Member

Through the Lincoln Limestone Member (306-314 m), the SID decreases, indicating increasingly stressed environmental conditions prevailed (Wall et al., 1977). In this interval, marine palynological assemblages are dominated by prasinophytes, and P-cysts remain the major constituent of the dinocyst community. Together with high TOC values (~3-6 wt. %; Fig. 4.5), these palynological data demonstrate stratified, eutrophic waters prevailed, under which organic-rich sediments could accumulate (Tyson, 1987; Prauss et al., 1991; Dodsworth, 2004; Eldrett et al., 2017). Similar palynomorph group distributions observed during the early Cenomanian in the Lower Eagle Ford Formation within the Iona-1 core (Eldrett et al., 2017) and from the Lozier Canyon outcrop in Texas (Dodsworth, 2015) are attributed to the introduction of relatively deeper waters from denitrification zones into the photic zone, either through the vertical expansion of the oxygen minimum zone or by upwelling (Dodsworth, 2015) when Tethyan waters migrated northward into the basin (Eldrett et al., 2017). These mechanisms could have promoted P-cyst and prasinophyte productivity through enhanced nitrite and ammonium availability, respectively (e.g., Prauss, 2007, 2012; Dodsworth, 2015). In RKB-1, significant enrichments of redox-sensitive TMs (e.g., V_{EF}: >3; U/Th: >1.25; Fig. 4.5), demonstrate bottom waters were oxygen-depleted (Jones and Manning, 1994; Tribovillard et al., 2006), thus suggesting a vertical expansion of the oxygen minimum zone may have stimulated P-cyst and prasinophyte productivity. High enrichments of Mo relative to U (Fig. 4.6) suggest euxinic conditions were also present (Algeo and Tribovillard, 2009), as has been shown in central Kansan and central Coloradan sites at the same latitude (Simons and Kenig, 2001). The identification of isorenieratene derivatives in coeval bioturbated strata on the east and west of our study locality demonstrate a dynamic water column structure was present during the Greenhorn Cyclothem, in which oxygenated bottom water conditions were punctuated by intermitted anoxia that extended upwards into the photic zone (Simons and Kenig, 2001). It is possible the MO_{EF}-U_{EF} record in RKB-1 is reflective of similar dynamics, further supporting the vertical expansion of the oxygen minimum zone into the photic zone. Increased microbial activity related to photic zone euxinia could have also led to enhanced Mo drawdown to the sediment-water interface as a strengthened Fe-Mn-oxyhydroxide particulate shuttle mechanism developed (Algeo and Tribovillard, 2009; Dellwig et al., 2010), similar to that seen when there was a greater Tethyan water mass influence during MCE I (Fig. 4.6; Chapter 3). Together with the dearth of the Boreal-affiliated *Cyclonophelium compactum–C. membraniphorum* dinocysts from the base of the Lincoln Limestone to the Bridge Creek Limestone (Fig. 4.5), these records show that Tethyan waters supplanted a local-WIS water mass during the deposition of the Lincoln Limestone, thus demonstrating the northerly migration of this southern watermass into the central WIS during the mid- to late Cenomanian.

However, from ~310m into the overlying Hartland Shale, there is a sharp decrease in absolute dinocyst and lower prasinophyte abundances, whilst carbonate contents remain ≥ ~40-50 %.

Intervals of increased bioturbation and a greater number of inoceramid shell fragments in the Lincoln Limestone compared to the underlying Graneros Shale (Figs. 4.3 and 4.4) demonstrate that benthic conditions, at least periodically, supported productivity at the seafloor, as also seen in central Colorado and Kansas (Simons and Kenig, 2001). As the flux of organic matter to the sea floor was persistent throughout the deposition of both units as evidenced by consistent TOC values, increased benthic activity has been attributed to increased ventilation, potentially resultant of increased upwelling or strengthened bottom currents (the latter represented by the identification of ripple marks; Fig. 4.3), demonstrating the dynamic nature of the stressed environmental conditions during the deposition of this member.

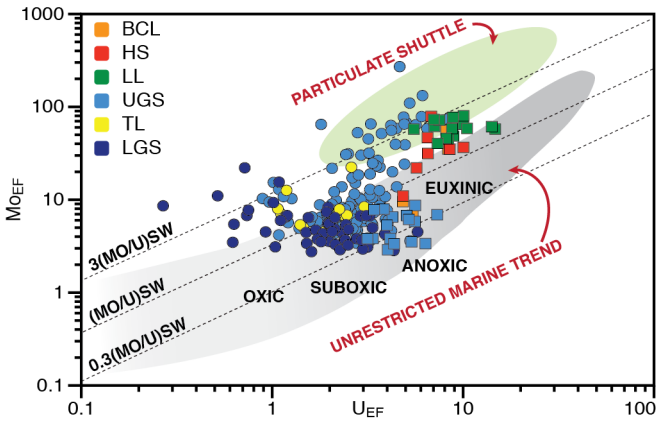

Figure 4.6: Mo:U enrichment ratios. Circles from this study; squares from Nakamura (2015); SW: seawater. Figure modified after Algeo and Tribovillard (2009) and Eldrett et al. (2014). LGS: Lower Graneros Shale; TL: Thatcher Limestone; UGS: Upper Graneros Shale; LL: Lincoln Limestone; HS: Hartland Shale; BCL: Bridge Creek Limestone.

4.4.2.4 Hartland Shale Member

In the Hartland Shale Member (301 - 306 m), the absolute abundances of marine palynomorphs and the SID both increase whilst the carbonate contents remain similar to the underlying Lincoln Limestone, indicating environmental conditions became less stressed (Wall et al., 1977). The P:G dinocyst ratio changes from being G-cyst dominated at the Lincoln Limestone/Hartland Shale contact to favouring P-cysts through the Hartland Shale (Fig. 4.5), indicating an increase of heterotrophic organic productivity. Sustained higher phytoclast abundances than those seen in the uppermost Lincoln Limestone (Fig. 4.4) show there may have been a relative increase in surface runoff from the eastern margin. Prasinophyte algae-dominated palynological assemblages (Fig. 4.5) indicate that the water column remained stratified throughout this part of the succession. However, lowered MO_{EF}:U_{EF} ratios (Fig. 4.6) suggest the particulate shuttle mechanism which was established during the deposition of the underlying Lincoln Limestone weakened and eventually ceased (Algeo and Tribovillard, 2009). Furthermore, although V_{EF}, U/Th, and MO_{EF} values decrease throughout the deposition of the Hartland Shale, they remain within suboxic-anoxic thresholds, indicating oxygen-depleted conditions were still present within deeper sections of water column (Jones and Manning, 1994; Tribovillard et al., 2006; Algeo and Tribovillard, 2009), and

still intermittently extended into the photic zone, as observed in other central-WIS sites (Simons and Kenig, 2001), thus providing a mechanism for enhanced ammonium and nitrite delivery to surface waters. Finely laminated mudstone-carbonate beds with infrequent low intensity bioturbation (BI 2), and few bivalve shell fragments further demonstrate bottom water ventilation was dynamic (Figs. 4.3 and 4.4), supporting similar observations from Colorado (Sageman, 1989).

4.4.2.5 Bridge Creek Limestone Member

The Bridge Creek Limestone contains a positive ~2 ‰ CIE denoting the global carbon cycle perturbation OAE 2, as also recorded in the Coloradan Portland-1 core (Fig. 4.2; Sageman et al., 1998; Joo and Sageman, 2014). Within OAE 2, increased bioturbation across the WIS (e.g., Colorado: Desmares et al., 2007; Texas: Eldrett et al., 2014), and diverse benthic foraminiferal assemblages (Keller and Pardo, 2004; Elderbak and Leckie, 2016) indicate that sediment-water interfaces across the basin were well ventilated, highlighting a "benthonic"/ "benthic oxic zone" developed across the seaway (Eicher and Worstell, 1970; Keller and Pardo, 2004; Eldrett et al., 2017). Together with occurrences of the Boreal-affiliated *Cyclonophelium compactum–C. membraniphorum* dinocyst complex in central and southern WIS localities (Eldrett et al., 2014, 2017; van Helmond et al., 2014), these data record a rapid southward incursion of Boreal waters (Elderbak and Leckie, 2016; Eldrett et al., 2017), as also observed in European and Atlantic sites representing the short-term climatic cooling episode known as the Plenus Cold Event (e.g., Gale and Christensen, 1996; Jarvis et al., 2011; van Helmond et al., 2016). In RKB-1, a marked decrease in TOC, AOM, and intense bioturbation consisting of large (≥ 1 cm diameter) burrows (Figs. 4.3 and 4.4) show that a benthic/benthonic oxic zone also developed at this site. Low Mo and V enrichment (~1) and U/Th values between 0.75-1.25 across OAE 2 further demonstrate that anoxic-euxinic benthic conditions were replaced by oxic-dysoxic/suboxic conditions (Jones and Manning, 1994; Algeo and Tribovillard, 2009). A decrease in prasinophyte phycomata and increased abundances of dinocysts (Fig. 4.5) illustrate that water column stratification weakened, and a shift to P-cyst dominated assemblages indicate that nutrient availability increased as the water column became more mixed. The re-appearance of the *Cyclonophelium compactum–C. membraniphorum* dinocyst complex within the benthic oxic zone interval (Fig. 4.5), and the presence of *Coscinophragma? codyensis*, a northern-affiliated benthic agglutinated foraminifera, in central Colorado (Elderbak and Leckie, 2016) indicate a there was a southward incursion of Boreal waters into the central WIS at this time, which could have promoted mixing of the local water mass.

However, the studied interval of the Bridge Creek Limestone is not uniformly bioturbated, and transitions between bioturbated limestones and laminated marlstone packages are observed (e.g., Figs. 4.2 and 4.3). In central Colorado, at the Global Boundary Stratotype Section Point (GSSP) for the Cenomanian – Turonian and neary localities, these limestone-marlstone packages within the Bridge Creek Limestone are interpreted to result from Milankovitch-paced orbital cyclicity (Sageman et al., 1998; Meyers et al., 2012b), which in turn influenced the climatic conditions that

controlled productivity and dilution cycles within the basin (e.g., Eicher and Diner, 1989; Elderbak and Leckie, 2016), leading to carbonate-rich deposits being produced during insolation maxima, and organic-rich sediments being deposited during insolation minima (Eldrett et al., 2015b).

Although the RKB-1 palynological record is of low resolution for the Bridge Creek Limestone interval studied, alternations within the P:G ratio can tentatively be discerned (Fig. 4.5), and variations in the phytoclast record are observed (Fig. 4.4). To determine if these are representative of Milankovitch-paced climatic variability, higher resolution studies would need to be undertaken.

4.4.3 Cenomanian WIS watermass evolution

4.4.3.1 Early Cenomanian

The central-eastern RKB-1 site was deposited in a continental – deltaic/coastal plain environment that extended from central Kansas to at least central Colorado in the early Cenomanian (Siemers, 1976; Hattin et al., 1987). In contrast, early Cenomanian deposits (~97.5 – 98 Ma) from the southern WIS (Eldrett et al., 2015a) and Canadian Albian-Turonian sections are of marine origin (Schröder-Adams et al., 1996; Eldrett et al., 2015a). Thus, as the WIS developed asymmetrically with western foredeep sub-basins thinning eastwards on a stable cratonic platform (Kauffman, 1985), a marine connection between northern Boreal waters and southern WIS became established on the western side of the basin at this time. Environmental reconstructions indicate southern WIS formations (e.g., Buda Limestone, Texas) were deposited under a local-WIS water mass (Eldrett et al., 2017), suggesting Tethyan waters had not yet migrated northwards into the seaway (Fig. 4.7).

Equatorial-Atlantic Tethyan waters first established a connection to the southern region of the WIS during the early Cenomanian (ca. 97 Ma), as recorded by sedimentological, geochemical, and palynological differences between the Lower Eagle Ford and the underlying Buda Limestone (Dodsworth, 2015; Eldrett et al., 2017). As a result, the local-WIS water mass, characterised by dysoxic waters, mixed dinocyst assemblages comprising of northern and Tethyan affiliated taxa (Eldrett et al., 2017) was displaced by Tethyan waters in the southern WIS (Fig. 4.7). The transition from the continental Dakota Sandstone transitioning into the marine Graneros Shale in RKB-1 confirms that that the central basin began to flood at this time. The Lower Graneros Shale in RKB-1 exhibits similar environmental attributes to sediments deposited under the local-WIS water mass from Texas, demonstrating that Tethyan waters had not yet reached the central basin, but rather the local-WIS watermass extended into the centre of the basin as sea levels rose (Fig. 4.7).

However, at the beginning of MCE I in the latest Early Cenomanian (~96.6 Ma; Eldrett et al. 2015a), the presence of Boreal-affiliated *Cyclonophelium compactum–C. membraniphorum* and *Crobroperidinium edwardsii* dinocysts alongside a dearth of Tethyan *Bosedia* spp. of Tethyan affinity, shows a short-lived southward migration of Boreal waters to this latitude in the WIS

temporarily replaced the local-WIS water mass. This southward Boreal migration mirrors temporally correlative incursions recorded in European sections, as represented by belemnites of Boreal affinity (e.g., Gale, 1995; Paul et al., 1994) and through neodymium stable isotope studies (Zheng et al., 2016). However, the *Cyclonophelium compactum–C. membraniphorum* dinocyst complex is not recorded further south than RKB-1 in the WIS during MCE I (e.g., it is absent from Texas; Eldrett et al., 2017), highlighting the limited extent of this Boreal water mass migration (Fig. 4.7). It is possible that this Boreal incursion has not been identified in sites of similar latitude as a number of hiatal surfaces have been identified through MCE I in successions such as that in the Coloradan Portland-1 core (Fig. 4.7; Eldrett et al., 2017). After this Boreal incursion, the mixed local-WIS watermass re-established as the dominant environmental driver in the central WIS, as evidenced by the presence of dinocyst assemblages of mixed Tethyan and Boreal affinities across MCE I, alongside low TM enrichments in the Lower Graneros Shale in RKB-1 (Chapter 2).

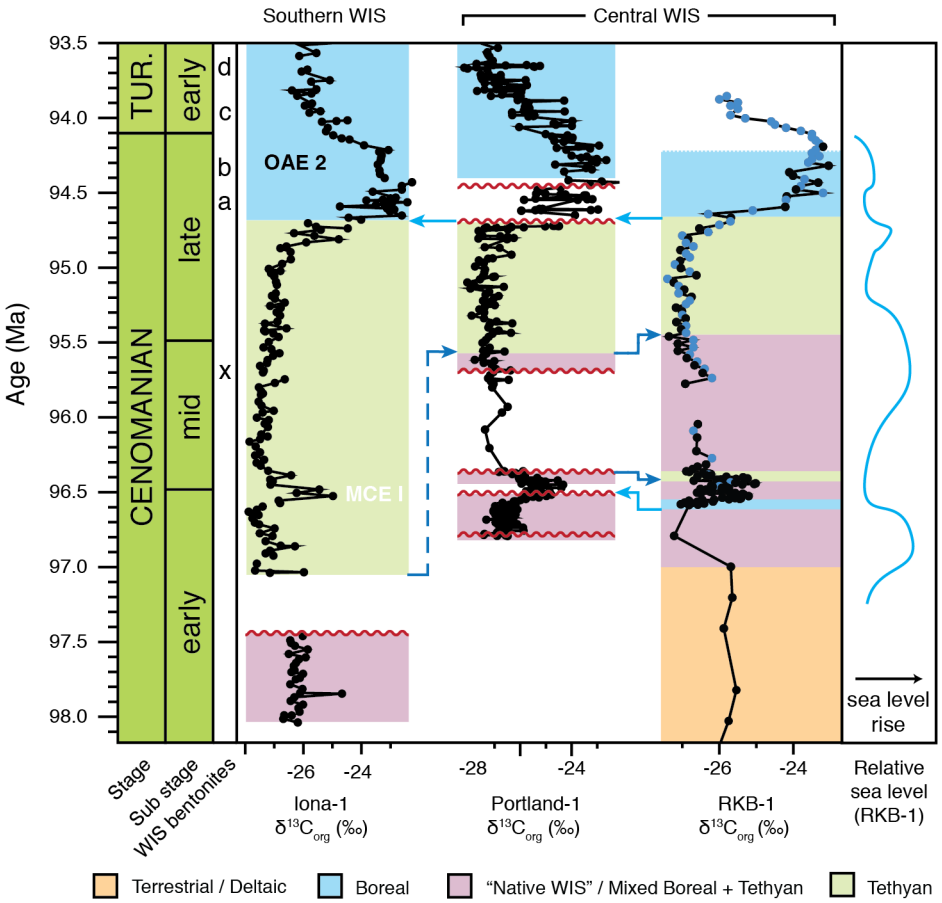

Figure 4.7: Cenomanian chronostratigraphic correlation of interpreted water masses in the Western Interior Seaway (WIS). Age model of Eldrett et al. (2015a) has been applied to the RKB-1 $\delta^{13}C_{org}$ record. Iona-1 and Portland-1 data from Eldrett et al. (2017). Blue RKB-1 data from Dean et al. (1995). Simplified WIS sea level curve of Kauffman and Caldwell (1993) modified to represent RKB-1. Arrows represent water mass movement (facing right = north, facing left = south).

4.4.3.2 Mid-Cenomanian

By the mid-Cenomanian, the Tethyan oceanic front had migrated northwards towards the central region of the WIS, as marked by significant increases in diversity and abundances of marine molluscan macrofauna and microplankton from the deposition of the Thatcher Limestone Member across Colorado and Kansas (Cobban and Scott, 1972; Kauffman, 1985, 1986; Cobban, 1993; Chapter 2). However, the mixed local-WIS watermass was not yet completely displaced at this latitude as evidenced by low TM redox-sensitive enrichments, high abundances of prasinophyte phycomata, and the presence of Boreal and Tethyan dinocysts in the Upper Graneros Shale (Eldrett et al., 2017; Chapter 2; this study). For a short period during the final stage of MCE I in the Upper Graneros Shale, Tethyan waters temporarily supplanted the local-WIS water mass in RKB-1, as shown by strengthened anoxic conditions and a lack of Boreal dinocysts (Figs. 4.5 and 4.7; Chapter 2). After MCE I, Boreal-affiliated dinocysts repopulated the water column, which also became slightly more oxygenated, illustrating that the mid-Cenomanian Tethyan incursion was short-lived at this latitude, and that the local-WIS water mass was the dominant long-term environmental driver in the central WIS.

4.4.3.3 Mid to Late Cenomanian

In the central WIS, a distinct lithological change to the carbonate-rich facies of the Greenhorn Formation is observed from the latest mid-Cenomanian (Cobban and Scott, 1972; Kauffman, 1977, 1988). The local-WIS water mass at RKB-1 was supplanted by Tethyan waters during the mid-late Cenomanian (Fig. 4.7), as evidenced by similar dinocyst assemblages and redox conditions as those seen during the latter stage of MCE I. Across the centre of the basin (e.g., Portland-1, Colorado) increased redox sensitive TM enrichments, abundant prasinophyte phycomata, and reduced diversities of dinocyst assemblages (containing abundant Tethyan-affiliated *Bosedinia* spp. dinocysts) occur from the deposition of the Lincoln Limestone and continue into the Hartland Shale, indicating the northwards migrating Tethyan oceanic front had now supplanted local-WIS environmental conditions in this area of the basin (Eldrett et al., 2017). This is also supported by increased abundances of Tethyan-related foraminifera across the centre of the basin (Sageman, 1985; Corbett et al., 2014).

4.4.3.3.1 Cenomanian-Turonian boundary

In the central WIS a positive carbon isotope excursion (CIE) representing OAE 2 commenced in the uppermost Hartland Shale Member and continued into the Bridge Creek Limestone Member (Dean et al., 1995; Sageman et al., 1998; Joo and Sageman, 2014; this study). From the onset of OAE 2, the reappearance of Boreal dinocysts, low enrichments of redox-sensitive TMs, decreased prasinophyte abundances, and increased bioturbation (Figs. 4.4 and 4.5) show the water column was more mixed, and that the sediment-water interface had become more oxygenated. These

conditions are associated with the rapid southward drawdown of Boreal waters into the WIS (e.g., Eldrett et al., 2017), which is also recorded in Colorado (Elderbak and Leckie, 2016), Texas (Eldrett et al., 2014), and New Jersey: (van Helmond et al., 2014), demonstrating the widespread nature of this oceanic change (Fig. 4.7). However, without palaeotemperature proxies available, it cannot be said if, at this site, the Plenus Cold Event is recorded within this seaway opening phase, which also led to longer term oceanographic and thus biotic changes.

Currently, although Eldrett et al. (2017) and Elderbak and Leckie (2016) both corroborate the existence of a Boreal incursion into the WIS during OAE 2, their conceptual models they use to interpret oceanographic changes during this climatic episode differ significantly. Eldrett et al. (2017) concluded from their multi-proxy, multi-site investigation that contemporaneous evidence for the Boreal incursion indicated that the numerically computed gyre-circulation model of Slingerland et al. (1996) (Fig. 4.8A; see Supplementary Information for model discussions) could not be supported for this interval, but rather, the Boreal incursion was representative of a southward migration of a basin-wide oceanic front, akin to the conceptual models of Hay et al. (1993) (Fig. 4.8B). Thus following this interpretation, the mechanism driving the rhythmic limestone-marlstone bedding couplets observed across OAE 2 in the Bridge Creek Limestone can be attributed to Milankovitch-paced climatic changes as proposed by Sageman et al. (1998) and Meyers et al. (2012a), with carbonate-rich deposits being produced during insolation maxima, and organic-rich sediments being deposited during insolation minima (Eldrett et al., 2015b).

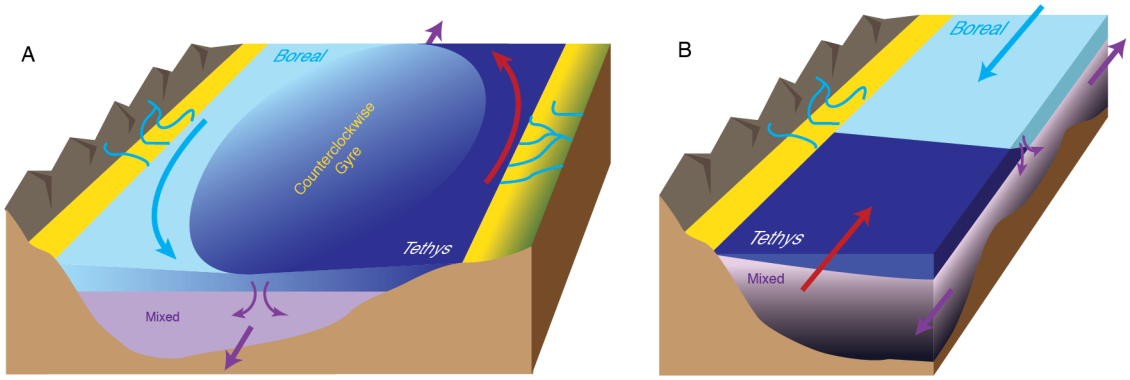

Figure 4.8: Mid-Cretaceous WIS oceanic circulation models. A) Estuarine surface water gyre numerical model of Slingerland et al. (1996), in which riverine fresh water input was deflected northwards on the eastern margin and southwards on the western margin due to the Coriolis effect. B) Conceptual surface water mass circulation model in which Tethyan and Boreal oceanic fronts meet, forming a third, denser, mixed local WIS water mass (Hay et al., 1993).

Conversely, Elderbak and Leckie (2016) adapted the gyre-circulation model of Slingerland et al. (1996) to account for changes between limestone and marlstone couplets within the Bridge Creek Limestone. They concluded that for the early phase of OAE 2, including the Plenus Cold Event, "Tethyan productivity cycles" drove the lithologic changes. In essence, during drier climatic intervals, heightened evaporation in the southeastern WIS coupled with increased precipitation in the north created a high-pressure gradient across the basin that strengthened the gyre. This, in turn,

enhanced Tethyan watermass migration along the eastern margin from the Gulf of Mexico and brought in greater abundances of associated calcareous plankton, increased productivity in surface waters, and ventilated the seafloor through the formation of a denser local-WIS; producing limestone deposits. The pressure gradient reduced during times of wetter climates in the southern WIS, leading to a weakened gyre system, which resulted in the deposition of marlstones and shales (Elderbak and Leckie, 2016). After the Plenus Cold Event, the authors determined "WIS-dilution cycles" drove the gyre, in which the regional climatic influences were inverted. Wetter climates led to increased continental runoff into the basin from the eastern and western margins that strengthened the gyre, which deflected continental sediment input away from the centre of the basin, allowing for limestone deposition. During drier periods the coastal jets weakened, allowing for detrital sediment to be transported further into the basin, leading to clastic sedimentary deposits to form (Elderbak and Leckie, 2016). However, the environmental records from RKB-1 indicate that the rapid southward migration of Boreal waters reached the central-eastern WIS, and thus extended across the width of the basin, supporting the conceptual oceanic front model of Eldrett et al. (2017). Furthermore, the proposed circulation models of Elderbak and Leckie (2016), which rely predominantly on single proxy (foraminiferal) data, do not sufficiently explain the occurrences of Boreal-affiliated dinocysts in the south or central-eastern WIS.

4.5 Conclusions

Our integrated palynological, geochemical, and sedimentological dataset records from the central-eastern WIS demonstrate the complexity of the Cenomanian oceanographic system in North America. In the early Cenomanian, mixing of Boreal and Tethyan waters along the western margin and southern regions of the WIS allowed for a third, denser local-WIS water mass to form, which flooded the terrestrial regions of the central-eastern basin during early to mid-Cenomanian. In RKB-1, a short-lived southward Boreal migration into the centre of the WIS is recorded during the beginning of MCE I, echoing contemporaneous Boreal incursions from Europe, thus indicating this was a transient, but global, oceanic reorganisation. Similarly, Tethyan waters supplanted the local-WIS water mass for a short interval at the end of MCE I, marking a precursor event to the northward Tethyan water mass migration during the Greenhorn Cyclothem. During the mid-late Cenomanian, the Tethyan oceanic front migrated northward to the centre of the basin, and the local-WIS water mass was fully supplanted by the Tethyan waters. Finally, from the initiation of OAE 2 in the late Cenomanian, a rapid southward Boreal water mass migration ventilated the water column. As this was observed across the basin and extended to southern regions of the WIS, we determine this Boreal incursion represents a migrating oceanic front, which does not support the conceptual oceanic gyre model as the dominant circulation driver for the late Cenomanian-early turonian.

4.6 Acknowledgements

This work is supported by an industrial CASE studentship award (NE/L50161X/1) granted by the Natural Environment Research Council UK and Shell International Exploration & Production Inc. We extend our gratitude to the USGS Core Repository Centre in Denver for granting us permission to sample and analyse the RKB-1 core. We appreciate the advice Dr. Paul Dodsworth offered regarding palynological identifications.

4.7 References

Akyuz, I., Warny, S., Famubode, O., Bhattacharya, J.P., 2016. Palynology of the Upper Cretaceous (Turonian) Ferron Sandstone Member, Utah, USA: identification of marine flooding surfaces and Milankovitch cycles in subtropical, ever-wet, paralic to non-marine palaeoenvironments. Palynology 40, 122–136.

Algeo, T.J., Tribovillard, N., 2009. Environmental analysis of paleoceanographic systems based on molybdenum-uranium covariation. Chem. Geol. 268, 211–225. doi:10.1016/j.chemgeo.2009.09.001

Archer, A.W., 1995. Modeling of cyclic tidal rhythmites based on a range of diurnal to semidiurnal tidal-station data. Mar. Geol. 123, 1–10.

Armstrong, R., 1968. Sevier orogenic belt in Nevada and Utah. Geol. Soc. Am. Bull. 79, 429-458.

Arthur, M.A., Sageman, B.B., 2004. Sea-level control on source-rock development: Perspectives from the Holocene Black Sea, the Mid-Cretaceous Western Interior Basin of North America, and the Late Devonian Appalachian Basin. SEPM Spec. Publ. 82, 35–59.

Bojesen-Koefoed, J.A., Nytoft, H.P., 2003. Petroleum Geochemistry: Cenomanian - Turonian succession of three core wells from the Cretaceous Western Interior Seaway, USA. Data report: USGS Escalante 1, USGS Portland 1 and AMOCO Rebecca K. Bounds 1 wells.

Brumsack, H.J., 2006. The trace metal content of recent organic carbon-rich sediments: Implications for Cretaceous black shale formation. Palaeogeogr. Palaeoclimatol. Palaeoecol. 232, 344–361. doi:10.1016/j.palaeo.2005.05.011

Cobban, W.A., 1993. Diversity and distribution of Late Cretaceous ammonites, Western Interior, United States. Evol. West. Inter. Basin Geol. Assoc. Canada Spec. Pap. 39, 435–451.

Cobban, W.A., Scott, G.R., 1972. Stratigraphy and Ammonite Fauna of the Graneros Shale and Greenhorn Limestone Near Pueblo , Colorado Stratigraphy and Ammonite Fauna of the

Graneros Shale and Greenhorn Limestone Near Pueblo , Colorado. Geol. Surv. Prof. Paper 645. 1–195.

Coccioni, R., Galeotti, S., 2003. The mid-Cenomanian Event: Prelude to OAE 2, in: Palaeogeography, Palaeoclimatology, Palaeoecology. pp. 427–440. doi:10.1016/S0031-0182(02)00617-X

Corbett, M.J., Watkins, D.K., Pospichal, J.J., 2014. A quantitative analysis of calcareous nannofossil bioevents of the Late Cretaceous (Late Cenomanian-Coniacian) Western Interior Seaway and their reliability in established zonation schemes. Mar. Micropaleontol. 109, 30–45. doi:10.1016/j.marmicro.2014.04.002

Dale, B., Fjellså, A., 1994. Dinoflagellate cysts as paleoproductivity indicators: state of the art, potential, and limits, in: Carbon Cycling in the Glacial Ocean: Constraints on the Ocean's Role in Global Change. Springer, pp. 521–537.

Dean, W.E., Arthur, M.A., Sageman, B.B., Lewan, M.D., 1995. Core descriptions and preliminary geochemical data for the Amoco Production Company Rebecca K. Bounds# 1 well, Greeley County, Kansas. US Geological Survey.

Dellwig, O., Leipe, T., März, C., Glockzin, M., Pollehne, F., Schnetger, B., Yakushev, E. V., Böttcher, M.E., Brumsack, H.J., 2010. A new particulate Mn-Fe-P-shuttle at the redoxcline of anoxic basins. Geochim. Cosmochim. Acta 74, 7100–7115. doi:10.1016/j.gca.2010.09.017

Desmares, D., Grosheny, D., Beaudoin, B., Gardin, S., Gauthier-Lafaye, F., 2007. High resolution stratigraphic record constrained by volcanic ash beds at the Cenomanian–Turonian boundary in the Western Interior Basin, USA. Cretac. Res. 28, 561–582.

Dodsworth, P., 2015. Palynostratigraphy and palaeoenvironments of the Eagle Ford Group (Upper Cretaceous) at the Lozier Canyon outcrop reference section, west Texas, USA. Palynology. 40(3), 357-378. doi:10.1080/01916122.2015.1073188

Dodsworth, P., 2004. The palynology of the Cenomanian-Turonian (Cretaceous) boundary succession at Aksudere in Crimea, Ukraine. Palynology 28, 129–141. doi:10.1080/01916122.2004.9989594

Eicher, D.L., 1965. Foraminifera and biostratigraphy of the Graneros Shale. J. Paleontol. 39, 875–909.

Eicher, D.L., Diner, R., 1989. Origin of the Cretaceous bridge creek cycles in the western interior, United States. Palaeogeogr. Palaeoclimatol. Palaeoecol. 74, 127–146. doi:10.1016/0031-0182(89)90023-0

Eicher, D.L., Worstell, P., 1970. Cenomanian and Turonian foraminifera from the Great Plains, United States. Micropaleontology 269–324.

Elder, W.P., 1985. Biotic patterns across the Cenomanian-Turonian extinction boundary near Pueblo, Colorado, in: Pratt, L.M., Kauffman, E.G., Zelt, F.B. (Eds.), Field Trip Guidebook No. 4, 157e169. Special Publications of SEPM.

Elderbak, K., Leckie, R.M., 2016. Paleocirculation and foraminiferal assemblages of the Cenomanian-Turonian Bridge Creek Limestone bedding couplets: Productivity vs. dilution during OAE2. Cretac. Res. 60, 52–77. doi:10.1016/j.cretres.2015.11.009

Elderbak, K., Leckie, R.M., Tibert, N.E., 2014. Paleoenvironmental and paleoceanographic changes across the Cenomanian-Turonian Boundary Event (Oceanic Anoxic Event 2) as indicated by foraminiferal assemblages from the eastern margin of the Cretaceous Western Interior Sea. Palaeogeogr. Palaeoclimatol. Palaeoecol. 413, 29–48. doi:10.1016/j.palaeo.2014.07.002

Eldrett, J.S., Dodsworth, P., Bergman, S.C., Wright, M., Minisini, D., 2017. Water-mass evolution in the Cretaceous Western Interior Seaway of North America and equatorial Atlantic. Clim. Past 13, 1–34. doi:https://doi.org/10.5194/cp-13-1-2017

Eldrett, J.S., Ma, C., Bergman, S.C., Lutz, B., Gregory, F.J., Dodsworth, P., Phipps, M., Hardas, P., Minisini, D., Ozkan, A., Ramezani, J., Bowring, S.A., Kamo, S.L., Ferguson, K., Macaulay, C., Kelly, A.E., 2015a. An astronomically calibrated stratigraphy of the Cenomanian, Turonian and earliest Coniacian from the Cretaceous Western Interior Seaway, USA: Implications for global chronostratigraphy. Cretac. Res. 56, 316–344. doi:10.1016/j.cretres.2015.04.010

Eldrett, J.S., Ma, C., Bergman, S.C., Ozkan, A., Minisini, D., Lutz, B., Jackett, S.J., Macaulay, C., Kelly, A.E., 2015b. Origin of limestone-marlstone cycles: Astronomic forcing of organic-rich sedimentary rocks from the Cenomanian to early Coniacian of the Cretaceous Western Interior Seaway, USA. Earth Planet. Sci. Lett. 423, 98–113. doi:10.1016/j.epsl.2015.04.026

Eldrett, J.S., Minisini, D., Bergman, S.C., 2014. Decoupling of the carbon cycle during ocean anoxic event 2. Geology 42, 567–570. doi:10.1130/G35520.1

Fisher, C.G., Hay, W.W., Eicher, D.L., 1994. Oceanic front in the Greenhorn Sea (Late Middle through Late Cenomanian). Paleoceanography 9, 879. doi:10.1029/94PA02114

Forster, A., Schouten, S., Moriya, K., Wilson, P.A., Damsté, J.S.S., 2007. Tropical warming and intermittent cooling during the Cenomanian/Turonian oceanic anoxic event 2: Sea surface

temperature records from the equatorial Atlantic. Paleoceanography 22, 1–14. doi:10.1029/2006PA001349

Friedrich, O., Erbacher, J., Wilson, P.A., Moriya, K., Mutterlose, J.J., 2009. Paleoenvironmental changes across the Mid Cenomanian Event in the tropical Atlantic Ocean (Demerara Rise, ODP Leg 207) inferred from benthic foraminiferal assemblages. Mar. Micropaleontol. 71, 28–40. doi:10.1016/j.marmicro.2009.01.002

Gale, A.S., 1995. Cyclostratigraphy and correlation of the Cenomanian Stage in Western Europe. Orbital Forcing Timescales and Cyclostratigraphy 85, 177–197. doi:10.1144/GSL.SP.1995.085.01.11

Gale, A.S., Christensen, W.K., 1996. Occurrence of the belemnite *Actinocamax plenus* in the Cenomanian of SE France and its significance. Bull. Geol. Soc. Denmark. 43, 68-77.

Gale, A.S., Voigt, S., Sageman, B.B., Kennedy, W.J., 2008. Eustatic sea-level record for the Cenomanian (Late Cretaceous) - Extension to the Western Interior Basin, USA. Geology 36, 859–862. doi:10.1130/G24838A.1

Gambacorta, G., Bersezio, R., Weissert, H., Erba, E., 2016. Onset and demise of Cretaceous Oceanic Anoxic Events: the coupling of surface and bottom oceanic processes in two pelagic basins of the western Tethys. Paleoceanography 732–757. doi:10.1002/2015PA002922

Gradstein, F.M., Ogg, J.G., Schmitz, M., Ogg, G., 2012. Chapter 27. Cretaceous, in: The Geologic Time Scale 2012. Elsevier B.V., pp. 793–853.

Hammer, Ø., Harper, D.A.T., Ryan, P.D., 2001. Paleontological statistics software package for education and data analysis. Palaeontol. Electron. 4, 9–18. doi:10.1016/j.bcp.2008.05.025

Hardas, P., Mutterlose, J., Friedrich, O., Erbacher, J., 2012. The Mid Cenomanian Event in the equatorial Atlantic: The calcareous nannofossil and benthic foraminiferal response. Mar. Micropaleontol. 96–97, 66–74. doi:10.1016/j.marmicro.2012.08.003

Hattin, D.E., Siemers, C.T., Stewart, G.F., 1987. Upper Cretaceous stratigraphy and depositional environments of western Kansas. Guideb. Kansas Geol. Surv. 3, 1–30.

Hay, W.W., Eicher, D.L., Diner, R., 1993. Physical oceanography and water masses in the Cretaceous Western Interior Seaway, in: Geological Association of Canada-Special Paper. Geological Association of Canada, pp. 297–318.

Hay, W.W., Floegel, S., 2012. New thoughts about the Cretaceous climate and oceans. Earth-Science Rev. 115, 262–272. doi:10.1016/j.earscirev.2012.09.008

Hook, S.C., Cobban, W.A., 2007. A condensed middle Cenomanian succession in the Dakota Sandstone (Upper Cretaceous), Sevilleta National Wildlife Refuge, Socorro County , New Mexico. New Mex. Geol. 29, 75–99.

Jarvis, I., Lignum, J.S., Gröcke, D.R., Jenkyns, H.C., Pearce, M.A., 2011. Black shale deposition, atmospheric CO_2 drawdown, and cooling during the Cenomanian-Turonian Oceanic Anoxic Event. Paleoceanography 26, 1–17. doi:10.1029/2010PA002081

Jones, B., Manning, D.A.C., 1994. Comparison of geochemical indices used for the interpretation of palaeoredox conditions in ancient mudstones. Chem. Geol. 111, 111–129. doi:10.1016/0009-2541(94)90085-X

Joo, Y.J.I., Sageman, B.B., 2014. Cenomanian to Campanian carbon isotope chemostratigraphy from the Western Interior Basin, USA. J. Sediment. Res. 84, 529–542. doi:dx.doi.org/10.2110/jsr.2014.38

Kauffman, E., 1977. Geological and biological overview: Western Interior Cretaceous basin. Mt. Geol. 14, 75–99.

Kauffman, E.G., 1985. Paleobiogeography and evolutionary response dynamic in the Cretaceous Western Interior Seaway of North America, in: Jurassic-Cretaceous Biochronology and Paleogeography of North America. Geol. Assoc. Can. Sp. Pap, pp. 273–306.

Kauffman, E. G., 1986. High-resolution event stratigraphy: Regional and Global Cretaceous Bio-events, In: O. Walliser, ed., Global Bio-Events, Lecture Notes in Earth History, v. 8, Springer, Berlin, p. 279-335.

Kauffman, E.G., 1988, Concepts and Methods of High-Resolution Event Stratigraphy. Ann. Rev. Earth Planetary Sci, v. 16, p. 605-653.

Kauffman, E.G., Caldwell, W.G.E., 1993. The Western Interior Basin in space and time. Evol. West. Inter. Basin Geol. Assoc. Canada, Spec. Pap. 39, 1–30.

Keller, G., Pardo, A., 2004. Age and paleoenvironment of the Cenomanian-Turonian global stratotype section and point at Pueblo, Colorado. Mar. Micropaleontol. 51, 95–128. doi:10.1016/j.marmicro.2003.08.004

Kump, L.R., Pavlov, A., Arthur, M.A., 2005. Massive release of hydrogen sulfide to the surface ocean and atmosphere during intervals of oceanic anoxia. Geology 33, 397–400. doi:10.1130/G21295.1

Kvale, E.P., Archer, A.W., 1991. Characteristics of two, Pennsylvanian-age, semidiurnal tidal deposits in the Illinois Basin, USA. In: Smith, D.G., Reinson, G.E., Zaitlin, B.A., Rahmani, R.A., (eds), Clastic tidal sedimentology. Canada Soc. Petrol. Geol. Mem. 16, 179-188.

Leckie, R.M., Yuretich, R.F., West, O.L.O., Finkelstein, D., Schmidt, M., 1998. Paleoceanography of the Southwestern Western Interior Sea During the Time of the Cenomanian-Turonian Boundary (Late Cretaceous). Stratigr. Paleoenviron. Cretac. West. Inter. Seaway, USA 6, 101–126. doi:10.2110/csp.98.06.0101

Meyers, S.R., Sageman, B.B., Arthur, M.A., 2012a. Obliquity forcing of organic matter accumulation during Oceanic Anoxic Event 2. Paleoceanography 27, 1–19. doi:10.1029/2012PA002286

Meyers, S.R., Siewert, S.E., Singer, B.S., Sageman, B.B., Condon, D.J., Obradovich, J.D., Jicha, B.R., Sawyer, D.A., 2012b. Intercalibration of radioisotopic and astrochronologic time scales for the Cenomanian-Turonian boundary interval, western interior Basin, USA. Geology 40, 7–10. doi:10.1130/G32261.1

Mitchell, S.F., 1996. Foraminiferal assemblages from the late Lower and Middle Cenomanian of Speeton (North Yorkshire, UK): relationships with sea-level fluctuations and watermass distribution. J. Micropalaeontology 15, 37–54.

Nakamura, K., 2015. Chemostratigraphy of the late Cretaceous Western Interior (Greenhorn, Carlile, and Niobrara Formations), Denver Basin, CO, USA. Colorado School of Mines.

Paul, C., Mitchell, S., Marshall, J., Leafy, P., 1994. Palaeoceanographic events in the Middle Cenomanian of Northwest Europe. Cretac. Res. 15, 707–738.

Prauss, M., Ligouis, B., Luterbacher, H., 1991. Organic matter and palynomorphs in the "Posidonienschiefer" (Toarcian, Lower Jurassic) of southern Germany. Geol. Soc. London, Spec. Publ. 58, 335–351. doi:10.1144/GSL.SP.1991.058.01.21

Prauss, M.L., 2012. The Cenomanian/Turonian Boundary event (CTBE) at Tarfaya, Morocco: Palaeoecological aspects as reflected by marine palynology. Cretac. Res. 34, 233–256. doi:10.1016/j.cretres.2011.11.004

Prauss, M.L., 2007. Availability of reduced nitrogen chemospecies in photic-zone waters as the ultimate cause for fossil prasinophyte prosperity. Palaios 22, 489–499.

Roberts, L.N., Kirschbaum, M.A., 1995. Paleogeography of the Late Cretaceous of the Western Interior of Middle North America - Coal Distribution and Sediment Accumulation, U.S. Geological Survey Professional paper.

Saeed, A., Evans, J.E., 2012. Subsurface Facies Analysis of the Late Cambrian Mt. Simon Sandstone in Western Ohio (Midcontinent North America). Open J. Geol. 2, 35.

Sageman, B.B., 1985. High-resolution stratigraphy and paleobiology of the Hartland Shale Member: analysis of an oxygen-deficient epicontinental sea. *In*: Fine-grained deposits and biofaces of the Cretaceous Western Interior Seaway: Evidence of cyclic sedimentary processes, L. M. Pratt, E. G. Kauffman, F. B. Zelt, eds., Society of economic paleontologists and mineralogists, 2nd annual midyear meeting. Fieldtrip guidebook 4, 110-121.

Sageman, B. B., 1989. The benthic boundary biofacies model: Hartland Shale Member, Greenhorn Formation (Cenomanian), Western Interior, North America. Palaeogeography, Palaeoclimatology, Palaeoecology. 74, 87-110.

Sageman, B.B., 1996. Lowstand tempestites: Depositional model for Cretaceous skeletal limestones, Western Interior basin. Geology 24, 888–892. doi:10.1130/0091-7613(1996)024<0888:LTDMFC>2.3.CO;2

Sageman, B.B., Rich, J., Arthur, M.A., Dean, W.E., Savrda, C.E., Bralower, T.J., 1998. Multiple Milankovitch cycles in the Bridge Creek Limestone (Cenomanian-Turonian), Western Interior Basin.

Schrank, E., 2010. Pollen and spores from the Tendaguru Beds, Upper Jurassic and Lower Cretaceous of southeast Tanzania: palynostratigraphical and paleoecological implications. Palynology 34, 3–42.

Schröder-Adams, C.J., Leckie, D.A., Bloch, J., Craig, J., Mcintyre, D.J., Adams, P.J., 1996. Paleoenvironmental changes in the Cretaceous (Albian to Turonian) Colorado Group of western Canada : microfossil , sedimentological and geochemical evidence. Cretac. Res. 17, 311–365. doi:10.1006/cres.1996.0022

Scott, R.W., Franks, P.C., Evetts, M.J., Bergen, J.A., Stein, J.A., 1998. Timing of mid-Cretaceous relative sea level changes in the Western Interior: Amoco No. 1 Bounds Core, in: Stratigraphy and Paleoenvironments of the Cretaceous Western Interior Seaway, USA. Special Publications of SEPM, pp. 35–58.

Siemers, C.T., 1976. Sedimentology of the Rocktown channel sandstone, upper part of the Dakota Formation (Cretaceous), central Kansas. J. Sediment. Res. 46, 97-123.

Simons, D.-J.H., Kenig, F., 2001. Molecular fossil constraints on the water column structure of the Cenomanian–Turonian Western Interior Seaway, USA. Palaeogeogr. Palaeoclimatol. Palaeoecol. 169, 129–152.

Simpson, E.H., 1949. Measurement of diversity. Nature 163, 688. doi:10.1038/163688a0

Sinninghe Damsté, J.S., Wakeham, S.G., Kohnen, M.E., Hayes, J.M., de Leeuw, J.W., 1993. A 6,000-year sedimentary molecular record of chemocline excursions in the Black Sea. Nature 362, 827.

Slingerland, R., Kump, L.R., Arthur, M.A., Fawcett, P.J., Sageman, B.B., Barron, E.J., 1996. Estuarine circulation in the Turonian western interior seaway of North America. Geol. Soc. Am. Bull. 108, 941–952. doi:10.1130/0016-7606(1998)110<0691

Sluijs, A., Pross, J., Brinkhuis, H., 2005. From greenhouse to icehouse; organic-walled dinoflagellate cysts as paleoenvironmental indicators in the Paleogene. Earth-Science Rev. 68, 281–315. doi:10.1016/j.earscirev.2004.06.001

Srivastava, S.K., 1976. The fossil pollen genus *Classopollis*. Lethaia 9, 437–457.

Sun, X., Zhang, T., Sun, Y., Milliken, K.L., Sun, D., 2016. Geochemical evidence of organic matter source input and depositional environments in the lower and upper Eagle Ford Formation, south Texas. Org. Geochem. 98, 66–81.

Taylor, A.M., Goldring, R., 1993. Description and analysis of bioturbation and ichnofabric. J. Geol. Soc. London. 150, 141–148. doi:10.1144/gsjgs.150.1.0141

Terwindt, J.H.J., 2009. Origin and sequences of sedimentary structures in inshore mesotidal deposits of the North Sea. Holocene Mar. Sediment. North Sea Basin 5, 4–26.

Tribovillard, N., Algeo, T.J., Lyons, T., Riboulleau, A., 2006. Trace metals as paleoredox and paleoproductivity proxies: An update. Chem. Geol. 232, 12–32. doi:10.1016/j.chemgeo.2006.02.012

Tyson, R.V., 1987. The genesis and palynofacies characteristic of marine petroleum source rocks. Mar. Pet. Source Rocks 47–67. doi:doi:10.1144/GSL.SP.1987.026.01.03

van Helmond, N.A.G.M., Sluijs, A., Papadomanolaki, N.M., Plint, A.G., Gröcke, D.R., Pearce, M.A., Eldrett, J.S., Trabucho-Alexandre, J., Walaszczyk, I., van De Schootbrugge, B., Brinkhuis, H., 2016. Equatorward phytoplankton migration during a cold spell within the Late Cretaceous super-greenhouse. Biogeosciences 13, 2859. doi:10.5194/bg-13-2859-2016

van Helmond, N.A.G.M., Sluijs, A., Reichart, G.-J., Sinninghe Damste, J.S., Slomp, C.P., Brinkhuis, H., 2014. A perturbed hydrological cycle during Oceanic Anoxic Event 2. Geology 42, 123–126. doi:10.1130/G34929.1

Wall, D., Dale, B., Lohmann, G.P., Smith, W.K., 1977. The environmental and climatic distribution of dinoflagellate cysts in modern marine sediments from regions in the North and South Atlantic Oceans and adjacent seas. Mar. Micropaleontol. 2, 121–200.

Williams, G.L., Fensome, R.A., MacRae, R.A., 2017. The Lentin and Williams index of fossil dinoflagellates 2017 edition. Contrib. Ser. Assoc. Stratigr. Palynol. 1–1097.

Zheng, X.-Y., Jenkyns, H., Gale, A., Ward, D., Henderson, G., 2016. A climatic control on reorganization of ocean circulation during the mid-Cenomanian event and Cenomanian-Turonian oceanic anoxic event (OAE 2): Nd isotope evidence. Geology 44, 151–154. doi:10.1130/G37354.1

4.8 Supplementary Information

4.8.1 Elemental analyses

4.8.1.1 ICP-MS sample preparation

To remove carbonate contents from samples, ~10 mg of powdered bulk sediment was digested in Teflon pots using a 0.5 ml, 10% solution of 6M hydrochloric acid (HCl). The pots were heated to 130-150°C on hot plates until all acid was evaporated (approx. 1 hour). Samples were further digested in 1 ml of Aqua Regia solution (3:1 HCl:HNO_3) and heated to 80°C for 12 hours remove sulphides and Fe/Mn oxides. Lids were placed on the pots to ensure no acid was lost due to evaporation over this time. The acid was subsequently removed via evaporation by increasing the hot plate temperature to 130-150°C and removing lids. Once dry, hydrofluoric acid (0.25 ml) and pechloric acid (0.25 ml) were added to each sample and heated to 80°C for 12 hours to remove any other minerals and organic matter (with lids kept on). Lids were removed and the temperature was increased to 160°C to evaporate the acids. Samples were dissolved in a 6M HCl solution (filling ~1/3 of a pot) and heated for 48 hours to ensure each sample was in a HCl matrix. Once samples were fully dissolved, acid was removed by evaporation. The samples were then diluted with 3% HNO_3 in preparation for ICP-MS analysis.

Each sample was diluted to 2000x by emptying pot contents into vials (weighed empty) and filled with 3% HNO_3 (20 ml), then re-weighed. The samples were further diluted to 4000x by taking 2.5ml of 2000x dilution solution and adding 2.5ml 3% HNO_3 in new vials which were weighed empty, with subsample, and once full. Finally, these were diluted to 80000x by taking 0.25ml of 4000x and adding 4.75ml of 3% HNO_3 in new vials which were weighed empty, with subsample, and once full.

Standards were also prepared. 2 ml of each standard (BAS 206, JA2, JB1A, BHVD2, JGB1, JB3, BRR1, and BIR1) was pipetted into Teflon pots, and the sample bottle was weighed before/after (standards start at 400x dilution). The standards were placed on a hot plate and evaporated overnight before being made up with 3% HNO_3 so they were also in a HCl matrix. These were then

diluted to 4000x by weighing: empty vials; vial + standard in; vial + standard + 20 ml 3% HNO_3 and re-weighing. These were then diluted to 80000x by taking 0.25ml of 4000x solution and adding 4.75ml of 3% HNO_3 in new vials. Each vial was weighed empty, with subsample, and when full. Finally, these were then diluted to 320000x by taking 1ml of 80000x and adding 3ml of 3% HNO_3 in new vials. Each vial was weighed empty, with subsample, and when full.

The samples were run on an Thermo Fisher Scientific ELEMENT 2XR ICP-MS at the University of Southampton (National Ocenaography Centre) and results were obtained for major elements: Na, Mg, Al, K, Ca, V, Cr, Mn, and Fe; and trace elements: Li, Sc, V, Cr, Co, Ni, Cu, Zn, Rb, Sr, Y, Zr, Nb, Mo, Sn, Cs, Ba, La, Ce, Pr, Nd, Sm, Eu, Gd, Tb, Dy, Ho, Er, Tm, Yb, Lu, Hf, Ta, Pb, Th, and U.

4.8.1.2 Portable XRF data acquisition

At the USGS Core Research Centre (Denver, Colorado), the RKB-1 core was analysed using a handheld Thermo Scientific Nikon XL3t GOLDD+ XRF Analyzer. This allowed the collection of elemental compositional data of the core in high resolution, in a non-destructive analysis. The following steps were taken to obtain data for the following elements: Mo, Zr, Sr, U, Rb, Th, Pb, As, Zn, Cu, Ni, Co, Fe, Mn, Cr, V, Ti, Sc, Ca, K, S, Ba, and Cs.

The core was marked at 10cm intervals from the base of the X-Bentonite down to the end of the Mid Cenomanian Event (MCE I) positive isotope excursion (CIE), from where the intervals were shortened to 5cm across MCE I. Below MCE I, sample resolution was increased back to 10cm. The handheld analyser was set to take readings over 120 seconds, and was calibrated by taking a reading of a factory standard (NIST LOW 2709). A reading was taken before and after each data recording session. Once calibrated, readings were taken for each interval, ensuring that no air gap was present between the analyser and the core, and that the analyser was not moved during three 120 second analysis.

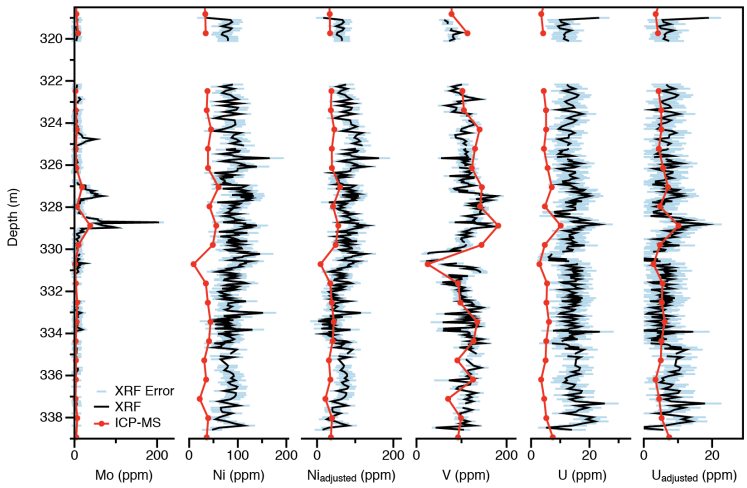

Figure 4.9: Comparisons between portable XRF and ICP-MS elemental counts, before and after adjusting for measurement drift during XRF data acquisition.

To calibrate for elemental measurement drift during sampling sessions, the difference between NIST LOW 2709 measurements and factory values from the beginning and end of each session was calculated for each element used. A linear positive or negative drift was assumed, and so interpolated drift coefficient values were calculated, based on number of readings taken per session. The interpolated coefficient values were then added to each sample reading to produce an adjusted elemental count (ppm). These adjusted records were validated by comparing to ICP-MS readings (e.g., Fig. 4.9).

4.8.1.3 Redox-sensitive trace element enrichments

Before palaeoenvironmental reconstructions using redox sensitive trace elements can be undertaken, it must first be determined if the trace element contents within sediments are controlled by the flux of detrital material into the marine system, or are authigenic. By comparing trace element accumulations against titanium (Ti) concentrations, correlative checks can be used to determine the main sources for these elements (see Tribovillard et al., 2006). As Ti is predominantly immobile during diagenesis and of terrigenous origin, a strong correlation would infer it is mainly controlled by detrital sources and, thus, would not be useful for paleoenvironmental analysis (Tribovillard et al., 2006). In this study, no redox-sensitive elements correlate with Ti, denoting their authigenic nature. Other major constituents of the continentally derived sedimentary matrix include Al_2O_3, and Fe_2O_3 (Fig. 4.10).

Trace element accumulation was determined by comparing values to average values in the Earth's crust or using "average shale" values (see Wedepohl, 1991) and determining whether they are relatively enriched or depleted, which infers reducing or oxidising conditions, respectively (Calvert and Pedersen, 1993). The only source of zirconium (Zr) in pelagic sediments is from terrigenous input, and so normalising to this element removes the effect of variable terrigenous input in these sediments (Milnes and Fitzpatrick, 1989). Furthermore, normalising elemental data to Zr has been used in previously WIS studies (e.g., Eldrett et al., 2014), as it corrects for highly variable carbonate contents (Snow et al., 2005). An enrichment factor of >3 represents a detectable enrichment of said element over crustal averages, and a value of >10 suggests a moderate to strong degree of enrichment (Algeo and Tribovillard, 2009). The following equation was used to obtain enrichment factors for each element:

$$Enrichement\ Factor\ (EF) = \frac{\left(\frac{\text{Element}}{\text{Zr}}\right) sample}{\left(\frac{\text{Element}}{\text{Zr}}\right) avg.shale}$$

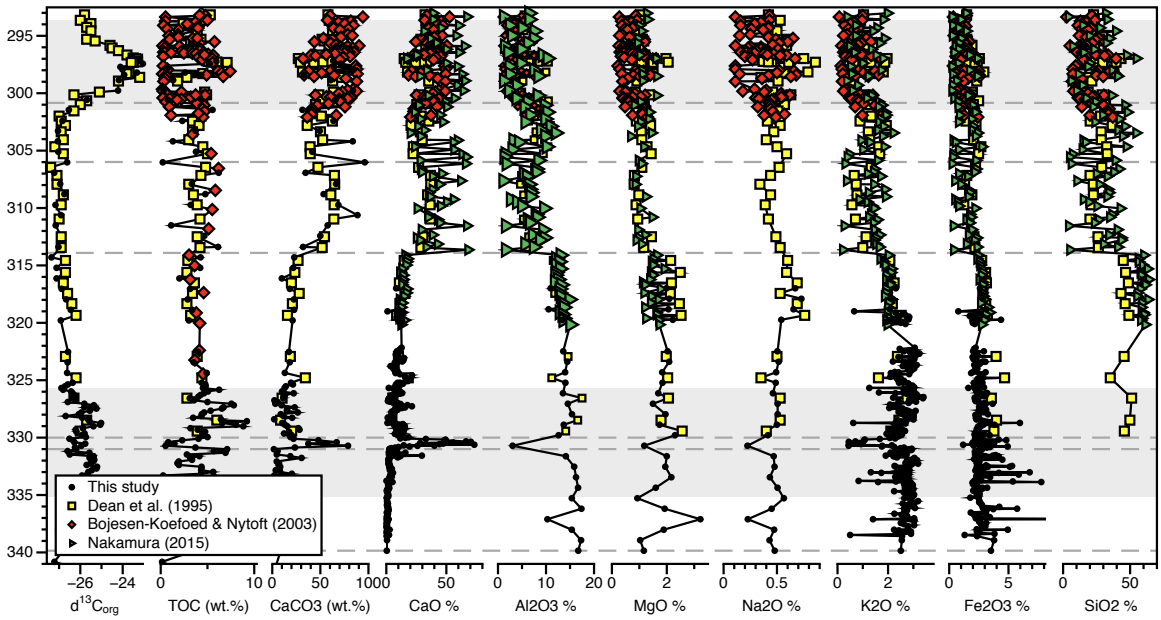

Figure 4.10: Distribution of major elemental oxides across study interval. Dashed lines indicate lithostratigraphic boundaries (see main text), and grey bars denote MCE I (326-336 m) and OAE2 (294-301 m).

4.8.2 Palynology

Different palynological subgroups thrive in their respective niche ecosystems, and thus can be as useful for assessing temporal environmental variability when compared with one another (Tyson, 1995).

4.8.2.1 Peridinoid vs. gonyaulacoid dinocysts (P:G ratio)

Marine productivity reconstructions using dinoflagellate cysts (dinocysts) mainly utilise the ratio of (proto-) peridinioid (P) vs. gonyaulacoid (G) cysts, as P-cysts are associated with high nutrient input, restricted marine or nearshore environments, and/or heterotrophic feeding mechanisms, while G-cysts reflect oligotrophic, open marine conditions and are generally autotrophic (see Sluijs et al., 2005; Eldrett et al., 2017). The P:G ratio can be influenced by the preferential preservation of P-cysts or G-cysts dependant on redox conditions of bottom and pore waters, age of deposition and/or location, and absolute abundances tend to provide more accurate sea surface productivity interpretations (discussion in Eldrett et al., 2017). However, in this study, palynological ratios are supported by other geochemical and sedimentological palaeoenvironmental proxies, which allow for more robust interpretations. Furthermore, the three marine palynological subgroups used for environmental analyses in this study are found to be mostly dominated by one genus or species (Fig. 4.11): P-cyst vs. *Palaeohystrichophora infusorioides* (r^2 = 0.85); G-cysts vs. *Spiniferites ramosus* group (r^2 = 0.53); prasinophytes vs. *Leiosphaeridia* spp. (r^2 = 0.95).

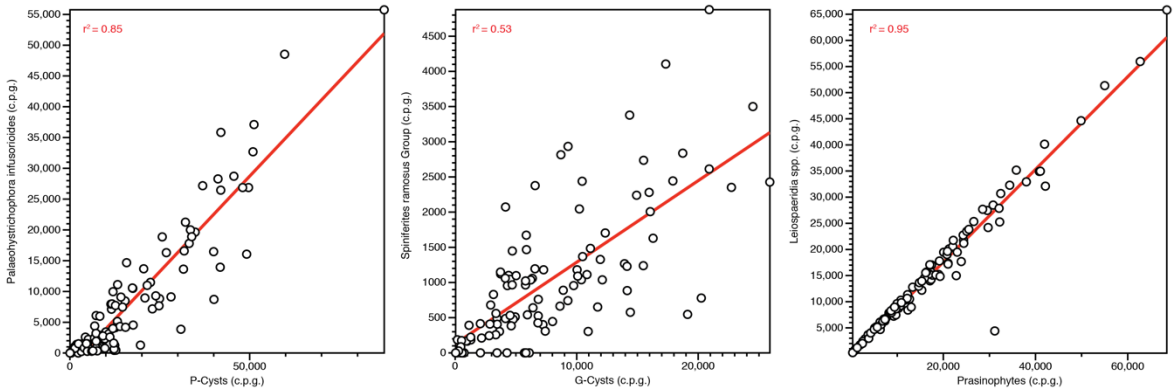

Figure 4.11: Correlations between palynological subgroups and species/genus distributions.

In this study, the following equation was used for the P:G ratio, in which values approaching 1 indicate P-cyst dominated assemblages, and values approaching -1 demonstrate G-cyst dominated assemblages:

$$\frac{\Sigma\, peridinioid\ dinocysts - \Sigma\, gonyaulacoid\ dinocysts}{\Sigma\, peridinioid\ dinocysts + \Sigma\, gonyaulacoid\ dinocysts}$$

4.8.2.2 Prasinophyte phycomata vs. dinocysts ratio

This ratio can be used to indicate distal/anoxic changes (Prauss and Riegel, 1989) or increased stability/stratification of the water column (Tyson, 1987), as prasinophytes are found in near shore environments and are indicators of deep chlorophyll maximums (Wawrik et al., 2003). The equation below was used to determine the distribution of these two palynological subgroups, and values approaching 1 indicate prasinophyte-dominated assemblages, and values approaching -1 demonstrate a dinocyst dominated assemblages:

$$\frac{\Sigma\, prasinophytes - \Sigma\, dinocysts}{\Sigma\, \text{prasinophytes} + \Sigma\, dinocysts}$$

4.8.2.3 Unclassified palynomaceral

In the Upper Graneros Shale, a significant number of an unidentified palynomaceral (Fig. 4.12), which has been tentatively catagorised as plant tissue, make up the palynological assemblages (main text Fig. 4.4). The specimens in question are large (>500 µm), and crescentic in shape. They contain thickened solid "ribs" in the centre, and lack any obvious large voids within them to indicate any sort of cellular structure or function as a 'cyst' of any type. Most specimens possess thinner lateral 'flanges' (these are variably preserved but can be quite wide in some specimens). The specimens can be found isolated or joined to another specimen, sometimes with the concave margins facing the second specimen. Under ultraviolet light they fluoresce as brightly as do many of the prasinophytes in the same assemblage do.

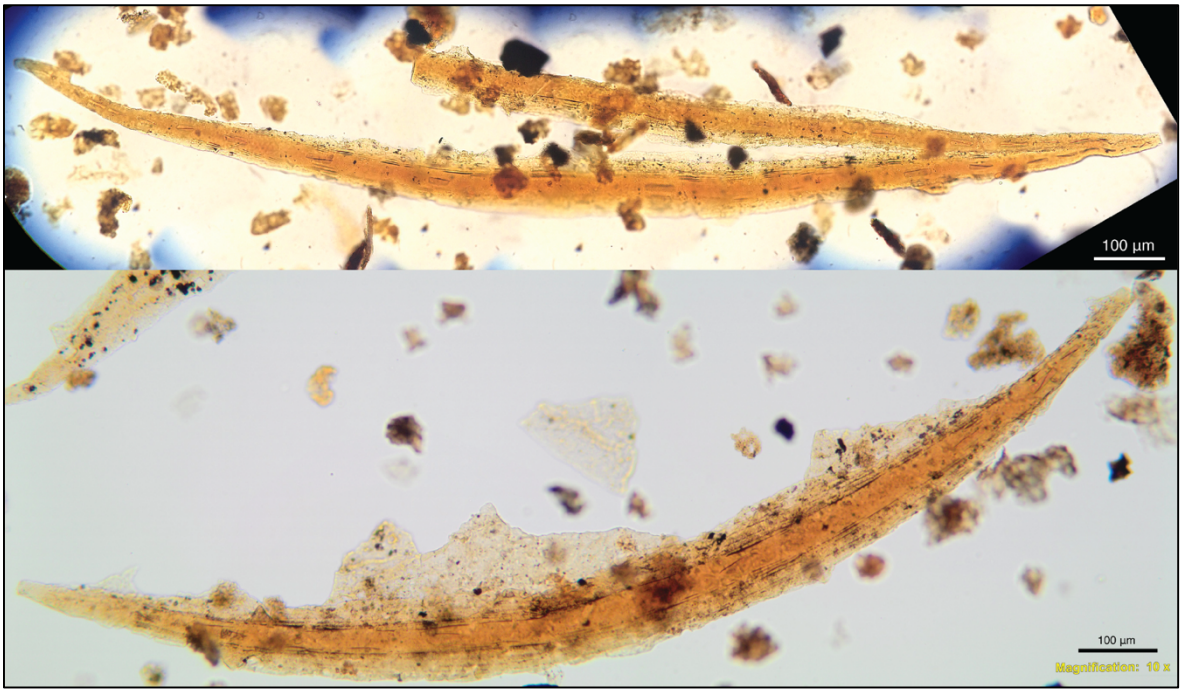

Figure 4.12: Examples of unidentified palynomacerals from the Upper Graneros Shale in RKB-1.

4.8.3 Bioturbation index

Examples of the different grades of bioturbation can be seen in Fig. 4.13.

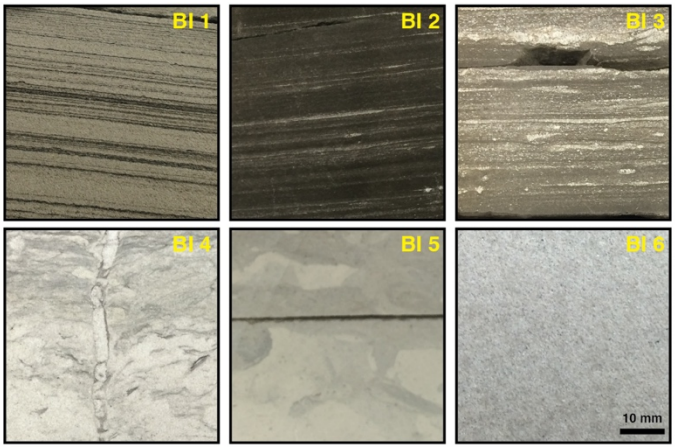

Figure 4.13: Examples of bioturbation index (BI) grades.

4.8.4 Coals and rootlets

Small rootlets (~0.5 – 1 cm; Fig. 4.14) below coal seams occur in a predominantly siliclastic sedimentary matrix, indicative of a lagoonal/swamp/coastal plain environment.

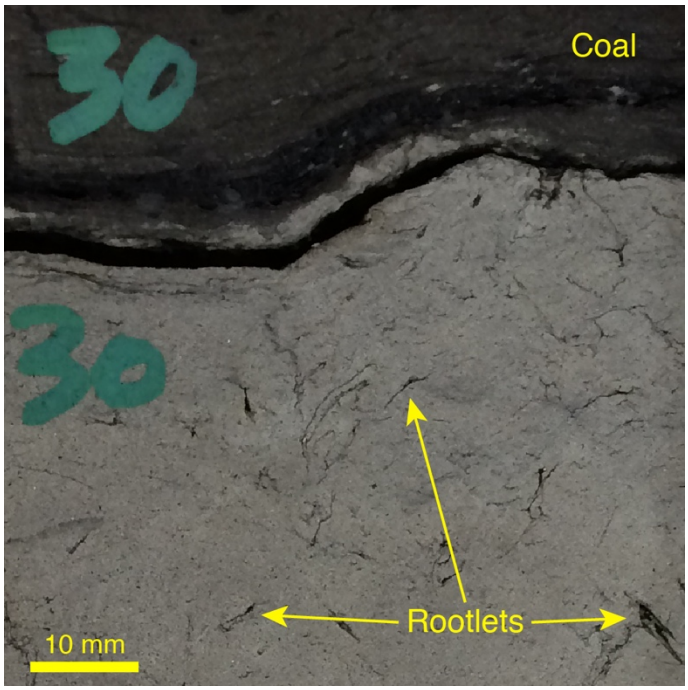

Figure 4.14: Example of coal seam and rootlet distributions within Dakota Sandstone Fm in RKB-1.

4.8.5 WIS circulation models

Basin-wide conceptual watermass circulation models (e.g., Hay et al., 1993; Elderbak and Leckie, 2016; Eldrett et al., 2017) and numerically constrained, computed circulation models (e.g., Slingerland et al., 1996; Kump and Slingerland, 1999) have been developed in order to better understand WIS oceanographic dynamics (e.g., Fig. 4.15) and help define key driving forces behind the alternating laminated organic-rich mudrocks and bioturbated carbonate-rich strata.

Hay et al. (1993) presented a number of scenarios in which strong watermass salinity gradients could have driven WIS circulation when shallow mid-Cretaceous pole-to-equator temperature gradients would have otherwise stagnated flow. The authors constrained temperatures and salinities of Boreal and Tethyan waters to modern Black Sea low-salinity surface water and high-salinity deep water values, respectively. As the two oceanic fronts met in the WIS, they mixed to form a third "local-WIS" intermediate watermass, either above dense, suboxic-anoxic Tethyan waters and below low-salinity Boreal waters (Fig. 4.15A), or below surface Tethyan/Boreal Waters (Fig. 4.15B): a process known as "caballing" (Hay et al., 1993; Elderbak and Leckie, 2016). This allowed for immediate increases in organic productivity in the newly formed nutrient-rich, ventilated intermediate waters, under which oxygen-depleted deep waters offered ideal conditions for the preservation of organic-rich material in areas where the basin configuration permitted (Hay et al., 1993). However, the authors noted that fresh water input from continental margins in the WIS would not have been sufficient enough to produce low-salinity waters for these conceptual models, but enhanced precipitation in warm, humid high-latitude regions could adequately account

for the formation of low-salinity Boreal waters that subsequently flowed into the basin from the north.

In contrast, Slingerland et al. (1996), computed a coastal ocean circulation model for the early Turonian WIS Greenhorn sea level highstand, which was, in part, constrained by North American continental precipitation-evaporation balances and associated fresh water input from the western and eastern margins. The authors' sensitivity studies demonstrated that of the modelled temperature, salinity, and wind drivers, thermohaline forcing was the most influential variable. Buoyant, riverine freshwater input from the margins travelled into the seaway along off-shore dipping water-surface flows. In the process, they were deflected to the right by the Coriolis force and collected along each coast until the offshore surface slopes pressure forces balanced the Coriolis force. These waters then moved isobathyally alongshore, avoiding the center of the seaway, which in turn created strong estuarine coastal jets (Slingerland et al. 1996). A resulting counter-clockwise gyre formed in surface waters (upper 100 m of the water column), in which Tethyan and Boreal waters were drawn in along the eastern and northern margins, respectively (Fig. 4.15C). In deeper waters (below 100 m in the water column), the model indicated that the two water masses sheared alongside each other in the centre of the basin-gyre, creating a third

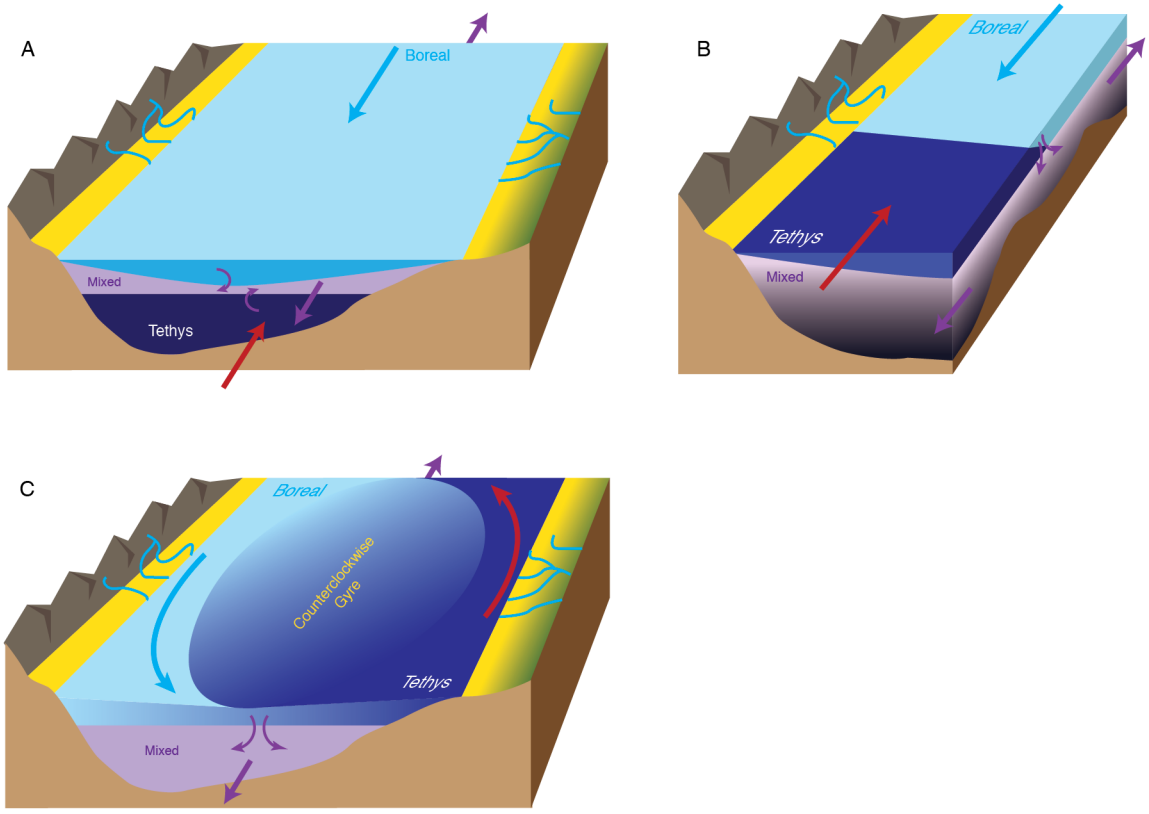

Figure 4.15: Conceptual Mid-Cretaceous WIS oceanic circulation models. A) Caballing model of Hay et al. (1993), in which dense southerly Tethyan waters and northerly Boreal waters mixed to form a local-WIS intermediate water mass. B) Surface water mass circulation model in which Tethyan and Boreal oceanic fronts meet, forming a third, denser, mixed local WIS water mass (Hay et al., 1993). C) Estuarine surface water gyre model of Slingerland et al. (1996), in which riverine fresh water input was deflected northwards on the eastern margin and southwards on the western margin due to the Coriolis effect.

intermediate watermass before flowing out of both basin entrances, favouring the northern side (Slingerland et al. 1996).

These models have been further constrained and developed as newer palaeoecological and environmental studies across the basin have been completed (e.g., Elderbak et al., 2014; Elderbak and Leckie, 2016; Eldrett et al., 2017). Alongside astronomically-tuned climatic changes that influenced lithologic changes on shorter timescales (e.g., ~40-50 kyr obliquity paced chalk-marl couplets in the late Cenomanian; Eldrett et al., 2015b; Meyers et al., 2012b), it is apparent that both circulation models influenced the distribution and extent of marine biotic and thus lithologic changes across the basin.

4.8.6 References

Algeo, T.J., Tribovillard, N., 2009. Environmental analysis of paleoceanographic systems based on molybdenum-uranium covariation. Chem. Geol. 268, 211–225. doi:10.1016/j.chemgeo.2009.09.001

Calvert, S., Pedersen, T., 1993. Geochemistry of recent oxic and anoxic marine sediments: implications for the geological record. Mar. Geol.

Elderbak, K., Leckie, R.M., 2016. Paleocirculation and foraminiferal assemblages of the Cenomanian-Turonian Bridge Creek Limestone bedding couplets: Productivity vs. dilution during OAE2. Cretac. Res. 60, 52–77. doi:10.1016/j.cretres.2015.11.009

Elderbak, K., Leckie, R.M., Tibert, N.E., 2014. Paleoenvironmental and paleoceanographic changes across the Cenomanian-Turonian Boundary Event (Oceanic Anoxic Event 2) as indicated by foraminiferal assemblages from the eastern margin of the Cretaceous Western Interior Sea. Palaeogeogr. Palaeoclimatol. Palaeoecol. 413, 29–48. doi:10.1016/j.palaeo.2014.07.002

Eldrett, J.S., Dodsworth, P., Bergman, S.C., Wright, M., Minisini, D., 2017. Water-mass evolution in the Cretaceous Western Interior Seaway of North America and equatorial Atlantic. Clim. Past 13, 1–34. doi:https://doi.org/10.5194/cp-13-1-2017

Eldrett, J.S., Ma, C., Bergman, S.C., Ozkan, A., Minisini, D., Lutz, B., Jackett, S.J., Macaulay, C., Kelly, A.E., 2015. Origin of limestone-marlstone cycles: Astronomic forcing of organic-rich sedimentary rocks from the Cenomanian to early Coniacian of the Cretaceous Western Interior Seaway, USA. Earth Planet. Sci. Lett. 423, 98–113. doi:10.1016/j.epsl.2015.04.026

Eldrett, J.S., Minisini, D., Bergman, S.C., 2014. Decoupling of the carbon cycle during ocean anoxic event 2. Geology 42, 567–570. doi:10.1130/G35520.1

Hay, W.W., Eicher, D.L., Diner, R., 1993. Physical oceanography and water masses in the Cretaceous Western Interior Seaway, in: Geological Association of Canada-Special Paper. Geological Association of Canada, pp. 297–318.

Kump, L.R., Slingerland, R.L., 1999. Circulation and stratification of the early Turonian Western Interior Seaway: Sensitivity to a variety of forcings. Spec. Pap. - Geol. Soc. Am. 181–190.

Meyers, S.R., Siewert, S.E., Singer, B.S., Sageman, B.B., Condon, D.J., Obradovich, J.D., Jicha, B.R., Sawyer, D.A., 2012. Intercalibration of radioisotopic and astrochronologic time scales for the Cenomanian-Turonian boundary interval, western interior Basin, USA. Geology 40, 7–10. doi:10.1130/G32261.1

Milnes, A.R., Fitzpatrick, R.W., 1989. Titanium and zirconium minerals. Miner. soil Environ. 1131–1205.

Prauss, M., Riegel, W., 1989. Evidence from phytoplankton associations for causes of black shale formation in epicontinental seas. Neues Jahrb. für Geol. und Paläontologie, Monatshefte 11, 671–682.

Slingerland, R., Kump, L.R., Arthur, M.A., Fawcett, P.J., Sageman, B.B., Barron, E.J., 1996. Estuarine circulation in the Turonian western interior seaway of North America. Geol. Soc. Am. Bull. 108, 941–952. doi:10.1130/0016-7606(1998)110<0691

Sluijs, A., Pross, J., Brinkhuis, H., 2005. From greenhouse to icehouse; organic-walled dinoflagellate cysts as paleoenvironmental indicators in the Paleogene. Earth-Science Rev. 68, 281–315. doi:10.1016/j.earscirev.2004.06.001

Snow, L.J., Duncan, R.A., Bralower, T.J., 2005. Trace element abundances in the Rock Canyon Anticline, Pueblo, Colorado, marine sedimentary section and their relationship to Caribbean plateau construction and ocean anoxic event 2. Paleoceanography 20, 1–14. doi:10.1029/2004PA001093

Tribovillard, N., Algeo, T.J., Lyons, T., Riboulleau, A., 2006. Trace metals as paleoredox and paleoproductivity proxies: An update. Chem. Geol. 232, 12–32. doi:10.1016/j.chemgeo.2006.02.012

Tyson, R.V., 1987. The genesis and palynofacies charac - teristic of marine petroleum source rocks. Mar. Pet. Source Rocks 47–67. doi:doi:10.1144/GSL.SP.1987.026.01.03

Tyson, R. V, 1995. Abundance of organic matter in sediments: TOC, hydrodynamic equivalence, dilution and flux effects, in: Sedimentary Organic Matter. Springer, pp. 81–118.

Wawrik, B., Paul, J.H., Campbell, L., Griffin, D., Houchin, L., Fuentes-Ortega, A., Muller-Karger, F., 2003. Vertical structure of the phytoplankton community associated with a coastal plume in the Gulf of Mexico. Mar. Ecol. Prog. Ser. 251, 87–101.

Wedepohl, K., 1991. The composition of the upper earth's crust and the natural cycles of selected metals. Metals in natural raw materials, in: Merian, E., Clarkson, T.W. (Eds.), Metals and Their Compounds in the Environment. VCH. 3-17.

Chapter 5: Conclusions and future work

5.1 Thesis summary and conclusions

The aims and objectives of this project included:

- Developing a high-resolution, multi-proxy framework for the Mid Cenomanian Event (MCE I) by integrating organic and inorganic datasets obtained from sedimentological, geochemical, and palynological analyses of organic-rich sediments from the Rebecca K Bounds-1 core (RKB-1), Kansas;
- Furthering our understanding of the driving forces behind MCE I by exploring environmental changes across this event in the Western Interior Seaway of North America (WIS);
- Evaluating longer-term oceanographic changes across Cenomanian WIS by creating a multiproxy environmental dataset from the central-eastern site and integrating it with other sites across the seaway.

The key findings from the preceding scientific chapters are summarised below, demonstrating how the aims and objectives of this project have been realised.

5.1.1 Identifying MCE I in RKB-1

A multi-proxy framework for MCE I has been constructed by analysing samples from the RKB-1 core, which was drilled in western Kansas, U.S.A., and represents a site from the central-eastern Cretaceous WIS. MCE I has been identified within RKB-1 by the discovery of a complex, yet distinct, positive dual-peaked bulk organic carbon isotope record. This mid-Cenomanian isotope curve is the most stratigraphically complete, highest-resolution record from the WIS, and thus constrains an excellent sequence with which to assess palaeoenvironmental and climatic change across this major carbon cycle perturbation within the basin.

5.1.2 Central-eastern WIS Water mass evolution during MCE I

A newly acquired high-resolution dataset consisting of trace metal contents, palynofacies and marine dinocyst records, lipid biomarker distributions, and sedimentological and microfacies analyses have demonstrated the complex nature of the evolution of the WIS water mass in the central-eastern part of the basin during the early to mid-Cenomanian. This dataset reveals that a fully connected North-South seaway developed during MCE I in this area, as equatorially-sourced Tethyan waters mixed with the Boreal-influenced northern arm of the seaway. Whilst previous interpretations from Colorado and Kansas have associated a major Tethyan connection during the deposition of the mid-Cenomanian Thatcher Limestone marker bed (e.g., Cobban and Scott, 1972;

Kauffman 1988; Sageman, 1996), this study demonstrates that the WIS water mass in this region consisted of Tethyan-Boreal waters during the first phase of MCE I, before the deposition of this tempestite.

Prior to MCE I, low enrichments of redox-sensitive trace metal, G-cyst dominated assemblages, and the higher absolute abundances of Boreal-affiliated *Cyclonephelium compactum–C. membraniphorum* and *Cribroperidinium edwardsii* dinocysts compared to Tethyan-affiliated *Bosedinia* spp. dinocysts demonstrate that, although mixed, the local-WIS watermass was predominantly influenced by oligotrophic, ventilated Boreal waters.

At the initiation of the first phase of MCE I (MCE 1a), Boreal dinocyst taxa reached their maximum abundances, whilst *Bosedinia* spp. became absent, indicating that a southward pulse of Boreal waters temporarily supplanted the mixed local-WIS water mass. This southward Boreal incursion mirrors similar southward migrations of Boreal-affiliated molluscan bivalves and elevated neodymium stable isotope records during MCE I into European sections (e.g., Gale and Christensen, 1996; Zheng et al., 2016), suggesting this was a globally contemporaneous oceanic reorganisation.

After this Boreal pulse, and throughout the remainder of MCE 1a, the co-occurrence of Boreal and Tethyan dinocysts, periodic changes to P-cyst dominated assemblages, and a relative increase in eukaryotic productivity indicate that nutrient-rich Tethyan waters were exerting a stronger influence on the local water mass. During the second phase of MCE I (MCE 1b) from the deposition of the Thatcher Limestone onwards, *Cribroperidinium edwardsii* is no longer observed, dinocyst assemblages are dominated by P-cysts, and numerous and abundance calcareous foraminifera and inoceramid shell fragments are identified throughout the succession. After the deposition of the Thatcher Limestone, the water column became strongly stratified, and anoxic-euxinic conditions developed at the sediment-water interface, *Bosedinia* spp. abundances increase significantly, the *Cyclonephelium compactum–C. membraniphorum* complex temporarily disappears, and overall eukaryotic and prokaryotic productivity increased, indicating that nutrient-rich Tethyan waters temporarily supplanted the local-WIS water mass.

After MCE I, the re-occurrence of Boreal dinocysts together with increasingly oxygenated waters indicate that the mixed local-WIS water mass re-established once again, remaining until the mid- to late Cenomanian Greenhorn Cyclothem.

5.1.3 Climatic controls on productivity during MCE I

Through microfacies analyses of polished thin sections of carbonate-rich and organic-rich horizons within the MCE I interval, the high-resolution bulk calcium (Ca) record obtained across the climatic event is shown to represent primarily a biogenic carbonate signal.

Multiple cyclostratigraphic statistical analyses demonstrate that the Ca record contains seven ~50 kyr obliquity cycles across MCE I, with the duration of these cycles being consistent to those resolved for contemporaneous strata from the southern WIS (Eldrett et al., 2015). Obliquity maxima in RKB-1 coincide with shifts to P-cyst dominated assemblages in the dinocyst record during MCE 1a and peaks in the Ca record during MCE 1b, indicating that at times of heightened solar insolation, planktic productivity increased at this latitude. This heightened productivity is attributed to the strengthening of meridional thermal gradients, which may have increased nutrient input into Tethyan surface waters in tropical equatorial regions through wind-driven upwelling.

5.1.4 Water mass related environmental evolution in the Cenomanian WIS

In lieu of biostratigraphic constraints available for the RKB-1 core, the Albian-Cenomanian to early Turonian $\delta^{13}C_{org}$ record was correlated to chronostratigraphically constrained $\delta^{13}C_{org}$ records from central Colorado and Texas by using a number of isotopic and bentonite tie-points. This provided a framework in which the environmental reconstruction of the RKB-1 study interval could be compared to others across the basin, ultimately providing new insights into the dynamic water mass evolution during the development of the Cenomanian WIS.

Sedimentological and palynofacies analyses determined that the early Cenomanian Dakota sandstone in the RKB-1 core represents a westerly extension of the large central Kansan large deltaic complexes onto the eastern coastal plain of the central WIS, and transitioned to a predominantly marsh/lagoonal environment as sea levels started to rise. The deposition of the Lower Graneros Shale records the transition from continental to completely marine settings at ~97 Ma, in a manner similar to that seen in Texas where Tethyan waters supplanted the southern WIS water mass. At the RKB-1 site, deposition continued under a mixed local-WIS water mass, aside from short-lived Boreal and Tethyan pulses at the beginning and end of MCE I, respectively (see above: Section 5.1.2). During the Greenhorn Cyclothem, northward-migrating Tethyan waters supplanted the local-WIS water mass in the mid- to late Cenomanian, as characterised by heightened redox-sensitive trace metal enrichments, increases in prasinophyte abundances, the absence of *Cyclonephelium compactum–C. membraniphorum* dinocysts, and greater carbonate contents from the deposition of the Lincoln Limestone Member onwards. However, from the deposition of the late Cenomanian Bridge Creek Limestone Member, bioturbation indices increase, redox-sensitive trace metal enrichments decrease, prasinophyte phycomata are no longer the dominant palynomorph in assemblages that now also favour G-cysts over P-cysts, and Boreal-affiliated dinocysts are observed once more. Together, these records demonstrate that the water column became more mixed and that an oxygenated benthic zone developed as Boreal waters exerted a dominant influence on the local environmental conditions. These changes are coincident with a positive CIE excursion that denotes OAE 2, and similar observations across the WIS at this time indicate that this southward Boreal migration represented a basin-wide oceanographic

reorganisation, mirroring similar oceanographic changes recorded in the North Atlantic and European sections, which are linked to the Plenus Cold Event.

5.2 Future work

While the research aims and objectives were met for this project, further research is planned in order to further constrain environmental and climatic changes during MCE I, which is briefly outlined below.

5.2.1 Further lipid biomarker analyses of RKB-1 sample material

Although palaeoenvironmental reconstructions through the use of lipid biomarker analyses provided interesting insights into the development of the central-eastern WIS water mass during MCE I, further sample processing may yield more robust data, which can then be used to enhance the conclusions put forward in Chapter 3.

Isorenieratene and its derivatives have been successfully identified in sections of the Graneros Shale in central Kansas and Colorado (Simons and Kenig, 2001). In order to do this, the authors completed an additional preparation when processing samples. They desulphurised the polar fraction of the total lipid fraction using nickel boride to liberate hydrocarbons which had been organically bound to sulphur.

Although aryl-isoprenoidal derivatives have been tentatively identified in RKB-1 samples, it is possible that isorenieratene itself has not been observed because it may have been organically bound to sulphur during diagenesis, and thus resides in the polar fraction of the total lipid extract. As the additional Raney-nickel desulphurisation process cannot be completed at the Organic Geochemistry Laboratory at Southampton, samples have been sent to the organic geochemistry laboratory at Curtin University, Australia, where Professor Kliti Grice and Dr. Alex Holman will desulphurise the samples, before assessing the polar fraction for isorenieratene. This newly acquired data will be analysed and incorporated into that already obtained and reported in Chapter 3 prior to submission of that manuscript.

5.2.2 Developing a North-South transect of the WIS

One of the key findings of this project is the identification of the interaction of Boreal and Tethyan waters as an important environmental driver. Both water masses had different palynological and geochemical characteristics, which have been observed across the central and southern Cenomanian WIS. By completing a high-resolution, multi-proxy transect that spans from the Boreally-influenced Canadian section in the north of the WIS, extending across the central and southern WIS, and terminating in the Tethyan-influenced equatorial North Atlantic, a more

comprehensive understanding of water mass migration throughout the WIS during both, MCE I and through the whole Cenomanian could be discerned (Fig. 5.1).

5.2.2.1 Boreal region, Canada

MCE I has been identified in the Cretaceous Colorado Group in the Western Canada Sedimentary Basin through a low-resolution positive bulk organic carbon isotope excursion at the contact between the Fish Scales Formation and the overlaying Belle Fourche Formation in northeastern Alberta (Schröder-Adams et al., 2012).

The Kennecott Crooked River core from east central Saskatchewan is here identified for future high-resolution, multi-proxy studies, as the Fish Scales and Belle Fourche formations and the WIS "x-bentonite" have been identified and described in this core (Gilboy, 1997), thus providing lithostratigraphic constraints on the study interval. Furthermore, published TOC and Rock Eval data at 1ft intervals (White et al., 1999), and low-resolution palynofacies records (Buckley and Tyson, 2003) can be used to develop a suitable sampling and analytical strategy.

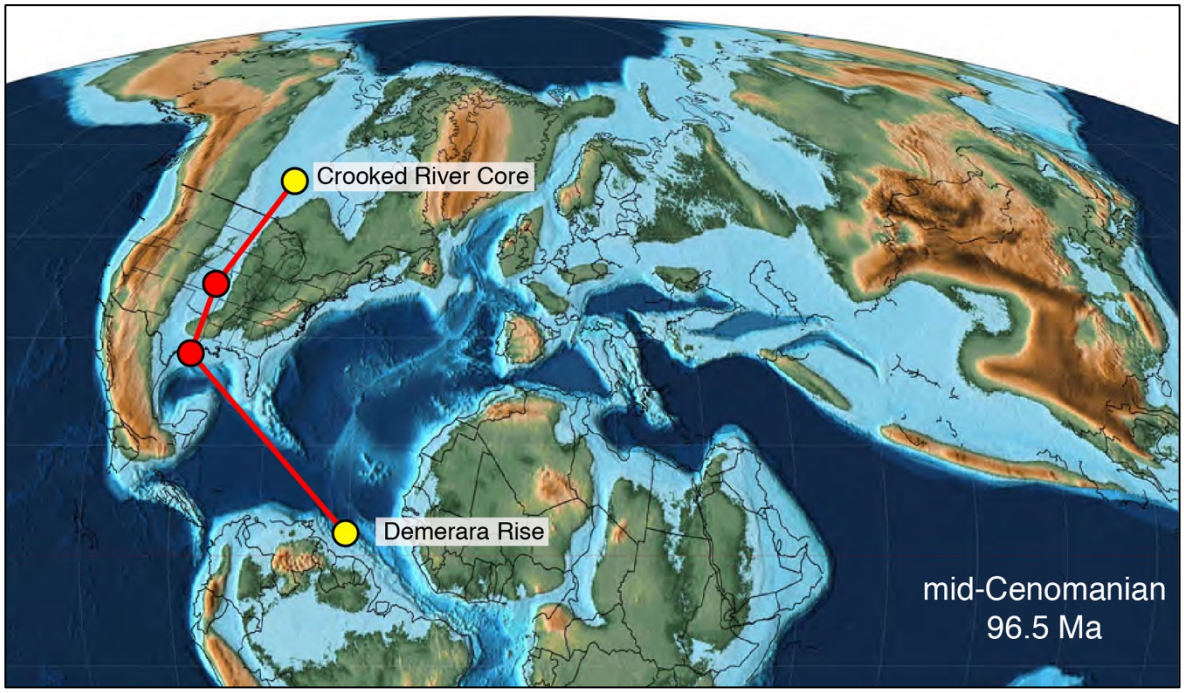

Figure 5.1: Palaeogeographic map showing study locations for a north-south transect of the WIS. Yellow circles represent proposed cores to be studied. Map adapted from Scotese, (2014).

5.2.2.2 Tethyan region, Demerara Rise

Multi-proxy analyses of Cenomanian organic-rich, black shale deposits from Sites 1258 and 1260 of Ocean Drilling Program (ODP) Leg 207 at Demerara Rise (tropical Atlantic Ocean) have provided an excellent foundation for an in-depth study of MCE I. Complex, multi-peaked mid-Cenomanian bulk organic carbon isotope profiles have been identified as MCE I using

foraminiferal biostratigraphic constraints (Friedrich et al., 2008). TOC, benthic and planktic foraminiferal records have determined that MCE I marks a turning point in the Cenomanian oceanographic system, in which bottom waters became progressively less oxygenated, and stepwise extinctions and turnovers of marine plankton commenced, lasting over a ~2 Myr period leading up to OAE 2 (Friedrich et al., 2008, 2009; Hardas et al., 2012). Recently, low-resolution inorganic geochemical and palynological analyses have been completed on these cores (Eldrett et al., 2017), further expanding the multi-proxy framework from which a detailed study of MCE I can be completed.

As part of this Ph.D. research, lipid biomarker analyses spanning MCE I have already been completed for these sites in a preliminary study. However, only *n*-alkanes could be reliably identified as considerable diagenetic alteration has led to much of the material to be organically bound to sulphur. As such, the polar fractions of the total lipid extracts will need to treated using Raney-nickel desulphurisaiton in order to liberate hopanes, steranes and aromatic hydrocarbons.

5.3 References

Buckley, L., Tyson, R. V., 2003. Organic facies analysis of the Cretaceous Lower and basal Upper Colorado Group, Western Canada Sedimentary Basin – a preliminary report. Saskatchewan Geol. Surv. Saskatchewan Ind. Resour. Misc. Rep. 2003–4.1, 13pp.

Cobban, W.A., Scott, G.R., 1972. Stratigraphy and Ammonite Fauna of the Graneros Shale and Greenhorn Limestone Near Pueblo , Colorado Stratigraphy and Ammonite Fauna of the Graneros Shale and Greenhorn Limestone Near Pueblo , Colorado. Geol. Surv. Prof. Pap. 1–195.

Eldrett, J.S., Dodsworth, P., Bergman, S.C., Wright, M., Minisini, D., 2017. Water-mass evolution in the Cretaceous Western Interior Seaway of North America and equatorial Atlantic. Clim. Past 13, 1–34. doi:https://doi.org/10.5194/cp-13-1-2017

Eldrett, J.S., Ma, C., Bergman, S.C., Ozkan, A., Minisini, D., Lutz, B., Jackett, S.J., Macaulay, C., Kelly, A.E., 2015. Origin of limestone-marlstone cycles: Astronomic forcing of organic-rich sedimentary rocks from the Cenomanian to early Coniacian of the Cretaceous Western Interior Seaway, USA. Earth Planet. Sci. Lett. 423, 98–113. doi:10.1016/j.epsl.2015.04.026

Friedrich, O., Erbacher, J., Moriya, K., Wilson, P.A., Kuhnert, H., 2008. Warm saline intermediate waters in the Cretaceous tropical Atlantic Ocean. Nat. Geosci. 1, 453–457. doi:10.1038/ngeo217

Friedrich, O., Erbacher, J., Wilson, P.A., Moriya, K., Mutterlose, J.J., 2009. Paleoenvironmental changes across the Mid Cenomanian Event in the tropical Atlantic Ocean (Demerara Rise,

ODP Leg 207) inferred from benthic foraminiferal assemblages. Mar. Micropaleontol. 71, 28–40. doi:10.1016/j.marmicro.2009.01.002

Gale, A.S., Christensen, W.K., 1996. Occurrence of the belemnite *Actinocamax plenus* in the Cenomanian of SE France and its significance. Bull. Geol. Soc. Denmark. 43, 68-77.

Gilboy, C.F., 1997. Lithological Description of Cretaceous Strata in Core from Kennecott Crooked River Kimberlite SK-16B-93. Summ. Investig. 1997, Saskatchewan Geol. Surv. 97, 188.

Hardas, P., Mutterlose, J., Friedrich, O., Erbacher, J., 2012. The Mid Cenomanian Event in the equatorial Atlantic: The calcareous nannofossil and benthic foraminiferal response. Mar. Micropaleontol. 96–97, 66–74. doi:10.1016/j.marmicro.2012.08.003

Kauffman, E.G., 1988, Concepts and Methods of High-Resolution Event Stratigraphy. Ann. Rev. Earth Planetary Sci, v. 16, p. 605-653.

Sageman, B.B., 1996. Lowstand tempestites: Depositional model for Cretaceous skeletal limestones, Western Interior basin. Geology 24, 888–892. doi:10.1130/0091-7613(1996)024<0888:LTDMFC>2.3.CO;2

Schröder-Adams, C., Herrle, J.O., Tu, Q., 2012. Albian to Santonian carbon isotope excursions and faunal extinctions in the Canadian Western Interior Sea: Recognition of eustatic sea-level controls on a forebulge setting. Sediment. Geol. 281, 50–58. doi:10.1016/j.sedgeo.2012.08.004

Scotese, C.R., 2014. Atlas of Late Cretaceous Paleogeographic Maps, PALEOMAP Atlas for ArcGIS, volume 2, The Cretaceous, Maps 16–22, Mollweide Projection, PALEOMAP Project, Evanston, IL.

Simons, D.-J.H., Kenig, F., 2001. Molecular fossil constraints on the water column structure of the Cenomanian–Turonian Western Interior Seaway, USA. Palaeogeogr. Palaeoclimatol. Palaeoecol. 169, 129–152.

White, T.S., Witzke, B.J., Ludwigson, G.A., Ravn, R., 1999. Chemostratigraphy and sequence stratigraphy of the Albian–Turonian (Cretaceous) portions of the Kennecott Crooked River SK-16B-93-1 Core, east-central Saskatchewan. Summ. Investig. 1, 94–99.

Zheng, X.-Y., Jenkyns, H., Gale, A., Ward, D., Henderson, G., 2016. A climatic control on reorganization of ocean circulation during the mid-Cenomanian event and Cenomanian-Turonian oceanic anoxic event (OAE 2): Nd isotope evidence. Geology 44, 151–154. doi:10.1130/G37354.1